

**Repair of Heavily Decayed Timber Piles  
Using Glass Fiber Reinforced Polymers (GFRP)  
and Cementitious Grout**

by

**Michael W. Hagos**

A Thesis Submitted to  
the Faculty of Graduate Studies  
in Partial Fulfillment of the  
Requirement for the Degree of

**Master of Science**

Department of Civil and Geological Engineering  
University of Manitoba  
Winnipeg, Manitoba  
Canada

© July 2001



National Library  
of Canada

Acquisitions and  
Bibliographic Services

395 Wellington Street  
Ottawa ON K1A 0N4  
Canada

Bibliothèque nationale  
du Canada

Acquisitions et  
services bibliographiques

395, rue Wellington  
Ottawa ON K1A 0N4  
Canada

*Your file Votre référence*

*Our file Notre référence*

The author has granted a non-exclusive licence allowing the National Library of Canada to reproduce, loan, distribute or sell copies of this thesis in microform, paper or electronic formats.

The author retains ownership of the copyright in this thesis. Neither the thesis nor substantial extracts from it may be printed or otherwise reproduced without the author's permission.

L'auteur a accordé une licence non exclusive permettant à la Bibliothèque nationale du Canada de reproduire, prêter, distribuer ou vendre des copies de cette thèse sous la forme de microfiche/film, de reproduction sur papier ou sur format électronique.

L'auteur conserve la propriété du droit d'auteur qui protège cette thèse. Ni la thèse ni des extraits substantiels de celle-ci ne doivent être imprimés ou autrement reproduits sans son autorisation.

0-612-62745-4

**Canada**

**THE UNIVERSITY OF MANITOBA**

**FACULTY OF GRADUATE STUDIES**

**\*\*\*\*\***

**COPYRIGHT PERMISSION PAGE**

**REPAIR OF HEAVILY DECAYED TIMBER PILES USING GLASS FIBER  
REINFORCED POLYMERS (GFRP) AND CEMENTITIOUS GROUT**

**BY**

**Michael W. Hagos**

**A Thesis/Practicum submitted to the Faculty of Graduate Studies of The University  
of Manitoba in partial fulfilment of the requirements of the degree**

**of**

**MASTER OF SCIENCE**

**MICHAEL W. HAGOS ©2001**

**Permission has been granted to the Library of The University of Manitoba to lend or sell copies of this thesis/practicum, to the National Library of Canada to microfilm this thesis/practicum and to lend or sell copies of the film, and to Dissertations Abstracts International to publish an abstract of this thesis/practicum.**

**The author reserves other publication rights, and neither this thesis/practicum nor extensive extracts from it may be printed or otherwise reproduced without the author's written permission.**

## **Abstract**

This experimental study has been conducted to evaluate the effectiveness of using Glass Fiber Reinforced Polymer (GFRP) systems and cementitious grout to restore heavily decayed timber piles to their original load-carrying capacity.

The proposed repair scheme involved trimming some of the decayed timber from around the circumference of the pile, followed by encasing the “sound” timber core with a 50 mm thick non-shrink cementitious grout shell. The “sound” timber core and the newly formed grout shell were then confined using external GFRP systems to improve the axial compression capacity of the piles. A total of 43 timber pile specimens were tested to failure in axial compression, while another ten pile specimens were tested in bending.

In general, test results demonstrated that a 50 mm thick cementitious grout shell confined by a single layer of GFRP wet-wrap can effectively restore the axial compressive strength of the piles to their original load-carrying capacity or greater. Furthermore, the proposed repair technique serves to reduce the variability in the load-carrying capacity of the repaired piles. The transition zone between the repaired length of pile and the “sound” timber below must be strengthened in order to utilize the full capacity of the unrepaired “sound” timber below. However, the transition zone cannot sustain high moment and should be located at depths with lower levels of applied moment.

A conservative design approach has been developed and detailed design recommendations are made. Suggestions for specific areas of further research are also given, and should be undertaken if further refinement of the repair technique and design procedure is required.

## **Acknowledgements**

First and foremost, the author wishes to express his profound gratitude and appreciation to his advisor, Dr. Robin L. Hutchinson. Throughout the course of this project, Dr. Hutchinson provided the author with invaluable guidance and advice. The author is also indebted to Dr. Hutchinson for providing financial support through ISIS Canada and listening to his personal concerns.

The author would like to gratefully acknowledge the specimens fabrication and testing performed by Mr. Kevin Amy.

The author would like to express his sincere appreciation to Mr. Moray McVey, Mr. Scott Sparrow, and Mr. Grant Whiteside for their invaluable assistance with the experimental work. The assistance provided by Mr. David Schnerch is also gratefully acknowledged.

Finally, the author would like to thank Mr. Bart Flisak, Mr. Shaun Hay and Grant Horeczy for their help in the structural lab.

## **Table of Contents**

<b>Abstract</b> .....	<b>ii</b>
<b>Acknowledgements</b> .....	<b>iii</b>
<b>Table of Contents</b> .....	<b>iv</b>
<b>List of Tables</b> .....	<b>viii</b>
<b>List of Figures</b> .....	<b>x</b>
<b>List of Symbols</b> .....	<b>xviii</b>

### **Chapter 1: Introduction**

1.1 General Overview.....	1
1.2 Objective.....	3
1.3 Scope and Contents.....	3

### **Chapter 2: Literature Review**

2.1 General.....	5
2.2 Strength of Timber Piles.....	6
2.3 Previous Studies of Timber Pile Repair.....	8
2.4 Concrete Columns Confined by FRP Systems.....	12
2.5 The Mechanics of Confinement.....	15

## **Chapter 3: Experimental Program**

3.1	General.....	23
3.2	The Repair Technique and Materials Used.....	24
3.2.1	Pile Repair Technique.....	24
3.2.2	Timber Piles.....	25
3.2.3	FRP Systems.....	26
3.2.3.1	GFRP Wet-Wrap System.....	26
3.2.3.2	GFRP Shell System.....	27
3.2.4	Cementitious Grout.....	27
3.2.5	Boron Rods.....	28
3.3	Axial Compression Specimens.....	29
3.3.1	General.....	29
3.3.2	200 mm Diameter Pile Specimens.....	30
3.3.2.1	“Timber Only” Control Specimens.....	30
3.3.2.2	Single Layer GFRP Wet-Wrap Specimens.....	31
3.3.2.3	Bearing Specimens.....	31
3.3.3	300 mm Diameter Pile Specimens.....	32
3.3.3.1	“Grout Only” Control Specimens.....	32
3.3.3.2	Single Layer GFRP Wet-Wrap Specimens.....	32
3.3.3.3	Double Layer GFRP Wet-Wrap Specimens.....	32
3.3.3.4	Prefabricated GFRP Shell Specimens.....	33
3.3.4	Instrumentation for Axial Compression Specimens.....	33
3.3.5	Test Set-Up for Axial Compression Specimens.....	34

3.4	Bending Specimens.....	35
3.4.1	General.....	35
3.4.2	Bending Specimen Design and Fabrication.....	35
3.4.3	Instrumentation for Bending Specimens.....	36
3.4.4	Test Set-Up for Bending Specimens.....	37

***Chapter 4: Test Results and Analysis:  
Axial Compression Series***

4.1	General.....	56
4.2	Control Specimens.....	57
4.3	Piles with a Single Layer of GFRP Wet-Wrap and Various Levels of Core Decay.....	60
4.4	Bearing Specimens Examining Load Transfer.....	63
4.5	Effect of Different GFRP Configurations.....	65
4.5.1	General.....	65
4.5.2	Piles with a Single Layer of GFRP Wet-Wrap.....	65
4.5.3	Piles with a Double Layer of GFRP Wet-Wrap.....	66
4.5.4	Piles with a Prefabricated GFRP Shell.....	67
4.6	Analysis of Axial and Lateral Strain Behaviour.....	69
4.7	Effect of Confinement on Compressive Strength.....	72
4.8	Effect of Core Size and Condition on Efficiency of Confinement.....	77
4.9	Recommended Design Approach.....	79



**Chapter 5: Test Results and Analysis:  
Bending Series**

5.1 General.....108  
5.2 Bending Control Specimens.....109  
5.3 Transition Zone Between Repaired and Unrepaired Pile Lengths.....111  
5.4 Effect of Axial GFRP and Timber Core Condition.....114  
5.5 Flexural Strain Analysis.....116

**Chapter 6: Summary and Conclusions**

6.1 Summary.....130  
6.2 Conclusions and Design Recommendations.....132  
6.3 Recommendations for Further Research.....135

**References.....137**

**Appendix A Load vs Strain Curves for Axial Compression Series.....142**

**Appendix B Load vs Flexural Strain Curves for Bending Series.....152**

## ***List of Tables***

### ***Chapter 2***

Table 2.1	Specified Strength and Modulus of Elasticity for Round Timber piles...	18
-----------	--	----

### ***Chapter 3***

Table 3.1	Physical Properties of Mbrace™ EG 900 E-glass Fiber Sheet.....	38
Table 3.2	Physical Properties of QM 6408 Prefabricated GFRP Shell.....	38
Table 3.3	Summary of 200 mm Overall Diameter Axial Compression Test Specimens.....	39
Table 3.4	Summary of 300 mm Overall Diameter Axial Compression Test Specimens.....	40
Table 3.5	Summary of Specimens Tested in Bending.....	41

### ***Chapter 4***

Table 4.1	Summary of 200 mm Overall Diameter Piles Tested in Axial Compression.....	85
Table 4.2	Summary of 300 mm Overall Diameter Piles Tested in Axial Compression.....	86
Table 4.3	Maximum Grout Stress Assuming Load is Carried by Grout Shell Only: 200 mm Diameter Piles.....	87

Table 4.4	Maximum Grout Stress Assuming Load is Carried by Grout Shell Only: 300 mm Diameter Piles.....	88
-----------	--	----

## ***Chapter 5***

Table 5.1	Summary of Results for Pile Specimens Tested in Bending.....	118
Table 5.2	Summary of Moment at Failure for Pile Specimens Tested in Bending.....	119
Table 5.3	Estimated Modulus of Rupture and Specified Strength for “Timber Only” Bending Control Specimens at Mid-Span.....	119

## ***List of Figures***

### ***Chapter 2***

Figure 2.1	Timber Pile Repair Scheme by Splicing Using Reinforced Concrete.....	19
Figure 2.2	Schematic of Cutting and Posting Timber Pile Repair.....	20
Figure 2.3	Reinforced Concrete Jacketed Timber Pile.....	20
Figure 2.4	Unconfined Uniaxially Loaded Concrete Showing Stress vs Longitudinal, Transverse Strain.....	21
Figure 2.5	Stress-Strain Curves for Unconfined and Confined Concrete Cylinders.....	21
Figure 2.6	Free Body Diagram Showing The Internal and External Forces on the FRP System and Concrete Core.....	22
Figure 2.7	Stress-Strain Curve for Confined and Unconfined Concrete.....	22

### **Chapter 3**

Figure 3.1(a)	Schematic of Bearing Specimens before Grout Injection and GFRP Wet-Wrap Sheets Application.....	42
Figure 3.1(b)	Schematic of Repair Technique Using GFRP Wet-Wrap Sheets.....	42
Figure 3.2(a)	Prefabricated QM 6408 GFRP Shell.....	43
Figure 3.2(b)	Schematic of Repair Technique Using the Prefabricated GFRP Shell.....	43
Figure 3.3	200 mm Diameter “Timber Only” Control Specimens.....	44
Figure 3.4	200 mm Diameter Single Layer GFRP Wet-Wrap Specimens.....	45
Figure 3.5	200 mm Diameter Bearing Specimens.....	46
Figure 3.6	300 mm Diameter “Grout Only” Control Specimens.....	47
Figure 3.7	300 mm Diameter Single Layer GFRP Wet-Wrap Specimens.....	48
Figure 3.8	300 mm Diameter Double layer GFRP Wet-Wrap Specimens.....	49
Figure 3.9	300 mm Diameter Specimens Repaired Using Prefabricated GFRP Shell.....	50
Figure 3.10	Axial Compression Specimens Fabricated Using the GFRP Wet-Wrap Technique.....	50
Figure 3.11	Schematic of Test Set-Up and Instrumentation Layout for Piles Tested in Axial Compression.....	51
Figure 3.12	Photo of Test Set-Up for Piles Tested in Axial Compression.....	51
Figure 3.13	Bending Test Specimens.....	52
Figure 3.14(a)	Trimmed Timber Piles for Bending Test.....	53

<b>Figure 3.14(b) Trimmed Timber Piles after Non-Shrink Cementitious</b>	
<b>Grout Injection.....</b>	<b>53</b>
<b>Figure 3.14(c) The Piles after Two Layers of GFRP Wet-Wrap</b>	
<b>System Application.....</b>	<b>53</b>
<b>Figure 3.14(d) Longitudinal Cross-Section of Bending Test Specimens</b>	
<b>Examining the Transition Zone.....</b>	<b>53</b>
<b>Figure 3.15(a) Instrumentation Layout for 200 mm Diameter “Timber Only”</b>	
<b>Bending Control Specimens Tested in Bending.....</b>	<b>54</b>
<b>Figure 3.15(b) Instrumentation Layout for 200 mm Diameter Repaired</b>	
<b>Specimens Tested in Bending.....</b>	<b>54</b>
<b>Figure 3.16 Schematic of Test Set-Up for Piles Tested in Bending.....</b>	<b>55</b>
<b>Figure 3.17 Photo of Test Set-Up for Piles Tested in Bending.....</b>	<b>55</b>

## **Chapter 4**

Figure 4.1(a) Maximum Load for all Control Pile Specimens.....	89
Figure 4.1(b) Summary of Test Results for 200 mm Overall Diameter Piles.....	90
Figure 4.1(c) Summary of Test Results for 300 mm Overall diameter Piles.....	90
Figure 4.2(a) Load vs Stroke for Mildly Decayed “Timber Only” Control Specimens.....	91
Figure 4.2(b) Load vs Stroke for “Grout Only” Control Specimens.....	91
Figure 4.2(c) Load vs Stroke for Heavily Decayed “Timber Only” Control Specimens.....	92
Figure 4.3(a) Cross-Section “Timber Only” Control Pile after Failure.....	93
Figure 4.3(b) “Timber Only” Control Pile after Failure.....	93
Figure 4.4(a) “Grout Only” Pile Specimens after Failure.....	94
Figure 4.4(b) Crack of the Grout Shell after Curing.....	94
Figure 4.5(a) Load vs Stroke for Piles with a Single Layer of GFRP Wrap and Mildly Decayed Core.....	95
Figure 4.5(b) Load vs Stroke for Piles with a Single Layer of GFRP Wrap and Heavily Decayed Core.....	95
Figure 4.5(c) Load vs Stroke for Piles with a Single Layer of GFRP Wrap and Void Core.....	96
Figure 4.6(a) Load vs Stroke Curves for Bearing Specimens.....	97
Figure 4.6(b) Load vs Stroke Curves for Piles with Strengthened Bearing Surface.....	97

Figure 4.7	200 mm Diameter Piles with a Single Layer of GFRP Wrap After Failure.....	98
Figure 4.8	Piles with Strengthened Bearing Surface after Failure.....	98
Figure 4.9(a)	Load vs Stroke for 300 mm Diameter Piles with a Single Layer of GFRP Wrap and Mildly Decayed Timber Core.....	99
Figure 4.9(b)	Load vs Stroke for 300 mm Diameter Piles with a Single Layer of GFRP Wrap and Void Core.....	99
Figure 4.10(a)	Load vs Stroke for 300 mm Diameter Piles with a Double Layer of GFRP Wrap and Mildly Decayed Timber Core.....	100
Figure 4.10(b)	Load vs Stroke for 300 mm Diameter Piles with a Double Layer of GFRP Wrap and Void Core.....	100
Figure 4.11(a)	Load vs Stroke for 300 mm Diameter Piles with a Prefabricated GFRP Shell and Mildly Decayed Timber Core.....	101
Figure 4.11(b)	Load vs Stroke for 300 mm Diameter Piles with a Prefabricated GFRP Shell and Heavily Decayed Timber Core.....	101
Figure 4.12(a)	300 mm Diameter Piles with a Single Layer of GFRP Wrap and Void Core after Failure.....	102
Figure 4.12(b)	Top View of 300 mm Diameter Piles with a Single layer of GFRP Wrap after Failure.....	102
Figure 4.13(a)	Piles with a Double Layer of GFRP Wrap and Mildly Decayed Timber Core after Failure.....	103



<b>Figure 4.13(b) Piles with a Double Layer of GFRP Wrap and Mildly</b>	
<b>Decayed Timber Core after Failure.....</b>	<b>103</b>
<b>Figure 4.14 Piles with a Double Layer of GFRP and Void Core after Failure.....</b>	<b>103</b>
<b>Figure 4.15 Pile with a Prefabricated GFRP Shell after Failure.....</b>	<b>104</b>
<b>Figure 4.16(a) Load vs Strain Curves for 2F1-V1.....</b>	<b>105</b>
<b>Figure 4.16(b) Load vs Strain Curves for 2F1-V2.....</b>	<b>105</b>
<b>Figure 4.16(c) Load vs Strain Curves for 2F1-V3.....</b>	<b>105</b>
<b>Figure 4.17(a) Load vs Strain Curves for 3F1-M1.....</b>	<b>106</b>
<b>Figure 4.17(b) Load vs Strain Curves for 3F1-M2.....</b>	<b>106</b>
<b>Figure 4.17(c) Load vs Strain Curves for 3F1-M3.....</b>	<b>106</b>
<b>Figure 4.18 Stress in Timber Core, <math>\sigma_T</math>, and Grout Shell, <math>\sigma_g</math>, vs Material</b>	
<b>Stiffness Ratio <math>E_G/E_T</math>.....</b>	<b>107</b>

## ***Chapter 5***

Figure 5.1	Summary of Bending Moment at Mid-Span and at Location of Failure.....	120
Figure 5.2	Load vs Mid-Span Deflection Curves for 200 mm “Timber Only” Bending Control Specimens.....	121
Figure 5.3	Load vs Mid-Span Deflection Curves for 200 mm Diameter Repaired Specimens Examining the Transition Zone.....	121
Figure 5.4	“Timber Only” Bending Control Specimen at Failure 2C-T-2.....	122
Figure 5.5	Failure at Transition Zone for Specimen 2LA-T-1.....	122
Figure 5.6	Failure at Transition Zone for Specimen 2LA-T-3.....	123
Figure 5.7	Failure at Transition Zone for Specimen 2LA-T-4.....	123
Figure 5.8	Failure at Transition Zone for Specimen 2LA-T-5.....	123
Figure 5.9(a)	Photo of Trimmed Timber Pile before Grout Injection.....	124
Figure 5.9(b)	Schematic of Longitudinal Cross-Section of Repair Specimen at Failure.....	124
Figure 5.9(c)	GFRP Sheet Rupture Over 200 mm Length.....	124
Figure 5.10	Specimen 3L-T with Lateral GFRP Wrap and Timber Core at Failure.....	125
Figure 5.11	Specimen 3LA-V with Axial and Lateral GFRP Wrap and Void Core at Failure.....	125

<b>Figure 5.12</b>	<b>Load vs Mid-Span Deflection Curves for 300 mm Diameter Piles</b>	
	<b>Tested in Bending.....</b>	<b>126</b>
<b>Figure 5.13</b>	<b>Load vs Flexural Strain Curves for 2C-T-1.....</b>	<b>127</b>
<b>Figure 5.14</b>	<b>Load vs Flexural Strain Curves for 2LA-T-3.....</b>	<b>128</b>
<b>Figure 5.15</b>	<b>Load vs Flexural Strain Curves for 3LA-V.....</b>	<b>129</b>

## List of Symbols

$A_g$	area of grout shell
$A_T$	area of timber core
$D$	diameter of the confined core
$E_f$	modulus of elasticity of the FRP system in the hoop direction
$E_g$	modulus of elasticity of grout
$E_T$	modulus of elasticity of timber
$f'_c$	compressive strength of unconfined concrete
$f'_{cc}$	compressive strength of confined concrete
$f_{cp}$	confining pressure provided by the FRP system
$f'_{cg}$	compressive strength of the confined grout
$f_f$	ultimate strength of the FRP system in the hoop direction
$f'_g$	compressive strength of the unconfined grout
$f_r$	modulus of rupture
$M_f$	bending moment at failure load
$P_g$	proportion of load carried by grout shell
$P_T$	proportion of load carried by timber core
$P_{total}$	total load carried by both timber core and grout shell
$S$	section modulus
$t_f$	thickness of the FRP system
$\epsilon'_c$	peak strain of unconfined concrete
$\epsilon'_{cc}$	peak strain of confined concrete
$\epsilon_f$	ultimate strain of the FRP system
$\epsilon_g$	strain in grout shell
$\epsilon_{i(hoop)}$	ultimate strain of the core in hoop direction
$\epsilon_T$	strain in timber core
$\sigma_g$	assumed maximum grout stress
$\sigma_T$	stress in timber core

# **Chapter 1**

## **Introduction**

### **1.1 General Overview**

Timber piles are widely used to support buildings, bridges, trestles, wharves and a variety of other structures. As an organic material, timber may be subject to decay and deterioration by natural organisms. Untreated timber piles that are fully embedded in soil below the permanent ground water level may last for many years. However, if untreated piles extend above the ground water level, they may be subject to decay. For portions of the pile above the ground water level, creosote pressure treatment is usually effective in preventing decay for the normal design life of a structure. However, in Canada's arctic region, due to the extremely cold climatic conditions, buildings were supported using untreated timber piles driven into the permafrost.

Permafrost is perennially frozen ground usually overlaid by one to ten feet of soil that thaws and refreezes each year and is known as "The Active Layer". Those parts of the

timber piles in the active layer and above ground require preservative treatments. A recent investigation into the condition of untreated timber piles in Inuvik, North West Territories, conducted by Ruddick (1999), revealed that medium to heavy decay is present in many of the existing untreated piles, prompting an immediate response to ensure the stability of the structures supported by the decayed timber piles.

In response to this problem, an innovative technique for the repair of these heavily decayed timber piles is being evaluated by the Network of Centers of Excellence on Intelligent Sensing for Innovative Structures, (ISIS Canada). The repair scheme includes the use of confining Glass Fiber Reinforced Polymer (GFRP) systems and cementitious grout to restore the heavily decayed timber piles to their original load-carrying capacity. The use of GFRP systems provides an advantage over other conventional materials due to their high-strength to weight ratio, resistance to corrosion, durability and ease of installation. For application in the Arctic, the used of these light-weight materials will significantly reduce the cost of transporting materials to these remote regions.

In order to evaluate the effectiveness of the proposed repair scheme, to make useful design recommendations, and to develop a reliable design procedure, an experimental program was conducted at the W. R. McQuade structural laboratory at the University of Manitoba.

## **1.2 Objective**

The main objectives of this research program are: to observe general trends in the behaviour of piles repaired using this technique, to examine the effect of various parameters on the capacity of the repaired piles, and to develop a design approach which may be modified with further testing. Recommendations for focused areas of further research are also made based on the results of this experimental program.

## **1.3 Scope and Contents**

The scope of this study involves an experimental investigation to examine the effectiveness of heavily decayed timber piles repaired using different GFRP systems and cementitious grout. The study encompasses the testing of 53 timber pile specimens repaired using a GFRP wet-wrap system and a prefabricated GFRP shell system. The experimental program includes 43 specimens tested in axial compression and 10 specimens tested in bending.

The thesis is organized in the following format:

- Chapter 2: This chapter presents a review of previous studies of timber pile repair found in the literature. Background on the use of GFRP systems to enhance the axial compressive performance of concrete columns is also briefly discussed, as related to the proposed pile repair technique.
- Chapter 3: This chapter presents the experimental program of both the Axial Compression Series of specimens and the Bending Series. Details of the

repair technique, the materials used and the different specimen parameters evaluated are described.

Chapter 4: Test results and analysis for the series of specimens tested in axial compression are presented and discussed in this chapter. Major areas of focus include the effect of different parameters, typical failure modes observed, the strength of the confined grout and design recommendations.

Chapter 5: Test results and analysis for the series of specimens tested in bending are presented and discussed in this chapter.

Chapter 6: This chapter presents a summary of and conclusions drawn from the present study. Recommendations for further research are also given in this chapter.



## **Chapter 2**

### **Literature Review**

#### **2.1 General**

This chapter presents a review of published timber pile repair studies. The repair methodologies discussed include: pile splicing, cutting and posting, grout injection, and concrete jackets. Also discussed in this chapter is the use of confining FRP systems to enhance the axial compressive performance of concrete columns. Test data on confined concrete columns has formed a basis for the development of equations describing the mechanics of confined concrete. Several of these equations are presented in this chapter, and with modification, may be applicable for pile repair techniques using confined grout.

## **2.2 Strength of Timber Piles**

Timber is a defect-filled anisotropic natural material. The anisotropy of the material and the presence of defects causes timber members to behave differently when subjected to compression, bending, or tension. Furthermore, the probability of defects occurring in timber increases with increased timber sizes.

Timber piles must be designed to resist the forces that they will be subjected to during installation as well as under service loading. The basic reference strength of timber piles is affected by many factors, and is often adjusted to account for defects and imperfections, load duration, treatment and in-use moisture content.

The general reference strength used in timber pile design for compression parallel to the grain is the crushing strength of small clear specimens. These small clear specimens of green wood are cut from a tree so that the grain runs parallel to the direction of loading and the specimens are free of defects or imperfections. The unit stress at failure of the specimens is referred to as the Green Small Clear Crushing Strength. Methods for performing these tests are given in the American Standards of Testing and Materials (ASTM) standard D 143.

The Green Small Clear Crushing Strength varies considerably between different species and between trees of the same species. The ASTM standard D 2555 contains a list of the average strengths, and standard deviations for various species and subspecies of timber. The standard also outlines methods for evaluating the five-percent exclusion limit for

species combinations, if the volume of the various species are known. Based on the data contained in the ASTM standard D 2555, Armstrong (1979) recommended that a design value of 17.2 MPa be used for the basic reference strength for axial compression in piles of Douglas Fir, Red Oak and Southern Pine timber. Armstrong's recommended value also agrees fairly well with the specified strength given by the Canadian Standards Association (CSA).

The structural design of timber piles in Canada is generally based on the requirements of the 1989 CSA standard CAN/CSA-O86.1, Engineering Design in Wood (Limit States Design) and the National Building Code of Canada (NBCC). For convenience, the specified strength and modulus of elasticity for round timber piles of three different species is reproduced and shown in Table 2.1. The specified strength given in this standard for Douglas Fir-Western Larch species in axial compression parallel to the grain is 18.7 MPa.

### **2.3 Previous Studies of Timber Pile Repair**

Relatively few experimental studies on the repair and rehabilitation of decayed timber piles are available in the literature. However, a few repair methodologies used in the past include: splicing, cutting and posting, grout injection, and concrete jackets.

There are many factors which may affect the selection of a repair method, including the strength and durability of the repaired pile, access to the existing pile, disruption of building functions due to pile repair activities, and in remote locations, the availability of craftsmen, material and equipment. Although cost tends to be the overriding factor in the selection of an appropriate repair method, strength and durability of the repaired pile is also an important objective. Ideally, the repair scheme should restore the timber pile to its original strength.

Repair by pile splicing involves the addition of new materials and connectors, such as attaching a new section of timber pile to the existing pile, bolting or splicing sections of steel, or adding steel or timber bracing. A typical splicing repair scheme is shown in steps one through seven in Figure 2.1. As shown in Figure 2.1, the deteriorated upper portion of the pile is removed and a new section of pile is installed and spliced to the existing timber below. If long, unsupported piles are spliced using new timber, the flexural strength at the splice is typically much less than that of the original pile. A stronger splice can be obtained with a reinforced concrete encasement as shown in Figure 2.1 US ARMY Field Manual (1985). However, the complexity of the technique,

the amount of additional material required, and the long term durability of the repair are concerns.

Cutting and posting is a repair technique that is similar to pile splicing, and involves cutting out the damaged section of pile and replacing it with a new section of timer pile. The extent of damage in the existing pile is first determined by drilling. The deteriorated pile section is then cut perpendicular to the longitudinal axis of the pile and removed. A jack is used to provide temporary support to the structure above. A new length of timber pile of similar diameter is then cut and placed into position, as shown in Figure 2.2. The new piece of timber is spiked or bolted to the existing pile and a relatively weak connection is formed. In order to increase the capacity of the repaired pile, a low viscosity epoxy may be pressure injected through a predrilled port connecting the new piece to the existing timber pile, as shown in Figure 2.2.

The effectiveness of the cutting and posting repair procedure using epoxy injection was evaluated by Avent (1986) both experimentally and in a field repair application on a bridge with timber piles. Avent reported that the repair procedure can restore the axial strength of timber piles to their original design strength. However, the flexural strength of the piles can be restored to only about one-half the original design capacity.

The injection of cementitious grout into voids in decayed timber piles is a repair technique that was explored by the Railway Track and Structures, USA, (1973). The procedure involved treating the existing timber to prevent further decay, then drilling

various holes and pumping the grout through hose nozzles into the drilled holes. According to the Railway Track and Structures, this procedure is expected to add 15 – 20 years of service life to the piles. If the pile damage is less severe, epoxy injection can be used to effectively repair the pile.

Reinforced concrete jackets have also been used to repair damaged timber piles. As shown in Figure 2.3, reinforcement is first placed in the annular space between the deteriorated timber pile and the formwork, followed by concrete injection. Concrete jackets have also been formed using a 25 mm – 50 mm thick coating of shotcrete reinforced with a wire mesh. In addition, precast concrete jackets have also been used for timber pile repair applications.

Since concrete is prone to deterioration from environmental effects such as the acids, alkalies or salts found in ground water, there is a concern regarding the durability of reinforced concrete jackets. Alternate freezing and thawing cycles accelerate the deterioration, since any water in the voids or cracks creates an expansive force when freezing, which furthers cracking and spalling. Cracking and spalling may lead to exposure and corrosion of the reinforcing steel as well as loss of the relatively thin concrete cross-section.

As proposed in the present study, reinforced concrete jackets can be an attractive repair solution if fiber reinforced polymer (FRP) reinforcement, which is not subjected to electrochemical corrosion, is used. In addition, it is proposed that the confinement

provided by the reinforcement would be significantly more effective if applied to the outer surface of the concrete using continuous sheets of FRP reinforcement. Studies on the use of externally bonded FRP systems for the repair of concrete columns have shown that the lateral confinement provided by the FRP is effective in increasing the axial capacity of the column Picher et al (1996).

## 2.4 Concrete Columns Confined by FRP Systems

In recent years, the repair and rehabilitation of concrete columns using fiber reinforced polymer (FRP) sheets has become increasingly popular. Typically, FRP sheets are wrapped around the column, overlapped, and bonded to themselves, resulting in effective confinement which enhances the axial capacity of the column Picher et al (1996).

As a concrete column is uniaxially compressed along its longitudinal axis, the Poisson effect induces transverse strain that results in radial expansion of the concrete. At low levels of longitudinal strain, the concrete behaves elastically and the transverse strain is related proportionally to the longitudinal strain by Poisson's ratio. At a critical value of longitudinal stress, typically 75% to 80% of the concrete strength,  $f'_c$ , additional cracks forming in the concrete paste between the aggregates result in a large increase in transverse strain with a relatively small increase in longitudinal stress. This rapid increase in transverse strain results in an equally rapid volumetric expansion. This behaviour of unconfined concrete is illustrated by the stress-strain curves provided in Figure 2.4 (MacGregor, 1997).

By wrapping the axially loaded concrete with a continuous confining FRP system, the transverse expansion of the concrete is restrained by the fibers. This resistance provides a confining pressure to the concrete. At low levels of longitudinal stress, the transverse strains are so low that the confining FRP system induces little confinement. However, at longitudinal stress levels above the critical stress which is 75 to 80% of the concrete strength,  $f'_c$ , the dramatic increase in transverse strain engages the confining FRP system



and the confining pressure becomes significant. The effect of the confining pressure is to induce a triaxial state of stress in the concrete. It is generally understood that concrete under triaxial compressive stress exhibits superior behaviour in both strength and ductility when compared to concrete in uniaxial compression (MacGregor, 1997).

The stress vs strain behaviour of concrete columns confined by an FRP system and subjected to axial load can be divided into three distinct regions, which can be seen in Figure 2.5. In the first region, the behaviour of confined concrete is similar to that of unconfined concrete, due to the fact that the confining effect of the FRP system has not yet been activated by the lateral expansion of the concrete core. Near the peak stress of the unconfined concrete, the confined concrete reaches a state of unstable volumetric growth caused by excessive cracking. At this stage, the confining FRP system is activated and starts to gradually restrain the rapid lateral expansion of the column. This region of the response is characterized by a transitional curve near the unconfined concrete strength,  $f'_c$ . Finally, the third region is that in which the confining FRP system is fully activated, and the stiffness is generally stabilized at an approximately constant rate. The response in this region is mainly dependent on the linear elastic behaviour of the confining FRP system (Mirmiran et al, 1997).

The reduced effectiveness of confinement for concrete cylinders with void cores was also examined in an experimental study conducted by Fam (2000). Fam examined the axial capacity of GFRP tubes totally and partially filled with concrete. Fam reported that although the void core offers material savings and a reduced self-weight, the maximum

confined strength is reduced when compared to totally filled GFRP tubes. A reduction in strength with increasing void size was observed. This behaviour was attributed to the fact that the void core allows an inward displacement or degree-of-freedom for the concrete as it expands under axial compression. However, if the central void is maintained by an inner GFRP tube, the confinement effectiveness is improved and could approach that of a totally concrete filled GFRP tube Fam (2000).

Fam (2000) tested two identical GFRP tubes filled with concrete having a compressive strength,  $f'_c$ , of 58 MPa, but with different void core sizes. While the overall diameter of both tubes was 219 mm, the first tube had a 95 mm diameter void core and the other tube had a 133 mm diameter void core. Fam reported that the maximum stress in the concrete shell with the 95 mm diameter void core slightly exceeded the compressive strength of the unconfined concrete,  $f'_c$ , while the tube with the larger 133 mm diameter void core failed at a stress level of only about  $0.91f'_c$ .

## 2.5 The Mechanics of Confinement

The mechanics of confinement, which were developed based on confined concrete column tests, may be applicable to confined grout shells used for timber pile repair with some modifications. The confining pressure provided by the FRP system is a function of the stiffness of the FRP and the expansion of the concrete or grout in the transverse direction. Therefore, in order to quantify the behaviour of concrete or grout confined by an FRP system, it is necessary to determine the confining pressure provided by the FRP system. Figure 2.6 illustrates the confining action provided by an FRP system applied with the continuous fibers oriented in the transverse or hoop direction.

The mechanics of confinement is dependent on two factors, the tendency of the concrete or grout to dilate and the radial stiffness of the FRP system restraining the dilation. Consequently, two conditions must always be satisfied: firstly, geometric compatibility between the core and the confining FRP system, and secondly, equilibrium of forces in the free-body diagram, as shown in Figure 2.6. According to the first condition, strain compatibility dictates that the strain in the confining FRP system is equal to the transverse strain of the concrete or grout. This leads to the following relationship:

$$\varepsilon_f = \varepsilon_{t(\text{hoop})} \quad (2.1)$$

The second equilibrium condition leads to the following relationship:

$$f_{cp} = \frac{2f_f t_f}{D} \quad (2.2)$$

$$f_{cp} = \frac{2E_f \varepsilon_{t(\text{hoop})} t_f}{D} \quad (2.3)$$

Where,

$D$  = diameter of the confined core

$E_f$  = modulus of elasticity of the FRP system in the hoop direction

$f_{cp}$  = the confining pressure provided by the FRP system

$f_f$  = ultimate strength of the FRP system in the hoop direction

$t_f$  = thickness of the FRP system

$\varepsilon_f$  = ultimate strain of the FRP system

$\varepsilon_{i(hoop)}$  = ultimate strain of the core in hoop direction

Various researchers have attempted to develop a generalized model to quantify the effect of confinement on the strength and ductility of concrete. The model proposed by Mander et al (1988) is, however, the most widely used. Although this model was originally developed for conventional reinforced concrete columns, it can be used to model the behaviour of concrete columns confined by a steel or FRP system.

Stress-strain curves for confined and unconfined concrete based on Mander's model are shown in Figure 2.7. Mander et al (1988) first proposed a unified stress – strain approach for confined concrete which is applicable to both circular and rectangular shaped sections subjected to axial compressive load. The confinement model proposed by Mander is based on a constant confining pressure,  $f_{cp}$ , acting during the entire loading history. The failure strain of the confined concrete is sought by an energy balance approach. The basis of this approach is that the additional ductility available in confined concrete is due to the energy stored in the confining member. Therefore in order to establish the first confining hoop fracture, the total strain energy in the confining

member is equated with the increase in strain energy of the confined concrete over its unconfined value.

The increased compressive strength of the concrete,  $f'_{cc}$  due to the confining pressure provided by the FRP system is a function of the unconfined strength,  $f'_c$ , and the confining pressure,  $f_{cp}$ . Hence the increased concrete strength,  $f'_{cc}$ , can be quantified using the following equation proposed by Mander et al (1988):

$$f'_{cc} = f'_c \left[ 2.254 \sqrt{1 + \frac{7.94 f_{cp}}{f'_c} - \frac{2 f_{cp}}{f'_c}} - 1.254 \right] \quad (2.4)$$

The peak strain of the confined concrete,  $\epsilon'_{cc}$ , is a function of the peak strain of the unconfined concrete,  $\epsilon'_c$ , and is given by Equation (2.5).

$$\epsilon'_{cc} = \epsilon'_c \left[ 1 + 5 \left( \frac{f'_{cc}}{f'_c} - 1 \right) \right] \quad (2.5)$$

By using Equations 2.1 through 2.5, the confined compressive strength of concrete or grout can be predicted.

Modifications to this model may be necessary in order to apply the model to columns using grout rather than concrete, and additional test data would be required to calibrate the revised model. Additional modification to the model would also be required for cross-sections with a void core rather than a solid circular section.

**Table 2.1: Specified Strength and Modulus of Elasticity for Round Timber Piles (MPa)**  
 Source: CAN/CSA-O86.1-M89

Species	Bending $f_b$	Longi- tudinal shear $f_v$	Compression		Tension parallel to grain $f_t$	Modulus of Elasticity	
			Parallel to grain $f_c$	Perp. to grain $f_{cp}$		$E$	$E_{05}$
Douglas Fir, Western Larch	20.1	1.4	18.7	7.7	13.6	11000	7000
Jack Pine	18.1	1.5	15.6	5.2	11.6	7000	5000
Lodgepole and Ponderosa Pine	14.2	1.0	13.2	5.2	9.7	7000	5000
Red Pine	13.6	1.2	11.7	5.2	9.0	7000	5000

**Notes:**

1. Tabulated values are listed for dry service condition and standard term duration of load.
2. Wood piles using Southern Yellow Pine may be assigned the same resistance as the Douglas Fir-Larch species group.

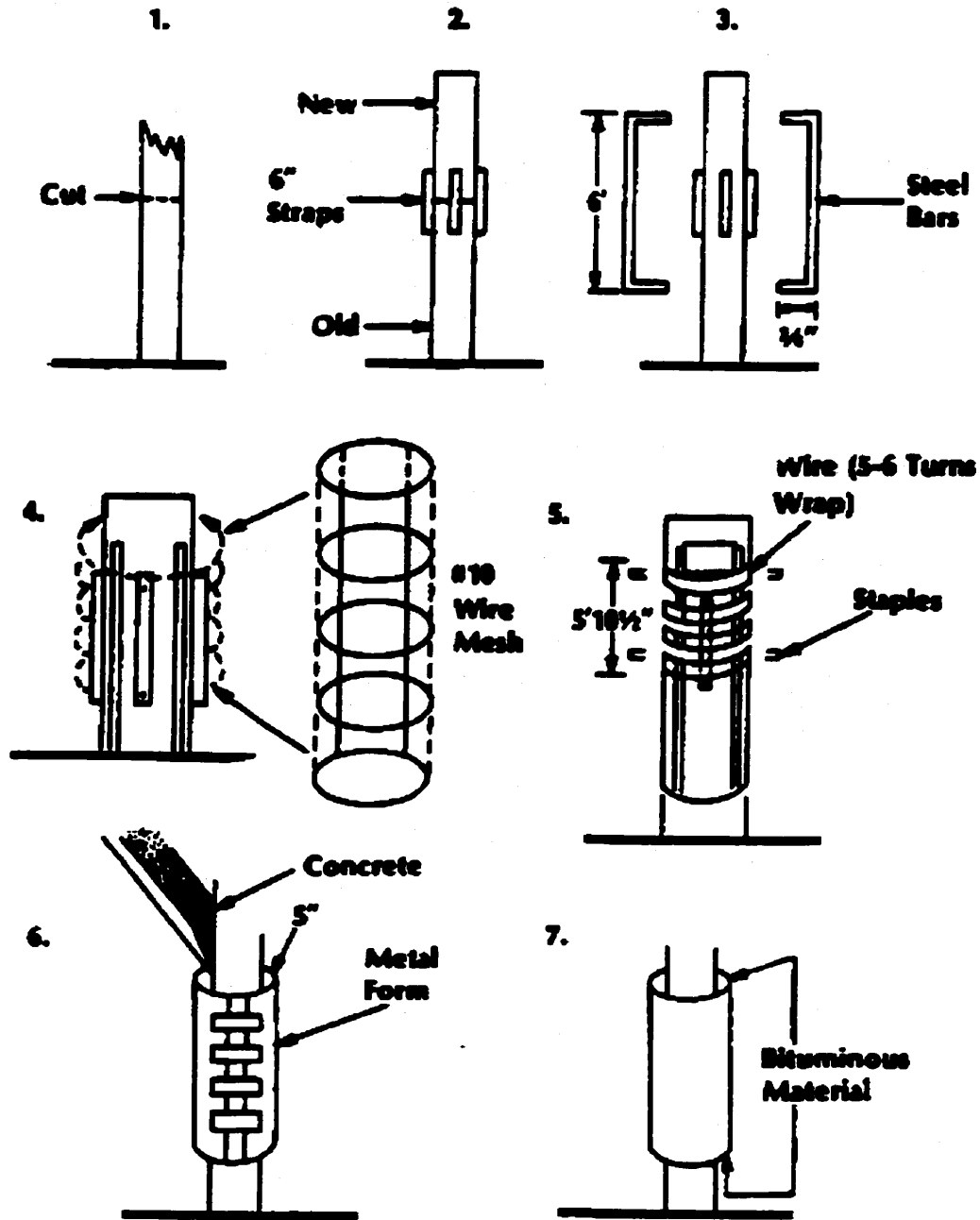


Figure 2.1: Timber Pile Repair Scheme by Splicing Using Reinforced Concrete.  
 After US ARMY FM 5-134 (1985)

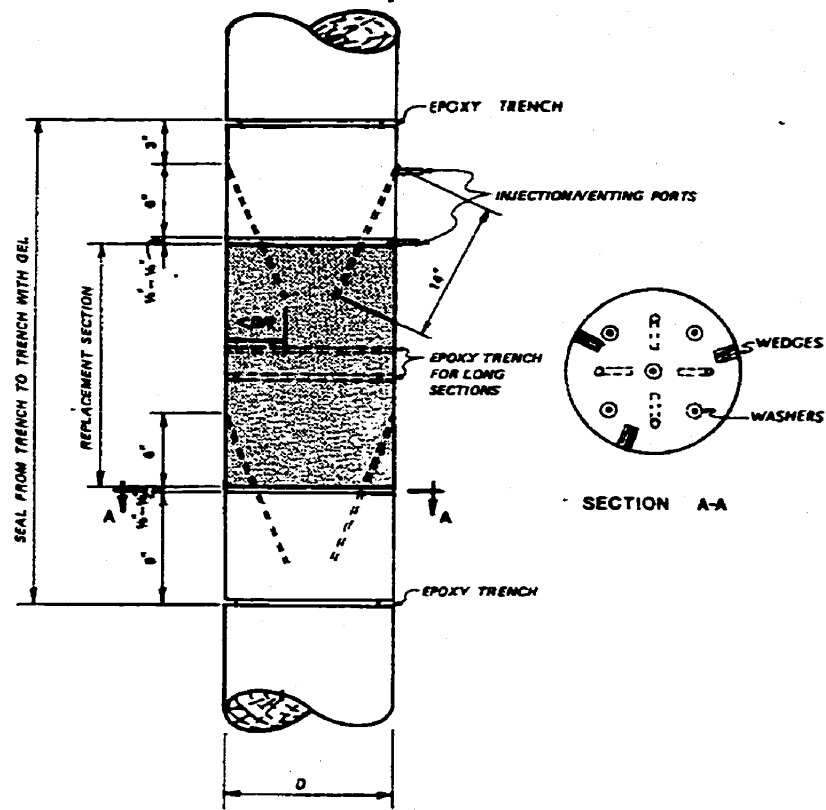


Figure 2.2: Schematic of Cutting and Posting Timber Pile Repair (Avent, 1986)

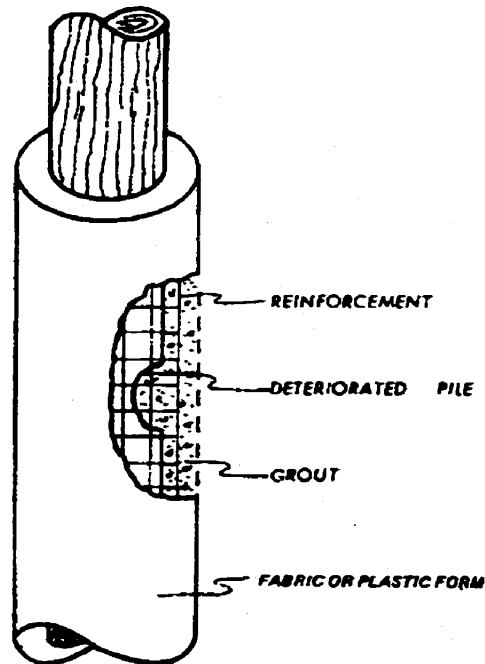


Figure 2.3: Reinforced Concrete Jacketed Timber Pile (Avent, 1986)



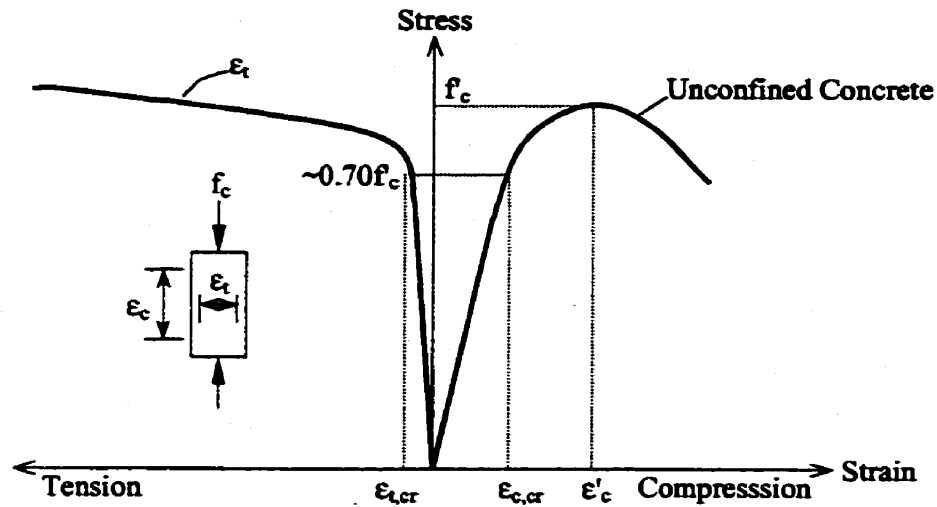


Figure 2.4: Unconfined Uniaxially Loaded Concrete Showing Stress vs Longitudinal, Transverse Strain (MacGregor, 1997)

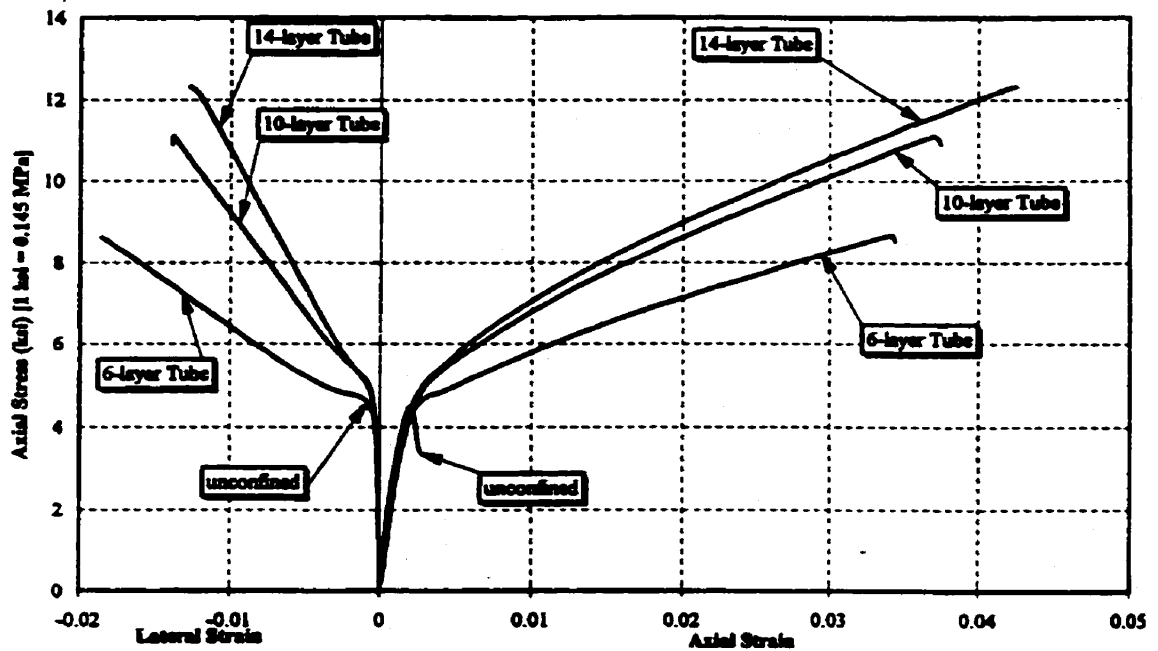


Figure 2.5: Stress-Strain Curves for Unconfined and Confined Concrete Cylinders (Mirmiran et al, 1997)

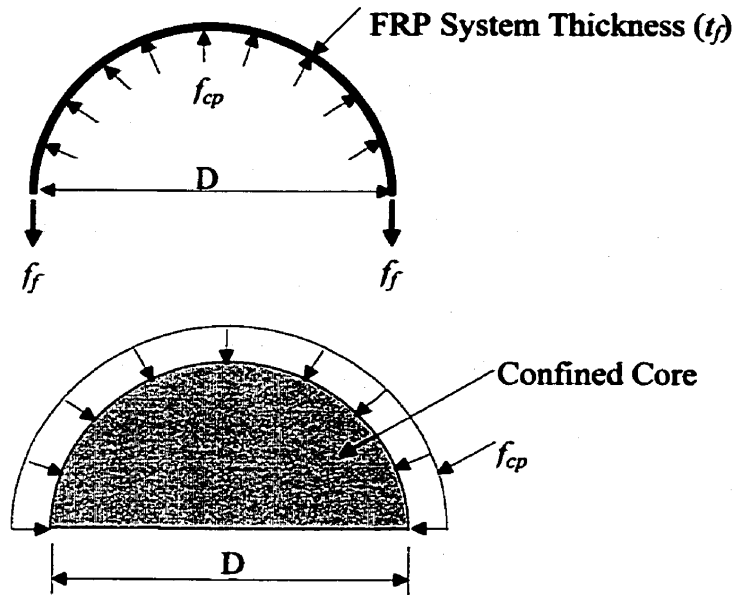


Figure 2.6: Free Body Diagram Showing the Internal and External Forces on the FRP System and Concrete Core

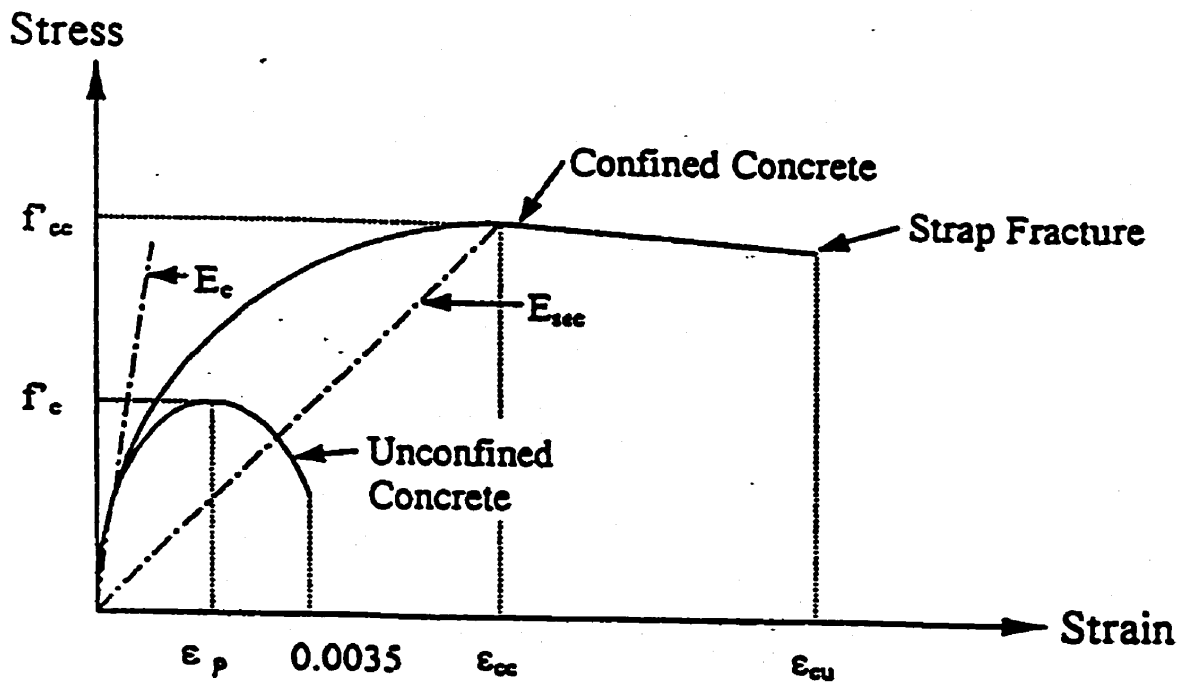


Figure 2.7: Stress-Strain Curve for Confined and Unconfined Concrete (Mander et al, 1988)

## **Chapter 3**

### **Experimental Program**

#### **3.1 General**

The experimental program consisted of 53 pile specimens repaired using cementitious grout and either a Glass Fiber Reinforced Polymer (GFRP) wet-wrap system or prefabricated GFRP shells. In order to determine the compressive strength of the repaired timber piles, a total of 43 specimens were fabricated and tested to failure in axial compression. In addition, the flexural behaviour of the repaired timber piles was examined using a total of ten specimens tested to failure in bending.

This chapter provides the details of specimen fabrication, presents the properties of the materials used in the experimental program, and describes the test set-ups and instrumentation used.

## **3.2 The Repair Technique and Materials Used**

### **3.2.1 Pile Repair Technique**

The first step in the proposed pile repair technique is removal of the most severely rotted surface wood. While removal of all of the decayed wood may not be required, enough wood must be removed around the pile circumference to provide sufficient bearing area for the grout shell on the sound pile below, as shown in Figure 3.1(a).

For the GFRP wet-wrap repair technique, after the timber pile is cut and shaped as shown in Figure 3.1(a), formwork is applied and the timber core is encased with non-shrink cementitious grout. The grout is allowed to cure for at least seven days before proceeding with the GFRP sheet application procedure. The wet-wrap procedure begins with a layer of epoxy resin or saturant applied to the surface of the grout, followed by a layer of dry glass fiber sheets, and then a final topcoat of the saturant resin. The resin is then allowed to cure for at least seven days at room temperature, between 5°C and 30°C, before testing.

As shown in Figure 3.1(b), the unidirectional continuous glass fibres are oriented horizontally around the circumference of the pile in order to provide maximum confinement for the grout shell and timber core, which are subjected to axial compression during loading. For piles subjected to significant bending, fibers oriented in the axial direction may also be applied. An overlap of at least 200 mm is provided to avoid any debonding failure at the ends of the sheets. In the case of multiple layers of

GFRP wet-wrap, the overlap should occur on alternating sides of the cross-section of the piles for each layer.

For the GFRP shell technique, after the timber is cut, the two-piece semi-circular prefabricated GFRP shell shown in Figure 3.2(a) is placed around the timber core. Adhesive supplied by the shell manufacturer is used to bond the two pieces together, and after curing of the adhesive, the GFRP shells serve as formwork for the grouting operation. As shown in Figure 3.2(b), a gap is maintained between the timber core and the GFRP shell which is equivalent to the intended thickness of the grout shell. High performance, non-shrink cementitious grout is used to fill this annular space between the timber and the GFRP shell.

### **3.2.2 Timber Piles**

Samples of heavily decayed timber piles shipped from Inuvik, N. W. T. were used for ten of the axial compression specimens. All of the other timber pile segments used in this experimental program were only mildly decayed, and were obtained from the Manitoba Hydro yard in Winnipeg, Manitoba. These mildly decayed timber piles had also been taken out of service, but were not in the severe state of decay that was observed in the group of piles shipped from Inuvik. The strength of the timber can be assessed by examining the load-carrying capacity of the unrepaired control specimens as will be discussed later.

### **3.2.3 FRP Systems**

As mentioned previously, two different types of commercially available glass fiber reinforced polymer (GFRP) systems were used to repair and fabricate the timber pile specimens. The first repair option used glass fibre reinforced polymer (GFRP) sheets applied using a wet lay-up, or wet-wrap procedure, while the second option used prefabricated GFRP shells.

#### **3.2.3.1 GFRP Wet-Wrap System**

The GFRP wet-wrap system used consisted of MBrace™ EG 900 E-glass fiber sheets, manufactured by Master Builders Inc in Cleveland, Ohio, USA. MBrace™ EG 900 E-Glass Fibers are manufactured by drawing molten glass through a die or bushing. The resulting "E" type glass filaments are grouped into tows that are then assembled into continuous unidirectional sheets. The physical properties of MBrace™ EG 900 sheets, as reported by the manufacturer, are provided in Table 3.1. The tensile strength and elastic modulus are determined by testing cured samples of the dry fiber and MBrace Saturant.

The MBrace™ Saturant LTC, a two-part low-viscosity epoxy was used to impregnate the dry glass fiber sheets. The resin and hardener (Parts A and B) were mechanically mixed using a 100 to 33 mixing ratio by weight, as recommended by the manufacturer. The MBrace™ Saturant was applied by napped roller to the grout surface or surface of the GFRP sheets.

### **3.2.3.2 GFRP Shell System**

The QM 6408 prefabricated GFRP shell system manufactured by Hardcore® Composites Inc, in New Castle, Delaware, USA were also used in this study. As shown in Figure 3.2(a), each prefabricated GFRP shell consisted of two semi-circular pieces, with fibers oriented at 0°, 90°, and ±45°. The physical properties of the QM 6408 prefabricated GFRP shell, as reported by the manufacturer, are given in Table 3.2.

### **3.2.4 Cementitious Grout**

Pre-blended non-shrink Sika® Grout 212 HP meeting the ASTM standard C1107 was used to encase all of the repaired timber pile specimens. The non-shrink grout, packaged in 25-kg bags, contains cement, dry sand, and a 2-stage component which compensates for shrinkage in both the plastic and hardened states. The consistency of the grout can range from dry-pack to fluid by adjusting the quantity of mix water. Unlike plain grout, the non-shrink grout exhibits little or no bleeding, expands slightly to squeeze out excess water and holds firmly against the grouted item. With the appropriate water to cement mix ratio, the grout has excellent pumpability and does not segregate, even in a fluid state. Also useful for this application, is the superior freeze/thaw resistance of this grout, as reported by the manufacturer.

A mix of 3.8 liters of water per 25-kg bag of grout was used in this particular experimental program, and was prepared using a mechanical mixer. Standard 100 mm x 200 mm cylinders were cast at the same time as the specimens were fabricated and were cured under the same conditions. The cylinders were tested at a loading rate of

0.2 mm/minute to determine the compressive strength of the grout at the time of pile testing. Compressive strength results for the grout cylinders are presented in Chapter 4.

### **3.2.5 Boron Rods**

Boron rods are reported by the manufacturer to be an effective preservative system for the prevention and control of fungal decay in timber structures and can control many destructive insects. The rods are typically installed in the timber in pre-drilled holes and will diffuse with an increased level of moisture content inside the timber.

In order to investigate any possible short-term effect of timber sterilization chemicals on the repair materials used, such as the non-shrink grout, Boron rods were inserted in a selected number of timber pile specimens. IMPEL™ Boron Rods, manufactured by Chemical Specialties Inc., Charlotte, NC, USA were used in this investigation. According to the manufacturer, IMPEL™ Boron rods have been used effectively in applications where the boron rods were in contact with concrete.



### **3.3 Axial Compression Specimens**

#### **3.3.1 General**

A total of 43 pile specimens with two different overall diameters were tested in axial compression, as summarized in Tables 3.3 and 3.4. Piles with an overall diameter of 200 mm are denoted by a specimen mark beginning with “2” and are listed in Table 3.3, while the specimen marks for piles with an overall diameter of 300 mm begin with “3” and are listed in Table 3.4. All of the repaired piles consisted of a 100 mm or 200 mm diameter timber core encased in a 50 mm thick grout shell.

In order to examine the effect of various levels of confinement on the behaviour of the repaired piles, three different GFRP configurations were used. The piles repaired using the prefabricated GFRP shell system are marked “FS”, while piles with a single or double layer of GFRP wet-wrap sheets are marked “F1” or “F2”, respectively. Nine control specimens were also tested, using timber only, and are marked “CT”. Two additional control specimens consisting of only, timber and an unconfined grout shell are marked “CG.”

In order to determine the effect that the condition of the timber core has on the behaviour of the repaired piles, three different levels of timber deterioration were examined. Timber with only mild decay, denoted by “M” in the specimen mark, was used, as well as heavily decayed timber shipped directly from the arctic and denoted by “H.” To simulate the worst case of completely deteriorated timber, pile specimens with a void rather than a timber core were tested and are marked “V.” Due to the variability in

material properties inherent in all large timber members, wherever possible, at least three identical piles were tested for each set of specimen parameters, as shown in Tables 3.3 and 3.4.

Load transfer between the repaired length of the pile and the existing timber below was examined using six longer pile specimens of only mildly decayed timber. The six “bearing” specimens used to examine load transfer were 900 mm long, while the 37 remaining axial compression specimens were 600 mm long. Figure 3.1(a) provides a schematic of the bearing specimens, which were used to study the load transfer behaviour. These specimens are shown shaded in Table 3.3 and are denoted using “B” and “SB”. Since the first group of three identical bearing specimens marked “B” exhibited bearing failure in the timber directly below the 50 mm thick grout shell, the bearing area was strengthened for the next three specimens which are denoted as “SB” in Table 3.3.

### **3.3.2 200 mm Diameter Pile Specimens**

#### **3.3.2.1 “Timber Only” Control Specimens**

The “timber only” control pile specimens consisted of two groups of 600 mm long piles. The first was a group of four timber piles with only mildly decayed timber obtained from Manitoba Hydro. The other group of five piles consisted of heavily decayed timber shipped directly from Inuvik. The heavily decayed piles were first tested to evaluate their existing capacity, and were then repaired and tested to examine the effectiveness of the repair technique for severely deteriorated piles. In order to avoid excessive damage

to the heavily decayed timber control piles, testing was terminated as soon as no increase in load was observed and prior to complete failure of the pile. Figure 3.3 provides a graphical representation of the “timber only” control specimens.

### **3.3.2.2 Single Layer GFRP Wet-Wrap Specimens**

A total of nine 200 mm diameter pile specimens were repaired using one layer of the GFRP wet-wrap system. Three of the piles had a mildly decayed timber core, three had a heavily decayed timber core, and the remaining three had a void core. Figure 3.4 presents a graphical representation of the 200 mm diameter piles repaired with a single layer of GFRP wet-wrap sheets.

### **3.3.2.3 Bearing Specimens**

As mentioned previously, six longer pile specimens were designed to examine the load transfer between the repaired pile and the existing timber below. These piles were 900 mm long with a 600 mm long section repaired using a single layer of GFRP wet-wrap and a 300 mm unrepaired section below as shown in Figure 3.1(a). In order to provide adequate bearing area for the 50 mm thick grout shell, a 50 mm thickness of timber was removed around the circumference of the 600 mm length of the pile. Since bearing failure occurred in the unrepaired timber for the first three specimens, the next group of three piles was prepared with a strengthened bearing surface.

Strengthening of the bearing surface included injecting the surface of the existing timber with epoxy resin and confining the first 100 mm length of timber below the bearing

surface with GFRP sheets. The group of three strengthened bearing piles also used the Impel Boron Rods to evaluate the short-term effect of timber sterilization. The Impel Boron Rods were inserted into the timber core prior to the grouting operation. Figure 3.5 provides a graphical representation of the bearing specimens.

### **3.3.3 300 mm Diameter Pile Specimens**

#### **3.3.3.1 “Grout Only” Control Specimens**

The “grout only” control specimens consisted of two mildly decayed 200 mm diameter timber piles encased in a 50 mm thick unconfined grout shell, as shown in Figure 3.6.

#### **3.3.3.2 Single Layer GFRP Wet-Wrap Specimens**

Six 300 mm diameter pile specimens were repaired with a single layer of GFRP wrap. The first three specimens had a 200 mm mildly decayed timber core while the remaining three had a 200 mm void core, as shown in Figure 3.7.

#### **3.3.3.3 Double Layer GFRP Wet-Wrap Specimens**

Six 300 mm diameter piles were repaired using a double layer of GFRP wrap. The first three specimens had a 200 mm diameter mildly decayed timber core, while the other three had a 200 mm diameter void core, as shown in Figure 3.8.

### **3.3.3.4 Prefabricated GFRP Shell Specimens**

This group consisted of five piles repaired using the prefabricated GFRP shell system. The first group of three piles had a 200 mm diameter mildly decayed timber core, while the other two piles had a 200 mm diameter heavily decayed timber core. Figure 3.9 provides a graphical representation of the specimens repaired using the prefabricated GFRP shells.

### **3.3.4 Instrumentation for Axial Compression Specimens**

Load, vertical displacement and strain were the general parameters measured during the axial compression tests. In addition to the load cell and stroke measurements of the MTS machine, instruments used included: electric resistance strain gauges, PI gauges and linear variable displacement transducers (LVDTs). Based on preliminary tests and failure observations, the instruments were concentrated around potential failure zones.

Strain gauges measuring hoop strain over a 5 mm gauge length were attached at 75 mm from the top and bottom of the pile and at mid height. Vertical strain was measured using 100 mm PI gauges attached on two opposite sides of the pile at mid height, and the vertical displacement was measured using an LVDT. A schematic diagram of the instrumentation layout is shown in Figures 3.11(a) and (b).

Data from the load cell and all other instruments mounted on the specimen was collected by a 32-channel data acquisition system. The data acquisition system was programmed to receive and record samples at every one second frequency for the duration of the test.

### **3.3.5 Test Set-Up for Axial Compression Specimens**

The test set-up used for the axial compression specimens is shown in Figures 3.11 and 3.12. A 5,000 kN closed loop MTS hydraulic testing machine was used to apply axial compression under stroke control. The stroke rate used was 0.5 mm/minute. Quickset plaster pads were used at the top and bottom of the specimens to ensure uniform load distribution and to facilitate proper alignment of the specimens in the testing machine.

## **3.4 Bending Specimens**

### **3.4.1 General**

In the majority of applications, timber piles are subjected to axial loads that are relatively high in comparison to any lateral loads that may be applied to the piles. However, piles may be subjected to horizontal or lateral forces due to wind, seismic activity, and earth or hydraulic pressure, which would induce bending stresses in the piles. Therefore, in order to examine the flexural behaviour of the repaired timber piles, ten pile specimens were tested in bending. Table 3.5 provides a summary of the specimen parameters used.

### **3.4.2 Bending Specimen Design and Fabrication**

A graphical representation of the ten 1200 mm long bending test specimens is provided in Figure 3.13. Eight of the bending specimens with an overall diameter of 200 mm are denoted by a specimen mark beginning with “2”, while the two specimens with an overall diameter of 300 mm are marked beginning with “3”. Only mildly decayed timber was used for this series of tests, and the presence of a timber core is denoted with “T” in the specimen mark. The specimen with a void core is denoted with “V” in the specimen mark.

The 200 mm diameter bending specimens included three “timber only” bending control piles and five repaired piles. The “timber only” bending control specimens marked 2C-T-1, 2C-T-2 and 2C-T-3 are shown in Figure 3.13. In order to examine the transition zone between the repaired and unrepaired zone of the piles, five of the timber piles were

trimmed and their diameter reduced to 100 mm over a 800 mm length as shown in Figure 3.14(a). The 800 mm long and 50 mm thick space was then filled with non-shrink cementitious grout. The specimens are shown in Figure 3.14(b) after grout injection. The GFRP wet-wrap system was then applied over a 1000 mm length which extended 200 mm over the untrimmed 200 mm diameter timber, as shown in Figure 3.14(c). Two layers of continuous GFRP wet-wrap fibers were applied in two orthogonal directions, axial, "A", and lateral, "L". The role of the lateral fibers around the circumference of the piles are to confine the grout, while the axial fibers are designed to carry flexural tension stresses. A longitudinal cross-section of these specimens used to examine the transition zone is shown in Figure 3.14(d).

In order to focus on the repair technique, the 300 mm diameter piles were repaired over the entire 1200 mm length of pile. The two specimens with an overall diameter of 300 mm are marked 3L-T and 3LA-V, and are shown in Figure 3.13. Pile specimen 3L-T consisted of a 200 mm diameter timber core and one layer of GFRP wrap fibers oriented laterally around the circumference of the pile. Pile specimen 3LA-V consisted of a 200 mm void core and two layers of GFRP wrap fibers in the two orthogonal directions, axial and lateral.

### ***3.4.3 Instrumentation for Bending Specimens***

Similar to the axial compression specimens, load, mid-span deflection and strain were the general parameters measured in the bending tests. In addition to the load cell and stroke measurements of the MTS machine, instruments used for the bending tests



included: electric resistance strain gauges, PI gauges and linear variable displacement transducers (LVDTs). Strain gauges and 100 mm PI gauges were used to measure the extreme fiber strain at the top and bottom of the specimen, while an LVDT was used to measure the deflection at mid-span. A schematic diagram of the instrumentation layout is shown in Figures 3.15(a) and (b).

The load cell, PI gauges and strain gauges were all connected to 32-channel data acquisition system, which was configured to receive data at every one second frequency for the duration of the test. In order to observe post-peak failure behaviour, when ever possible, reading was continued beyond the maximum load.

#### **3.4.4 Test Set-Up for Bending Specimens**

The test set-up used for the bending specimens is shown in Figures 3.16 and 3.17. A 1,000 kN closed loop MTS hydraulic testing machine was used for all bending tests. Testing was conducted under stroke control at a rate of 0.5 mm/minute. All beams were tested under three-point bending using a concentrated load at mid-span. A roller support was fastened to a concrete block base at each end of the specimen, as shown in Figure 3.16. The load from the testing machine was transferred to the round surface of the timber through a curved loading plate. Plaster pads were used to ensure uniform load distribution.

*Table 3.1: Physical Properties of Mbrace™ EG 900 E-glass Fiber Sheet*

Property	Uni-Directional Fibers
Ultimate Tensile Strength (MPa)	1730
Tensile Modulus (GPa)	72.4
Ultimate Tensile Strain	2%
Thickness (mm)	0.353

*Table 3.2: Physical Properties of QM 6408 Prefabricated GFRP Shell*

Property	Multi-Axial Fibers 0°, 90°, ±45°
Ultimate Tensile Strength (MPa) Primary Axis	434
Ultimate Tensile Strength (MPa) y – y Axis	324
Tensile Modulus (GPa) Primary Axis	25.9
Tensile Modulus (GPa) y - y Axis	16.3
Ultimate Tensile Strain	1.8%
Thickness (mm)	3.175

Table 3.3: Summary of 200 mm Overall Diameter Axial Compression Test specimens

Overall Diameter (mm)	GFRP Repair System	Timber or Core Condition	Timber or Void Diameter (mm)	Specimen Mark		
200	Control: Timber Only	Mild	200	2CT-M1		
				2CT-M2		
				2CT-M3		
				2CT-M4		
				2CT-H1		
		Heavy	200	2CT-H2		
				2CT-H3		
				2CT-H4		
				2CT-H5		
				2F1-M1		
	Single Layer GFRP Wet-Wrap	Mild	100	2F1-M2		
				2F1-M3		
				2F1-H1		
				Heavy	100	2F1-H2
						2F1-H3
		Void	100	2F1-V1		
				2F1-V2		
				2F1-V3		
		Bearing (Mild)	100/200	2F1-B1		
				2F1-B2		
	2F1-B3					
Improved Bearing (Mild)	100/200	2F1-SB1				
		2F1-SB2				
		2F1-SB3				

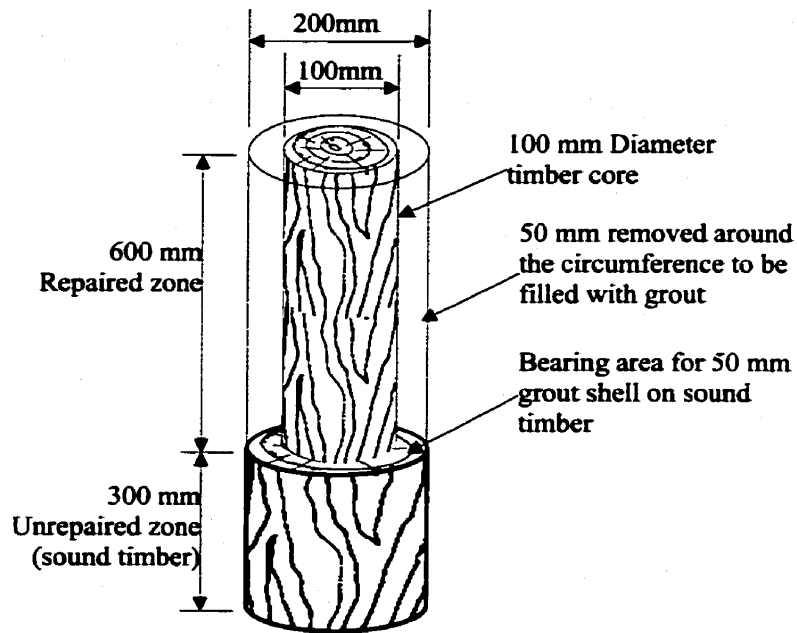
 Bearing Specimens

*Table 3.4: Summary of 300 mm Overall Diameter Axial Compression Test specimens*

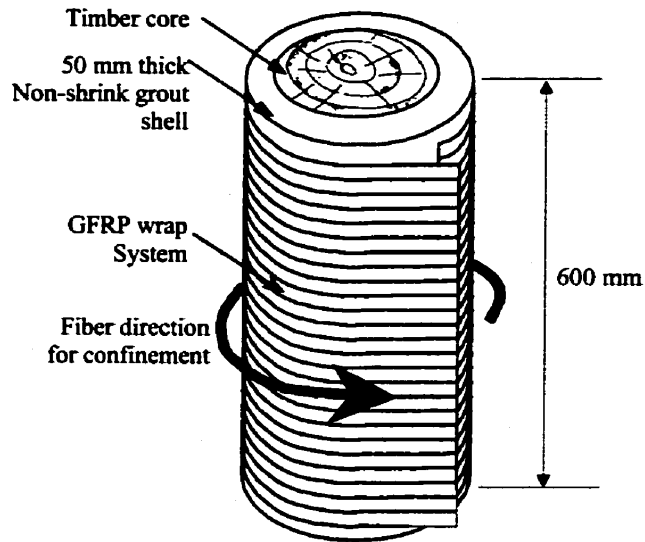
Overall Diameter (mm)	GFRP Repair System	Timber or Core Condition	Timber or Void Diameter (mm)	Specimen Mark
300	Control: Grout only	Mild	200	3CG-M1
				3CG-M2
	Single Layer	Mild	200	3F1-M1
				3F1-M2
				3F1-M3
	GFRP Wet-Wrap	Void	200	3F1-V1
				3F1-V2
				3F1-V3
	Double Layer	Mild	200	3F2-M1
				3F2-M2
				3F2-M3
	GFRP Wet-Wrap	Void	200	3F2-V1
				3F2-V2
				3F2-V3
	GFRP Shell	Mild	200	3FS-M1
3FS-M2				
Heavy		200	3FS-M3	
			3FS-H1	
			3FS-H2	

Table 3.5: Summary of Specimens Tested in Bending

Overall Diameter (mm)	GFRP Repair System	Timber or Core condition	Timber Diameter (mm)	Specimen Mark
200	Control			2C-T-1
	Timber	Mild	200	2C-T-2
	Only			2C-T-3
				2LA-T-1
	Lateral			2LA-T-2
	& Axial	Mild	100/200	2LA-T-3
	GFRP			2LA-T-4
				2LA-T-5
300	Lateral GFRP	Mild	200	3L-T
	Lat. & Axial	Void	200	3LA-V



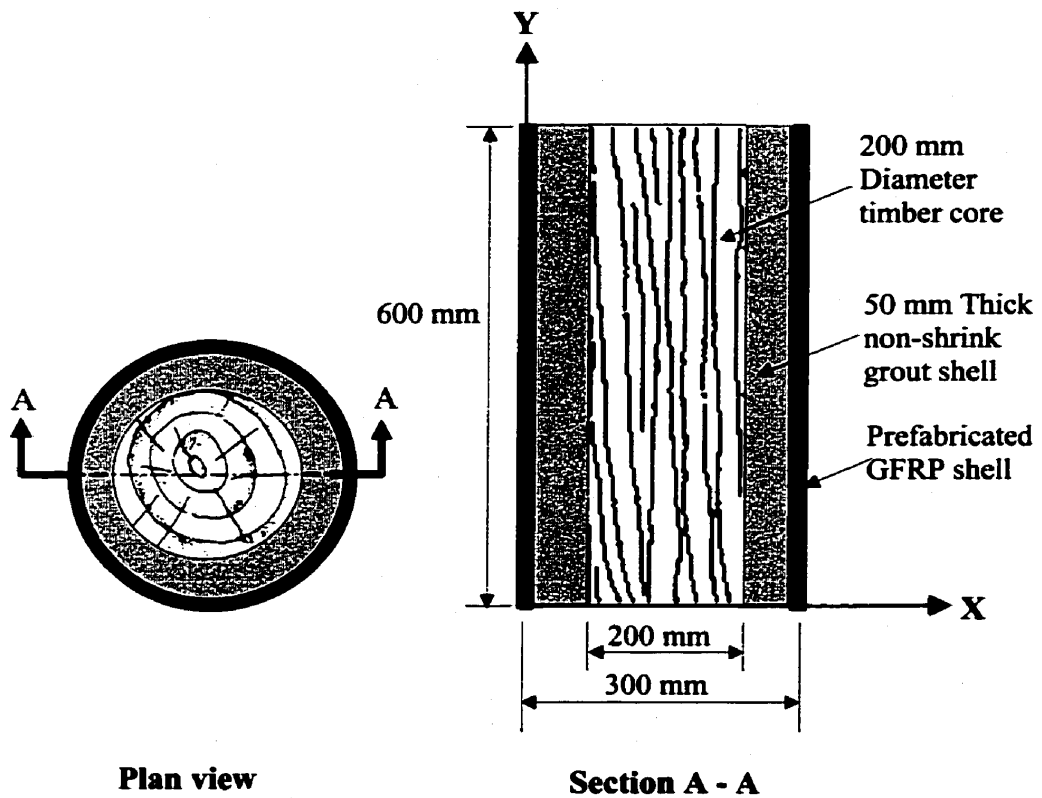
*Figure 3.1(a): Schematic of Bearing Specimens before Grout Injection and GFRP Wet-Wrap Application*



*Figure 3.1(b): Schematic of Repair Technique Using GFRP Wet-Wrap Sheets*



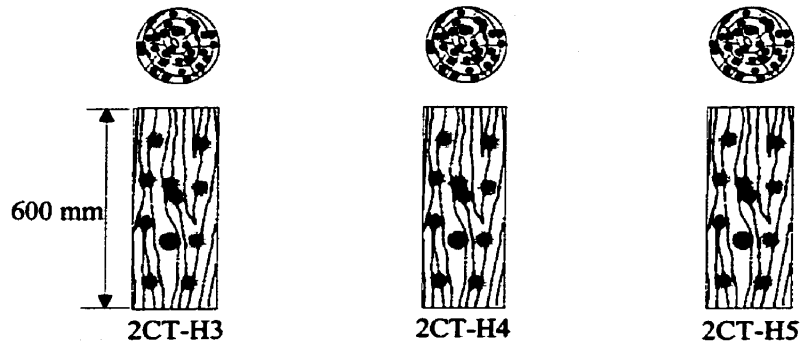
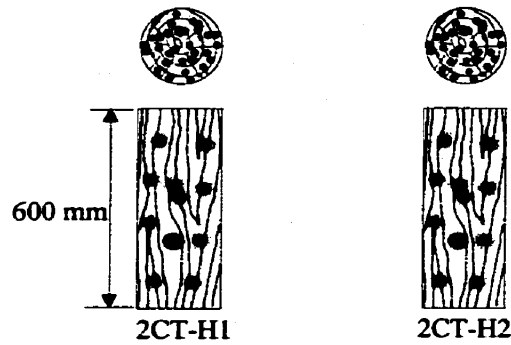
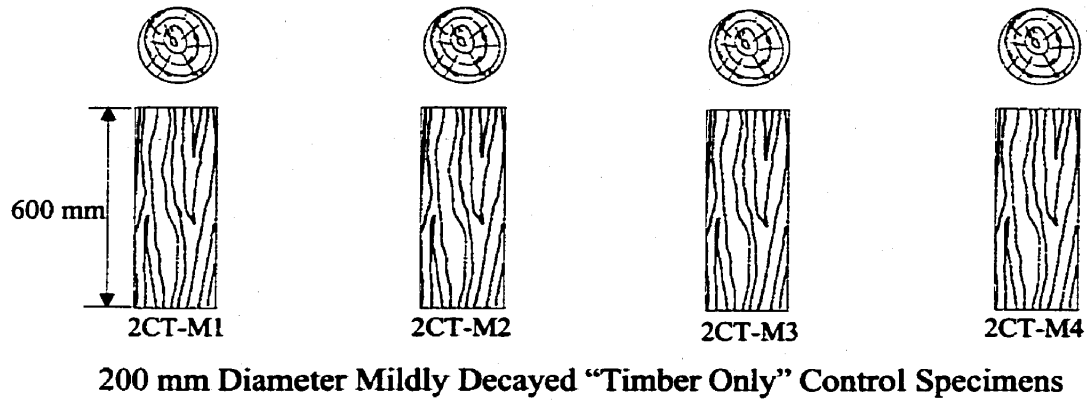
Figure 3.2(a): Prefabricated QM 6408 GFRP Shell



Plan view

Section A - A

Figure 3.2(b): Schematic of Repair Technique Using the Prefabricated GFRP Shell

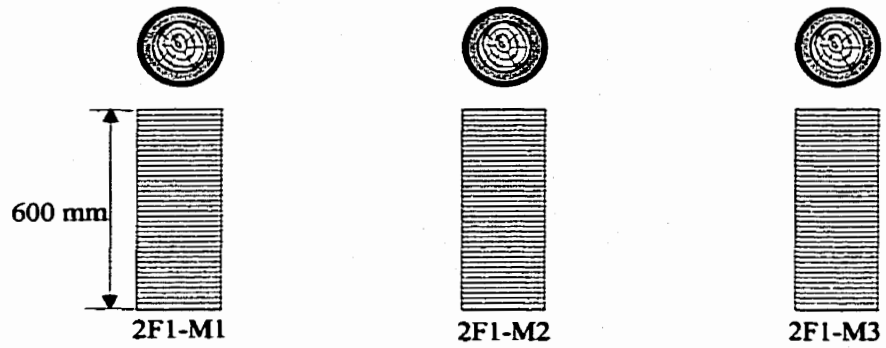


200 mm Diameter Heavily Decayed "Timber Only" Control Specimens

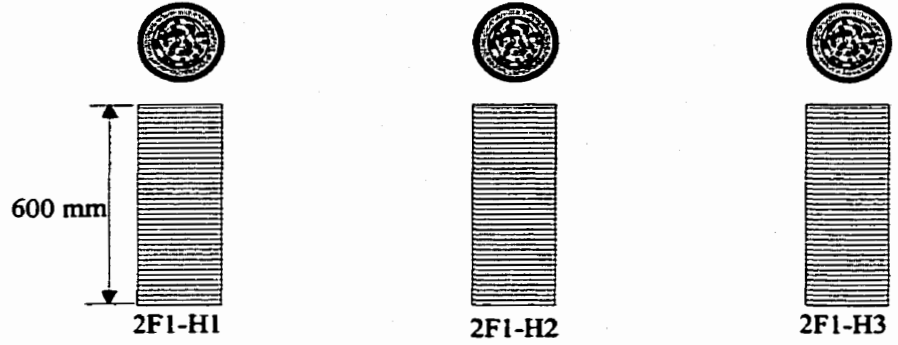
Figure 3.3: 200 mm Diameter "Timber Only" Control Specimens



200 mm Diameter Piles with 100 mm Diameter Mildly Decayed Timber Core



200 mm Diameter Piles with 100 mm Diameter Heavily Decayed Timber Core



200 mm Diameter Piles with 100 mm Diameter Void Core

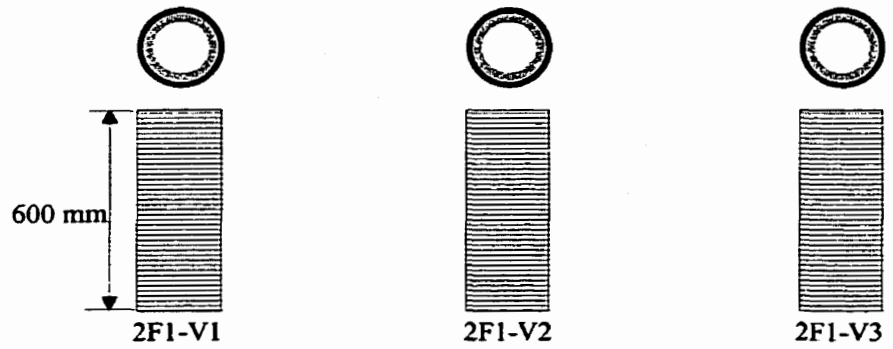
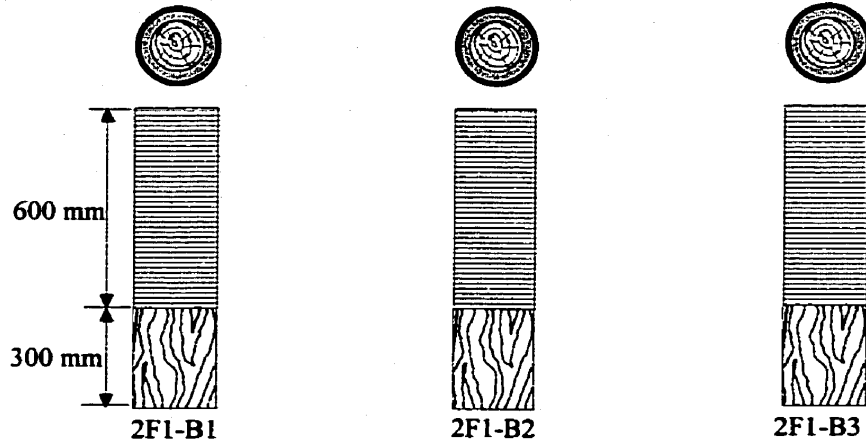


Figure 3.4: 200 mm Diameter Single Layer GFRP Wet-Wrap Specimens

200 mm Diameter Bearing Specimens



200 mm Diameter Specimens with Bearing Surface Strengthened

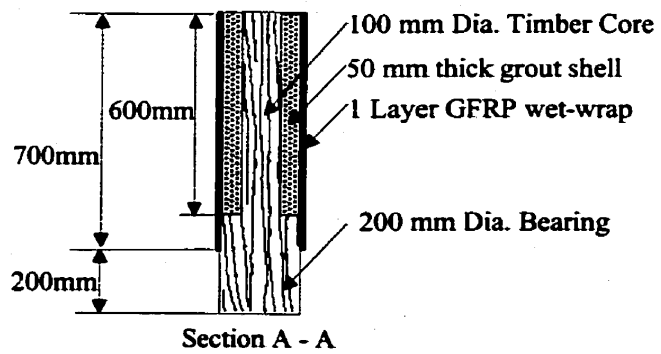
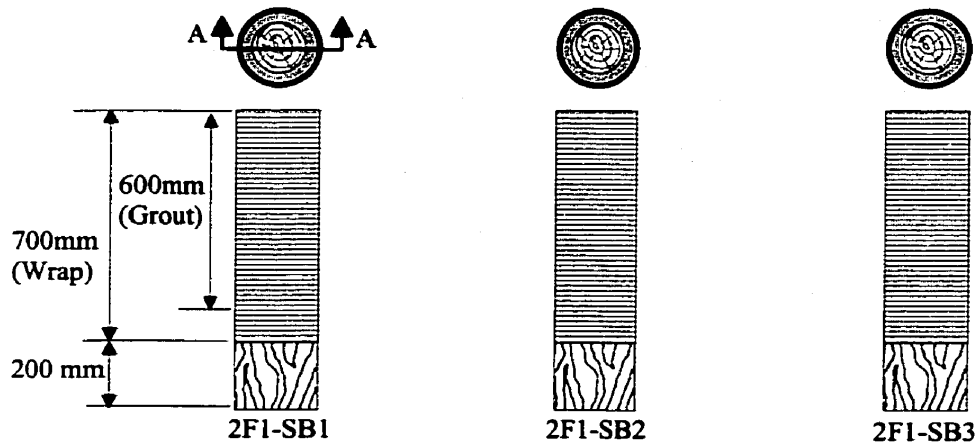


Figure 3.5: 200 mm Diameter Bearing Specimens

300 mm Diameter Piles with 200 mm Diameter  
Mildly Decayed Timber Core

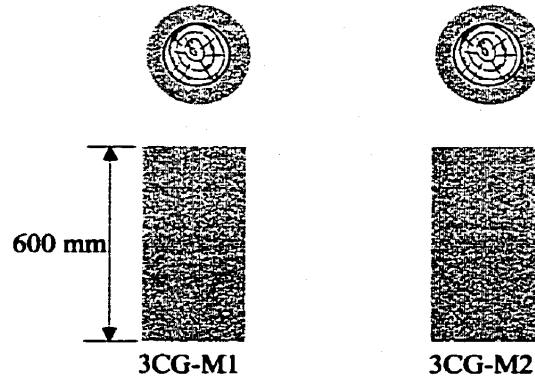
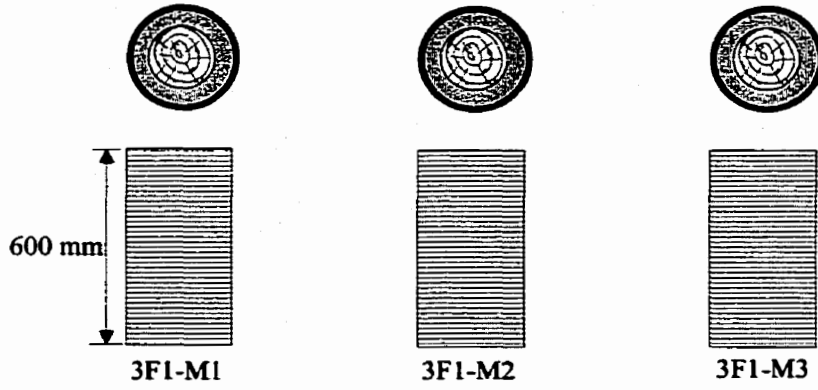


Figure 3.6: 300 mm Diameter "Grout Only" Control Specimens

300 mm Diameter Piles with 200 mm Diameter Mildly Decayed Timber Core



300 mm Diameter Piles with 200 mm Diameter Void Core

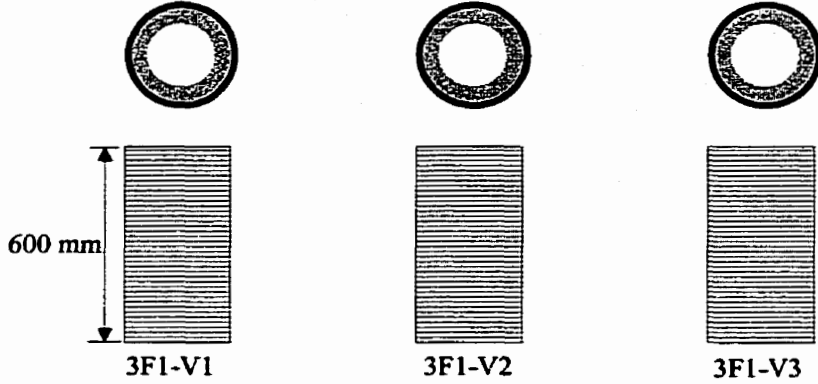
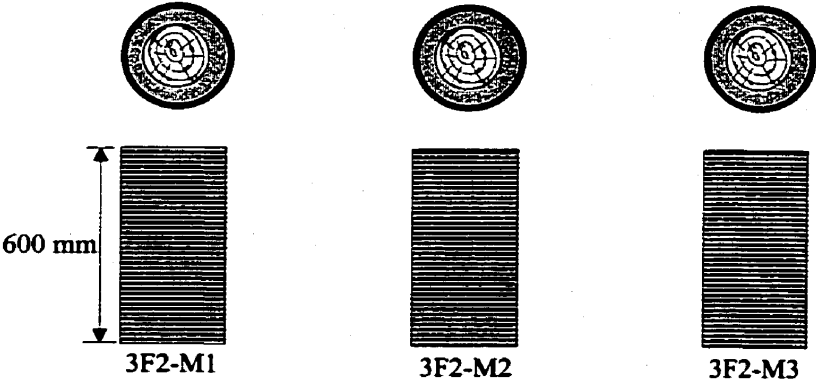


Figure 3.7: 300 mm Diameter Single Layer GFRP Wet-Wrap Specimens

300 mm Diameter Piles with 200 mm Diameter Mildly Decayed Timber Core



300 mm Diameter Piles with 200 mm Diameter Void Core

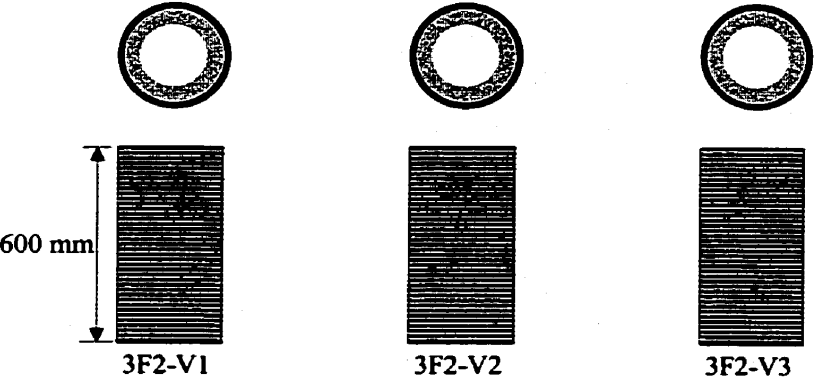
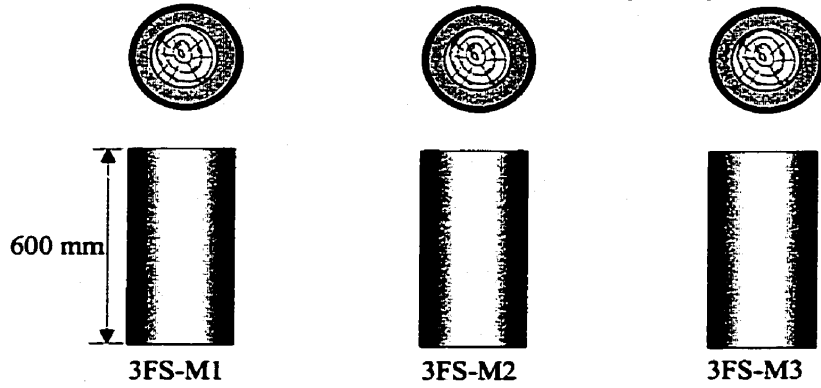


Figure 3.8: 300 mm Diameter Double Layer GFRP Wet-Wrap Specimens

300 mm Diameter Piles with 200 mm Diameter Mildly Decayed Timber Core



300 mm Diameter Piles with 200 mm Diameter Heavily Decayed Timber Core

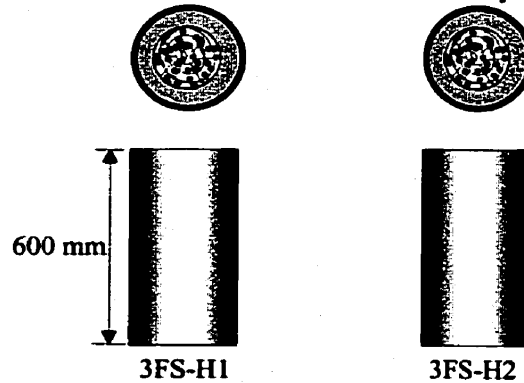


Figure 3.9: 300 mm Diameter Specimens Repaired Using Prefabricated GFRP Shell

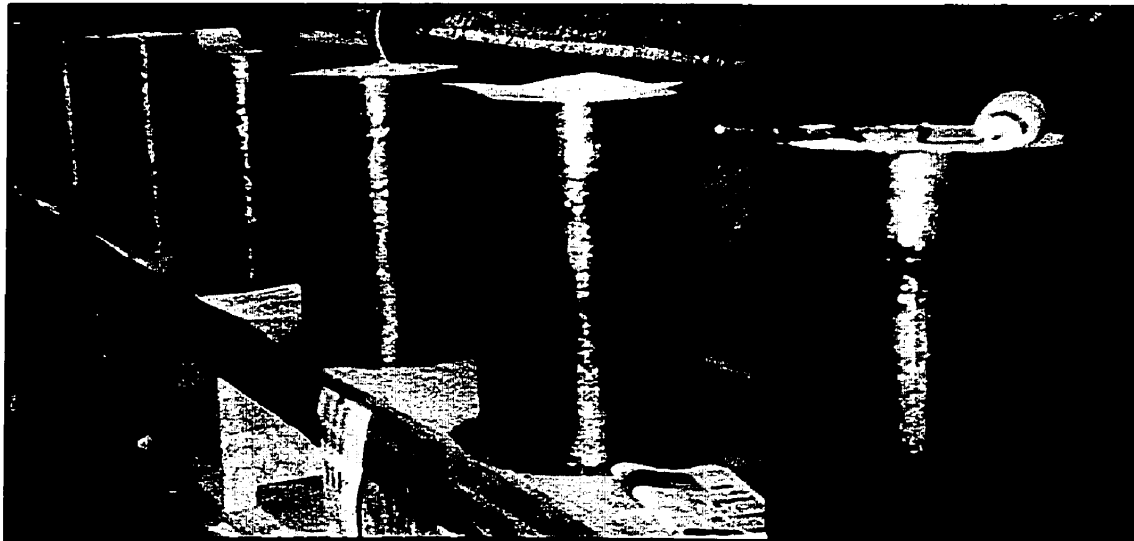
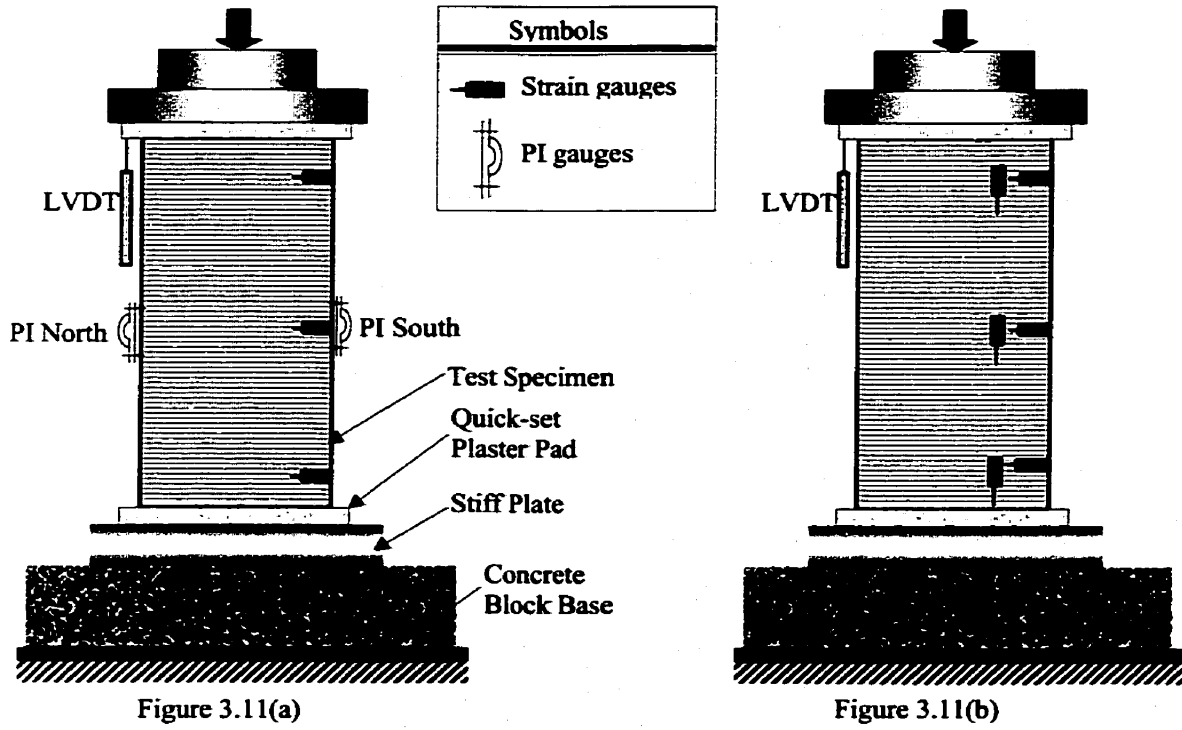


Figure 3.10: Axial Compression Specimens Fabricated Using the GFRP Wet-Wrap Technique



Figures 3.11(a) and (b): Schematic of Test Set-Up and Instrumentation Layout for Piles Tested in Axial Compression



Figure 3.12: Photo of Test Set-Up for Piles Tested in Axial Compression

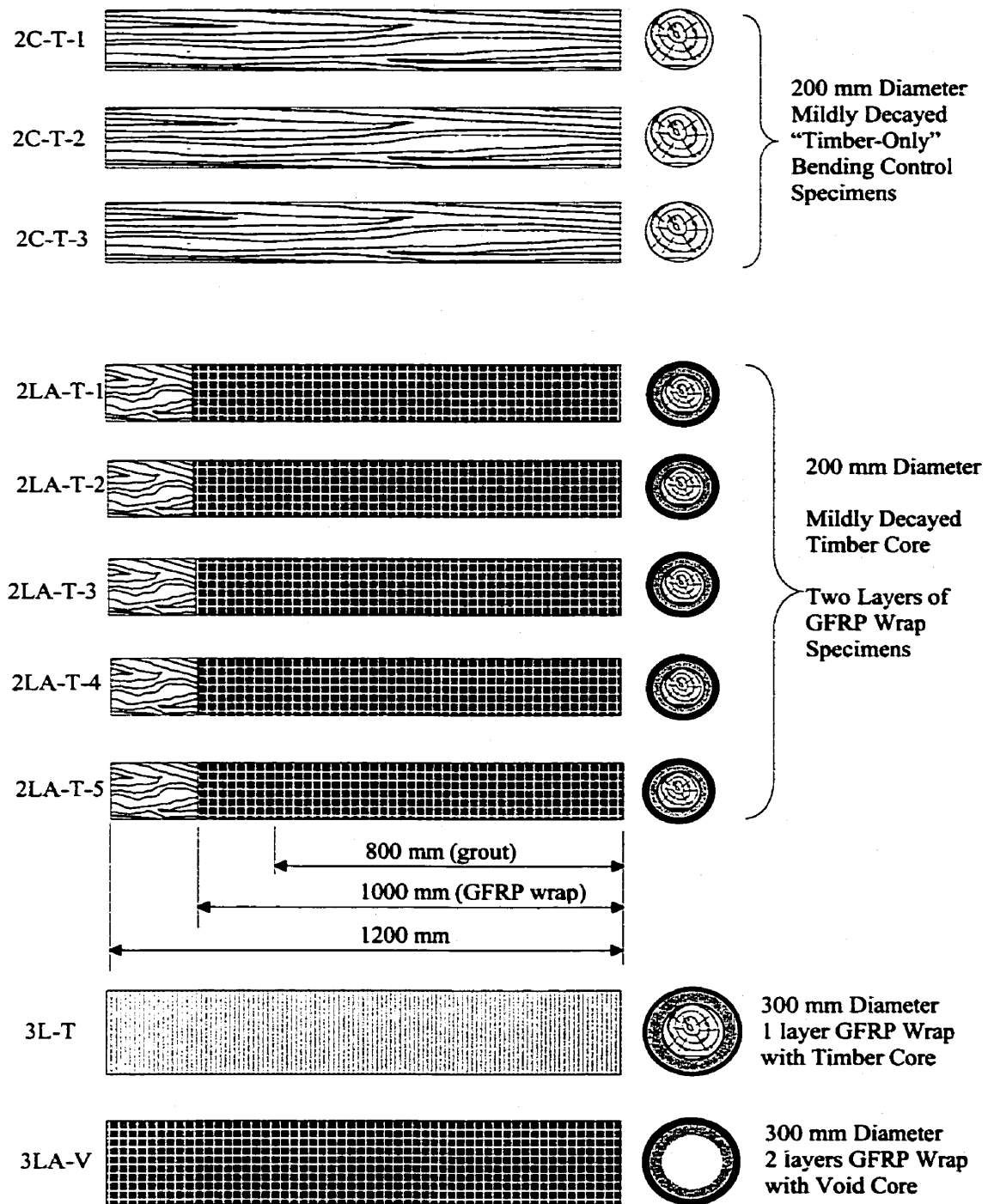


Figure 3.13: Bending Test Specimens



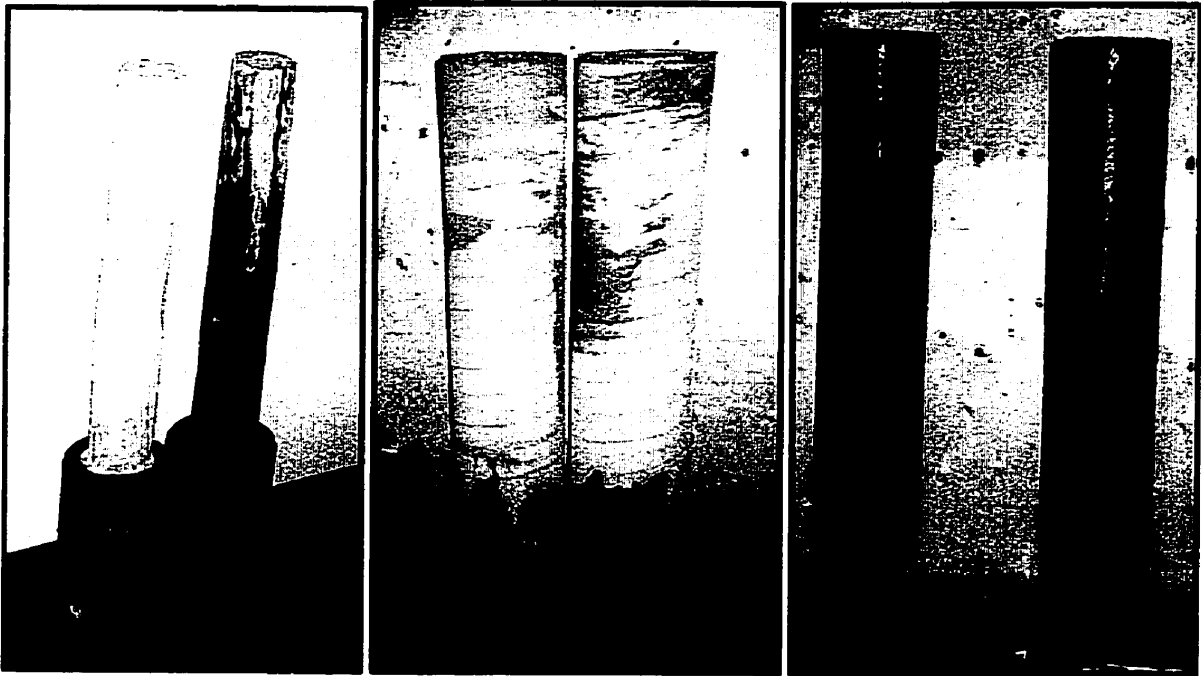


Figure 3.14(a)

Figure 3.14(b)

Figure 3.14(c)

Figure 3.14(a): Trimmed Timber Piles for Bending Test

Figure 3.14(b): Trimmed Timber Piles After Non-Shrink Cementitious Grout Injection

Figure 3.14(c): The Piles After Two Layers of GFRP Wet-Wrap System Application.

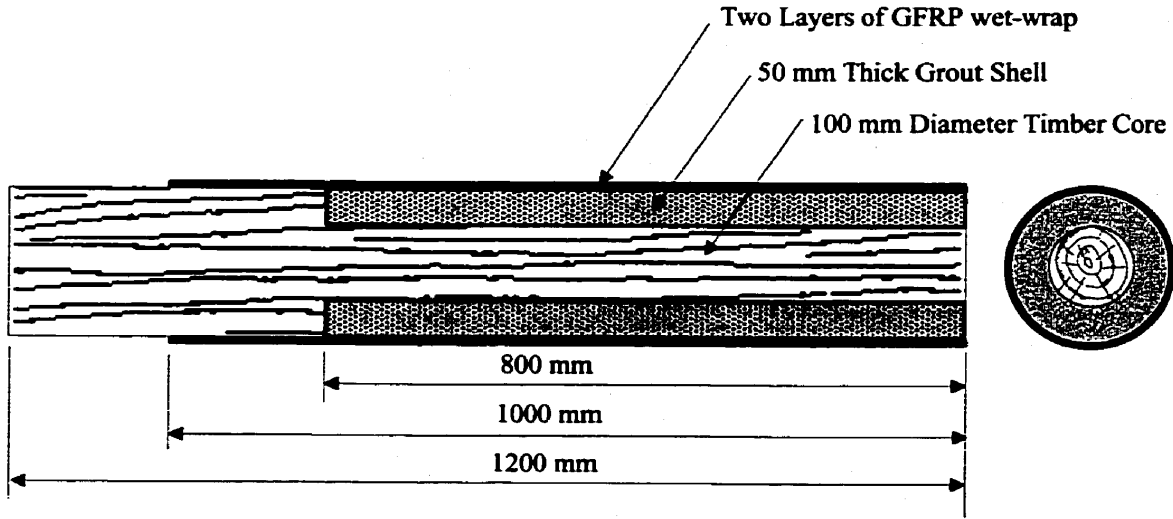


Figure 3.14(d): Longitudinal Cross-Section of Bending Specimens Examining the Transition Zone

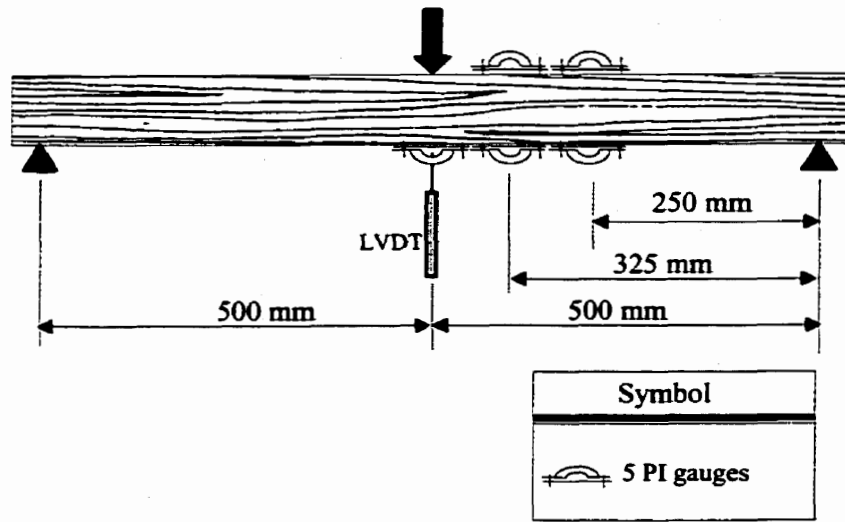


Figure 3.15(a): Instrumentation Layout for 200 mm "Timber Only" Bending Control Specimens Tested in Bending

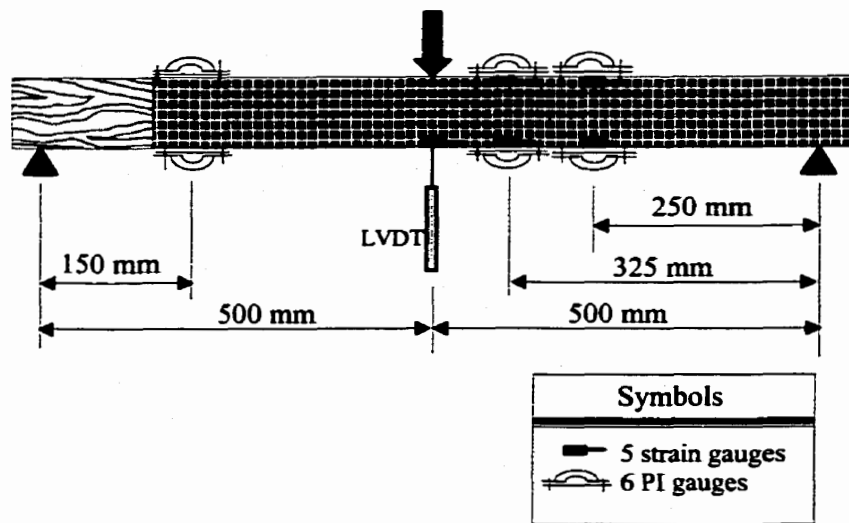
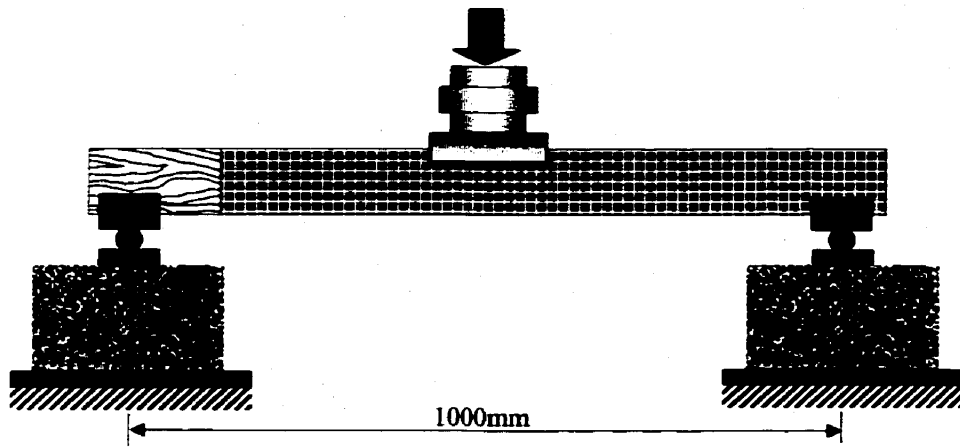


Figure 3.15(b): Instrumentation Layout for 200 mm Diameter Repaired Specimens Tested in Bending



*Figure 3.16: Schematic of Test Set-Up for Piles Tested in Bending*



*Figure 3.17: Photo of Test Set-Up for Piles Tested in Bending*

## **Chapter 4**

# **Test Results and Analysis: Axial Compression Series**

### **4.1 General**

Test results and analysis for the series of specimens tested in axial compression are presented and discussed in this chapter. A total of 43 pile specimens were tested in the Axial Compression Series, as described in Chapter 3. Table 4.1 provides a summary of test results and specimen parameters for the 24 pile specimens with an overall diameter of 200 mm, while Table 4.2 presents results for the 19 specimens with an overall diameter of 300 mm. A comparison of the ultimate load obtained for all 200 mm diameter piles is illustrated in Figure 4.1(b), while Figure 4.1(c) provides comparison of the ultimate load obtained for all of the 300 mm diameter piles.

## **4.2 Control Specimens**

Four 200 mm diameter unrepaired timber control piles with only mild decay were tested as control specimens. In addition, two 200 mm diameter timber piles encased in a 50 mm thick grout shell, but without confining GFRP, were also tested for control purposes. In order to examine the existing capacity of heavily decayed timber piles shipped directly from Inuvik, five 200 mm diameter heavily decayed timber control specimens were tested. Figure 4.1(a) illustrates the maximum and average loads for all of the control piles tested.

The load versus stroke curves for all four of the mildly decayed timber control piles tested are shown in Figure 4.2(a). As shown in Table 4.1, the mildly decayed timber control piles failed at an average ultimate load of 953 kN. However, due to the high variability in material properties inherent in larger timber members, the ultimate load-carrying capacity of each timber pile varies considerably from the average for the group. According to the published design values given in Chapter 2, the design strength of the 200 mm diameter control specimen is about 540 kN, which is significantly lower than the average strength obtained during testing.

Figures 4.3(a) and (b) show the timber control specimen 2CT-M1 after failure in cross-section and in elevation, respectively. The timber piles failed by splitting parallel to the grain. All four mildly decayed timber control specimens tested exhibited similar modes of failure.

The load versus stroke curves for the “grout only” control piles are shown in Figure 4.2(b). Since the grout shell was not confined with a GFRP system, the grout was not expected to develop its full capacity. Consequently, as reported in Table 4.2, the unconfined “grout only” specimens failed at an average ultimate load of 958 kN which is comparable to the mildly decayed “timber only” control piles at failure. It should be noted that the overall diameter of the “timber only” control specimens was only 200 mm compared with an overall diameter of 300 mm for the “grout only” specimens as shown in Figure 4.1(a).

The “grout only” piles suffered from excessive lateral expansion due to the applied axial load, and the grout shell failed just prior to failure in the timber core. The grout shell cracked vertically and separated from the timber as shown in Figure 4.4(a). Crushing of the top surface of the grout shell was also observed at failure. It should be noted that for one specimen, a continuous vertical crack was observed in the grout shell after curing and prior to testing, as shown in Figure 4.4(b).

The five timber piles shipped directly from Inuvik were severely decayed. As shown in Figure 4.1(a), the high level of decay resulted in an average maximum load of only 184 kN which is significantly lower than the average maximum load of 953 kN obtained for the mildly decayed timber control specimens. In order to avoid causing significant damage to the heavily decayed timber control specimens which were to be repaired and re-tested, the control tests were terminated when no further increase in load could be achieved, but prior to complete failure. The variation in maximum load was even greater

for the heavily decayed timber control piles, as shown in Figure 4.1(a). This large variation in load-carrying capacity is attributed to the different levels of heavy decay present in the individual timber piles included in this group.

### **4.3 Piles with a Single Layer of GFRP Wet-Wrap and Various Levels of Core Decay**

In order to determine the effect of various levels of timber core decay on the capacity of the repaired piles, nine 600 mm long piles were repaired using a single layer of GFRP wrap and tested to failure. The three pile specimens marked 2F1-M1, 2F1-M2 and 2F2-M3 consisted of a 100 mm diameter mildly decayed timber core encased in a 50 mm thick grout shell and wrapped with a single layer of GFRP wrap. These piles, with an overall diameter of 200 mm, can be compared to the group of piles marked 2F1-H1, 2F1-H2 and 2F1-H3, which have identical specimen parameters except for the heavy decay present in the 100 mm diameter timber core. In order to simulate the worst possible case of complete timber deterioration, another group of specimens marked 2F1-V1, 2F1-V2 and 2F1-V3 were tested with identical specimen parameters, but with a 100 mm diameter void core rather than a timber core. Test results for all three types of specimens are summarized in Figure 4.1(b).

Since the “timber only” control specimens discussed in the previous section are all 200 mm in diameter, the maximum loads obtained can be directly compared to those for the 200 mm diameter GFRP wet-wrap repaired piles. For the 200 mm diameter specimens repaired with a single layer of GFRP wrap, the highest average ultimate load was obtained for the piles with a 100 mm diameter void core as shown in Table 4.1. Specimens 2F1-V1, 2F1-V2 and 2F1-V3 failed at an average ultimate load of 1214 kN, while the average ultimate load for the piles with a heavily decayed timber core was only 1003 kN. The reduced load-carrying capacity for the piles with a heavily decayed



timber core, marked 2F1-H1, 2F1-H2 and 2F1-H3, is attributed to the lower grout strength used for this group of piles, when compared to the piles with a void core. The grout strength for each type of specimen is based on cylinder tests and is given in Tables 4.1 and 4.2.

The load versus stroke curves for the piles with a void core and heavily decayed timber core are shown in Figures 4.5(c) and 4.5(b) respectively. As shown in Figure 4.1(b), the confining GFRP wrap increased the load-carrying capacity of the piles and reduced the standard deviation and variation in capacity between similar piles, when compared to results for the group of control piles.

Pile specimens 2F1-M1, 2F1-M2 and 2F1-M3, with a mildly decayed timber core, exhibited the lowest average ultimate load-carrying capacity of only 857 kN. The reduced strength of these piles could be due to the lower grout strength used, as well as the fact that these piles had been previously tested as 900 mm long load bearing specimens with the damaged bearing zone removed prior to re-testing. In general, the behaviour of these three re-tested specimens is not consistent with the general trends observed for all of the other specimens tested in this experimental program. Therefore, it is assumed that damage not visible on the exterior of the piles occurred during the bearing tests and that this damage may render the results of the re-testing unreliable. The load versus stroke curves for the piles with a mildly decay timber core are shown in Figure 4.5(a).

The typical failure mode for the piles repaired using a single layer of GFRP wrap was localized rupture of the GFRP wrap within the top or bottom 50 mm to 100 mm of the piles. For one of the piles tested with a void core, rupture of the GFRP wrap was distributed over a longer length of the pile as shown in Figure 4.7.

#### **4.4 Bearing Specimens Examining Load Transfer**

In order to examine the effectiveness of load transfer between the repaired portion of the pile and the sound timber below, six 900 mm long bearing specimens were tested. All of the 900 mm long bearing specimens consisted of a 600 mm long repaired zone and a 300 mm long zone of unrepaired sound timber below the repaired zone. A single layer of GFRP wrap was used as confinement for all of the bearing specimens.

The load versus stroke curves for the bearing specimens marked 2F1-B1, 2F1-B2, and 2F1-B3 are shown in Figure 4.6(a). These piles reached an average maximum load of only 652 kN which was only 68% of the average ultimate load obtained for the “timber only” control piles. Failure consistently occurred due to bearing in the unrepaired zone, leaving the repaired zone above relatively undamaged.

For the three bearing specimens marked 2F1-SB1, 2F1-SB2 and 2F1-SB3 the bearing area was strengthened during fabrication as described in Chapter 3. As reported in Table 4.1, the strengthened bearing specimens failed at an average maximum load of 956 kN, which is comparable to the average of 953 kN obtained for the mildly decayed timber control piles. However, even with the bearing area strengthened, these piles exhibited bearing failure in the timber below the repaired zone. Figure 4.8 shows the typical failure mode observed for the piles with a strengthened bearing area. As can be seen in Figure 4.8, the repaired zone typically remained intact after bearing failure occurred. Therefore, it is suggested that more efficient and effective methods of strengthening the bearing surface be examined in future experimental work.

During testing of specimens 2F1-SB1, 2F1-SB2 and 2F1-SB3, it was also observed that the Impel Boron sterilization had no short term effect on these piles.

## **4.5 Effect of Different GFRP Configurations**

### **4.5.1 General**

In order to compare the effect of different GFRP configurations on the capacity of the repaired piles, seventeen 600 mm long piles with an overall diameter of 300 mm were tested using three different GFRP configurations. Six of the 300 mm diameter piles were repaired with a single layer of GFRP sheets, six piles were repaired with a double layer of GFRP sheets, and prefabricated GFRP shells were used for the remaining five pile specimens. For each different GFRP configuration, three piles were tested with a mildly decayed 200 mm diameter timber core. The remaining piles in each group were tested with a void core, except for the piles with a GFRP shell where heavily decayed timber was used for the remaining two specimens. Test results for all of the 300 mm diameter piles with three different GFRP configurations are summarized in Figure 4.1(c).

### **4.5.2 Piles with a Single Layer of GFRP Wet-Wrap**

The load versus stroke curves for the specimens with a single layer GFRP wrap and a mildly decayed timber core are shown in Figure 4.9(a). The average ultimate load-carrying capacity obtained for these specimens was 1392 kN, as reported in Table 4.2. A comparison of test results for the control piles with unconfined grout indicates that the ultimate load was 45% higher for the specimens confined with a single layer of GFRP as shown in Figure 4.1(b). In addition, a comparison of load versus stroke curves indicates

that, the piles with a single layer of confining GFRP exhibit an increase in ductility reduced variability in load-carrying capacity for similar piles.

The load versus stroke curves for the piles with a single layer of GFRP wrap and a void core are shown in Figure 4.5(b). The average ultimate load-carrying capacity for these piles was 1313 kN as reported in Table 4.2. The capacity of the piles with a void core was only 94% of that obtained for the piles with a mildly decayed timber core, which suggests that the timer core does carry at least a portion of the load or serve to improve the confinement of the grout shell.

The typical mode of failure for the 300 mm diameter piles with a single layer of GFRP wrap was similar to that observed for the 200 mm diameter piles. The piles failed due to rupture of the GFRP wrap within the outer 50 to 100 mm length of the pile, followed by crushing of the grout shell as shown in Figures 4.12(a) and (b).

### ***4.5.3 Piles with a Double Layer of GFRP Wet-Wrap***

The load versus stroke curves for the specimens with two layers of GFRP Wrap and a mildly decayed timber core are shown in Figure 4.10(a). The average ultimate load-carrying capacity for these piles is 2585 kN, as shown in Table 4.2. The piles repaired with a double layer of GFRP wrap achieved the highest average ultimate load for all of the specimens tested in this experimental program. A comparison of load-carrying capacity for the piles with a single and double layers of GFRP wrap and with a mildly decayed timber core, indicates an increase of 86% for the doubly wrapped specimens.

Although an increase in pile capacity was observed with an increase in GFRP fiber content, it is not expected that adding further layers will continue to increase the load-carrying capacity proportionally. Even with increased GFRP fiber content, the capacity will eventually be limited by the strength of the confined grout.

The load versus stroke curves for the specimens with a double layer of GFRP wrap and a void core are shown in Figure 4.10(b). The average ultimate load-carrying capacity for these piles was 1617 kN, as shown in Table 4.2. Again, the capacity was not as high as that obtained for the piles with a timber core and two layers of GFRP. However, when compared to the piles with a single layer of GFRP and a void core, the addition of a second layer of GFRP does increase the capacity of 300 mm diameter piles with a void core by 23%.

For the specimens with a double layer of GFRP wrap, rupture in the GFRP was distributed over a longer length of pile and was followed by crushing of the grout shell, as shown in Figures 4.13(a), (b) and 4.14. Some debonding between the layers of GFRP within the 200 mm long lap length was also observed for a few of these higher capacity piles. It was observed that a thin layer of grout remained bonded to the inner layer of the GFRP wrap after failure

#### **4.5.4 Piles with a Prefabricated GFRP Shell**

The load versus stroke curves for the piles repaired using a prefabricated GFRP shell and with a mildly decayed timber core are shown in Figure 4.11(a). The average ultimate

load-carrying capacity obtained for these piles was 1886 kN, as reported in Table 4.2. A comparison of test results for the piles repaired with a GFRP shell and the “grout only” control specimens, indicates that an increase of 97% was obtained for the piles confined with the GFRP shells. A comparison of the piles with a single layer of GFRP sheet, 3F1-M1, 3F1-M2 and 3F1-M3, and the piles with a GFRP shell, 3FS-M1, 3FS-M2 and 3FS-M3, suggests that the confinement provided by the GFRP shell results in a higher load-carrying capacity. This difference in ultimate capacity is attributed to the different material characteristics of the glass fiber wrap in comparison to the prefabricated GFRP shell, as described in detail in Chapter 3. For the GFRP wrap system, the glass fibers are unidirectional and oriented in the horizontal (hoop) direction, while the prefabricated GFRP shells consist of fibers oriented in multi-axial directions. Furthermore, the prefabricated GFRP shells contain a higher volume of fibers.

The load versus stroke curves for the piles repaired with a prefabricated GFRP shell and with a heavily decayed timber core are shown in Figure 4.11(b). The ultimate load-carrying capacity for these piles was 898 kN, as reported in Table 4.2. The low average ultimate load-carrying capacity may be due to the fact that these piles were re-tested.

Figure 4.15 shows the typical failure mode observed for specimens repaired using the prefabricated GFRP shells. Rupture of the GFRP fibers was initiated at the top or bottom of the pile and propagated toward mid-height of the pile. Bulging of the shell around mid-height of the piles was also observed.



## **4.6 Analysis of Axial and Lateral Strain Behaviour**

The load versus strain curves obtained for the specimens with a single layer of GFRP wrap and a void core, 2F1-V1, 2F1-V2 and 2F1-V3, are shown in Figures 4.16(a), (b) and (c) respectively. In addition, load versus strain curves for the 300 mm diameter pile specimens, with a single layer of GFRP wrap and a mildly decayed timber core, 3F1-M1, 3F1-M2 and 3F1-M3, are shown in Figures 4.17(a), (b) and (c) respectively. Load versus strain curves for the other specimens tested in this experimental program are provided in Appendix A. On the left side of the load versus strain diagrams, the axial load is plotted as a function of axial strain, while on the right side, axial load is expressed as a function of the lateral or hoop strain. The instrumentation layout for piles 2F1-V1, 2F1-V2 and 2F1-V3 is shown in Figure 3.11(a), while Figure 3.11(b) shows the instrumentation layout for piles 3F1-M1, 3F1-M2 and 3F1-M3.

At an early stage of loading, the vertical and lateral or hoop strain curves are linearly proportional to the applied load as shown in Figures 4.16 and 4.17. As the load increases to approximately 50% of maximum load, increased cracking in the grout results in a rapid increase in lateral strain with a relatively small increment in axial load. As discussed in Chapter 2, the GFRP wrap is activated at this stage, and begins to restrain the rapid lateral expansion. Therefore, the response beyond this point is dependent on the stiffness of the GFRP wrap.

As described previously, failure is typically initiated by sudden rupture of the GFRP system. After failure occurs in the GFRP, the now unconfined grout shell is unable to withstand the applied load at stress levels near the maximum unconfined strength of the grout,  $f'_g$ .

As shown in Figures 4.16 and 4.17, the measured strains were typically highest at the top or bottom of the pile specimens. As discussed earlier, the typical failure mode was localized rupture of the GFRP wrap within the top or bottom 50 mm to 100 mm of the piles. The maximum strains measured in the GFRP sheets ranged from 2 to 6 millistrain, which is significantly lower than the rupture strain of 18 to 20 millistrain reported by the manufacturers. Although the low strain readings may be in part attributed to the use of localized electric resistance strain gauges with only a 5 mm gauge length, similarly lower strain readings were also reported by Fam (2000) and Picher et al (1996).

Picher, Rochette and Labossiere (1996) performed axial compression tests on three 152x304 mm solid concrete cylinders confined by CFRP. The CFRP sheets consisted of three 0.3 mm thick layers, each with a tensile strength of 1266 MPa, and wrapped around the circumference of the cylinders. Although the ultimate tensile strain of the sheets in the hoop direction was reported to be 15 millistrain, average strains of only 8.4 millistrain were recorded at failure.

The behaviour of load versus axial and lateral strain of GFRP tubes totally and partially filled with concrete was examined by Fam (2000). Although some of the totally filled

tubes exhibited strains as high as 11 millistrain at failure, the partially filled tubes failed with strains in the range of 2.5 to 6 millistrain. Fam reported that as the void core size decreased, the strain readings at failure increased. Therefore, the lower strain readings observed at failure in this experimental program may also be attributed to presence of the void or timber core.

## 4.7 Effect of Confinement on Compressive Strength

As shown in the previous sections, the axial capacity of the repaired piles is enhanced by confining the grout shell against lateral expansion using a GFRP jacket or wrap. As discussed in Chapter 2, the axial capacity of confined concrete or cementitious grout is related to the lateral confining stress provided by GFRP jackets or wrap, and may be predicted using the relationship proposed by Mander et al (1988).

$$f'_{cg} = f'_g \left[ 2.254 \sqrt{1 + \frac{7.94 f_{cp}}{f'_g} - \frac{2 f_{cp}}{f'_g}} - 1.254 \right] \quad (4.1)$$

Where,

$f'_{cg}$  = compressive strength of the confined concrete or grout

$f'_g$  = compressive strength of the unconfined concrete or grout

$f_{cp}$  = lateral confining stress provided by the GFRP jacket or wrap

The lateral confining stress,  $f_{cp}$ , can be computed from the following relationship:

$$f_{cp} = \frac{2 f_f t_f}{D} \quad (4.2)$$

Where,

$D$  = diameter of the confined core

$f_f$  = strength of the GFRP jacket or wrap in hoop direction

$t_f$  = thickness of the GFRP jacket or wrap

The lateral confining stress is often reduced by a factor,  $k$ , to account for the possibility of imperfect bond between the GFRP system and the core surface, as well as any

localized debonding that may result in incompatibility between the lateral strain in the core and the confining GFRP. A general reduction factor of 0.75 – 0.95 is recommended by various publications such as ISIS-M05-00 and the Mbrace™ manufacturer, Master Builders Inc. A reduction factor of 0.95 is recommended by CSA (CSA-S806-00). A reduction factor of 0.85 was assumed in order to predict the lateral confining stresses in this experimental program.

It is recognized that the Mander model is based on test data for solid circular concrete sections and may not be directly applicable to solid circular grout columns, without some modification based on test data. In addition, the presence of a timber or void core rather than a solid circular grout cross-section may also reduce the applicability of the model. However, as a first step is assessing the applicability of this model, the model is used without modification to predict the strength of the confined grout in this experimental program. Additional testing may be required to properly calibrate or modify the model, as will be discussed later.

The unconfined compressive strength of the grout used in this experimental program,  $f'_g$ , was determined using standard 100 mm diameter cylinders, and is provided in Tables 4.3 and 4.4. In these tables, the unconfined compressive strength is compared to the confined compressive strength of the grout,  $f'_{cg}$ , as predicted using Equations 4.1 and 4.2. Also provided in Tables 4.3 and 4.4, is the maximum stress in the grout shell during testing if the maximum applied load is assumed to be carried by the

grout shell only. This assumed maximum grout stress,  $\sigma_g$ , was calculated by dividing the maximum applied load by the area of the grout shell.

This conservative assumption, that the load is carried by the grout shell only, is used to simplify the analysis and to facilitate a comparison of the unconfined grout strength,  $f'_g$ , and the upper bound confined grout strength,  $\sigma_g$ , obtained during testing. Although the behaviour of the bearing specimens does suggest that a significant portion of the load is carried by the grout shell only, the possibility of load sharing between the grout and timber core is discussed in more detail in Section 4.9.

For most pile specimens, the assumed maximum stress in the grout shell,  $\sigma_g$ , calculated based on test results, was found to be even lower than the compressive strength of the unconfined grout,  $f'_g$ , as determined by the standard cylinder tests. However, for the piles with a higher degree of confinement, piles 3F2-M1, 3F2-M2, and 3F2-M3, with a double layer of GFRP wrap, and piles 3FS-M1, 3FS-M2, and 3FS-M3, with the prefabricated GFRP shells, the assumed maximum grout stress,  $\sigma_g$ , did exceed the compressive strength of the unconfined grout,  $f'_g$ .

A comparison of the maximum grout stress achieved for the 300 mm diameter piles with a mildly decayed timber core and various levels of confinement, indicates that only the double layer of GFRP wrap and the GFRP shells provided enough confinement for the grout stress,  $\sigma_g$ , to exceed the unconfined grout strength,  $f'_g$ , by 20 %. For piles 3F1-M1, 3F1-M2, and 3F1-M3, with similar parameters, but only a single layer of GFRP wrap,

the ratio of maximum grout stress to unconfined grout strength,  $\sigma_g/f'_g$ , was only 0.85. Those 300 mm piles with similar parameters, but with a void core, exhibited even lower ratios of 0.76 for the piles with a double layer of GFRP wrap and 0.61 for the piles with a single layer of GFRP wrap.

None of the specimens tested in this experimental program reached the confined grout strength,  $f'_{cg}$ , predicted using the unmodified Mander model. As mentioned previously, the model is unconservative for two reasons, the use of grout rather than concrete, and the presence of a void or timber core. With the specimen parameters used in this experimental program, it is not possible to separate the two effects in order to calibrate or modify the model. However, a sufficient number of different specimen parameters were used in order to provide a qualitative assessment of the effect of the void or timber core on the confinement, as will be discussed in the next section.

It is expected that the effect of using grout rather than concrete would be a reduction in the increased compressive strength normally provided by lateral confinement. The surface of the cracks which occur in grout are smoother than those occurring in concrete containing strong aggregates. The rough crack surface in concrete may contribute to a larger lateral expansion and Poisson effect, and therefore a greater confining effect, than that which can be achieved with grout. In order to modify Mander's model for use with grout rather than concrete, tests on confined solid grout cylinders should be conducted, and the possible correlation between Poisson's Ratio and the effect of confinement should be investigated in detail.

It should also be noted that when applying Mander's model, the full strength of the FRP system,  $f_f$  was used to predict the confined grout strength,  $f'_{cg}$ . However, as mentioned in Section 4.6, the strain in the FRP at failure was much lower than the rupture strain. The use of a reduced FRP strength at failure is one possible approach to modifying the Mander model which would require calibration through further testing.



## **4.8 Effect of Core Size and Condition on Efficiency of Confinement**

As discussed in the previous section, the ratio of maximum grout stress to unconfined grout strength,  $\sigma_g/f_g$ , was consistently lower for the 300 mm diameter piles with a 200 mm diameter void core when compared to similar specimens with a 200 mm diameter mildly decayed timber core. This observation suggests that the timber core contributes to the efficiency of the external confinement to some degree. As mentioned in Chapter 2, a similar trend was observed by Fam (2000) in an experimental study of concrete filled FRP tubes with a void core and with and without an inner FRP tube.

For the piles with an overall diameter of 200 mm and a core diameter of only 100 mm, the ratio of maximum grout stress to unconfined grout strength,  $\sigma_g/f_g$ , was 1.05 for the specimens with a heavily decayed timber core and 0.96 for the specimens with a void core. The condition of the core appears to have less effect on the efficiency of the confinement for these specimens with a smaller core diameter. In addition, these 200 mm diameter piles were confined with only one layer of GFRP wrap, and exhibit larger  $\sigma_g/f_g$  ratios than the 300 mm diameter piles with a single layer of GFRP wrap. These results suggest that there is a reduction in the efficiency of confinement with an increase in timber or void core size, which is in agreement with the observations made by Fam (2000) and discussed in Chapter 2. It also follows, that the condition of the core has a greater influence on the confinement for those specimens with a larger core.

Although general trends in the effect of core size and condition on the efficiency of confinement have been observed in this experimental program, further testing is required in order to quantify the effect of the core size on the maximum stress that can be achieved in the grout.

## **4.9 Recommended Design Approach**

The main objectives of this experimental program are to identify general trends in the behaviour of the repaired piles and the effect of various parameters, to determine the optimum combination of parameters for use in the field, and to develop a simplified design approach, which may be refined with further research. In the previous sections, the applicability of the Mander model for predicting the strength of the confined grout was considered, and recommendations for modifying the model based on further experimental investigation were made. In this section, a more simplified design approach is suggested, based on the experimental observations and data available to date.

In the previous sections, it was observed that the presence of a sound timber core enhances the confinement provided by the external FRP system. It was also suggested previously, that the sound timber core may also contribute to the axial capacity of the pile by directly carrying a portion of the axial load applied to the pile. However, the bearing failure observed in the sound timber below the grout shell, for both groups of bearing specimens, suggests that a greater proportion of the load is carried by the stiff grout shell.

The proportion of the total axial load,  $P_{total}$ , carried by the timber core,  $P_T$ , and by the grout shell,  $P_g$ , can be predicted by assuming equivalent strain in the two materials as follows:

$$\varepsilon_g = \varepsilon_T \quad (4.3)$$

$$\frac{P_g}{P_T} = \frac{A_g E_g}{A_T E_T} \quad (4.4)$$

$$P_T = \frac{P_{total}}{1 + \frac{P_g}{P_T}} \quad \text{or} \quad P_T = \frac{P_{total}}{1 + \frac{A_g E_g}{A_T E_T}} \quad (4.5)$$

$$P_g = P_{total} - P_T \quad (4.6)$$

Where,

- $\varepsilon_g$  = Strain in grout shell
- $\varepsilon_T$  = Strain in timber core
- $A_g$  = Area of grout shell
- $A_T$  = Area of timber core
- $E_g$  = Modulus of elasticity of grout
- $E_T$  = Modulus of elasticity of timber

The modulus of elasticity of the grout is expected to range between 23 – 26 GPa (Sika Canada data 2001). However, the modulus of elasticity for the timber core,  $E_T$ , will vary greatly depending on the quality of the original timber pile and also on the level of decay present in the timber. Based on data observed in this experimental program, the modular ratio  $E_g/E_T$  is expected to range from minimum values of about 2 to values greater than 10 for heavily decayed timber. In order to consider the effect of variations in the modular ratio, the timber stress,  $\sigma_T$ , and the grout stress,  $\sigma_g$ , are calculated using the expressions shown above, for increasing values of  $E_g/E_T$  at values of  $P_{total}$  equal to 800 kN, 1000 kN and 1200 kN, which are in the range of the maximum loads observed for the 200 mm diameter piles. Figure 4.18 illustrates that it is both conservative and

reasonable to assume that the total axial load,  $P_{total}$ , is carried completely by the grout shell.

A conservative design approach would therefore be to assume no contribution from the timber core, either for load sharing or confinement purposes, and to use a grout shell strength that is lower than the full compressive strength of the grout,  $f'_g$ , as determined by standard cylinder tests. Based on the test results obtained in this experimental program, a grout shell strength of  $0.6f'_g$  is recommended. It may be possible to increase the grout shell strength to  $0.75f'_g$  for greater degrees of confinement such as is provided by double layers of GFRP wrap and GFRP shells. However, test data is more limited for this case, and the conservative value of  $0.6f'_g$  is suggested until more test data is available.

The following design example, including both a 200 mm and 300 mm diameter pile, is provided in order to demonstrate the recommended design procedure.

*Design Example*

Pile Diameter (mm)	Pile Area (mm <sup>2</sup> )	Grout Shell Area (mm <sup>2</sup> )
200	31416	23562
300	70686	39270

**200 mm Diameter Pile Design:**

Using the timber pile design strength of 17.2 MPa, as discussed in Chapter 2, the axial capacity of a 200 mm diameter timber pile is 540 kN.

$$P_{\text{original}} = 31416 \text{ mm}^2 \times 17.2 \text{ MPa}$$

$$P_{\text{original}} = 540 \text{ kN}$$

This value of 540 kN represents the original capacity of the timber pile,  $P_{\text{original}}$ , and the capacity of the repaired pile,  $P_{\text{repaired}}$ , must meet or exceed this value.

Using the lowest unconfined grout strength obtained during the experimental work,  $f'_g = 41 \text{ MPa}$ , and considering the effect of the timber core in reducing the strength of the confined grout shell to 60% of  $f'_g$ , the stress carried by the grout shell,  $(f'_{cg})_{\text{shell}}$ , is as follows:

$$(f'_{cg})_{\text{shell}} = 0.6f'_g$$

$$(f'_{cg})_{\text{shell}} = 24.6 \text{ MPa}$$

Since conservatively, the confined grout shell is assumed to carry all of the applied load, the capacity of the repaired pile is 580 kN.

$$P_{\text{repaired}} = 23562 \text{ mm}^2 \times 24.6 \text{ MPa}$$

$$P_{\text{repaired}} = 580 \text{ kN}$$

Since the design capacity of the repaired pile exceeds that of the original timber pile, the repair technique is adequate even with the use of the lower strength grout. Based on the test results discussed previously, a single layer of GFRP wrap will provide sufficient confinement to achieve the design strength given above. The bearing surface of the existing timber directly below the grout shell must also be strengthened, as discussed in sections 3.3.2.3 and 4.4.

**300 mm Diameter Pile Design:**

Using the same procedure as that used above for the 200 mm diameter pile, the original design capacity,  $P_{\text{original}}$ , and the capacity of the repaired 300 mm diameter pile,  $P_{\text{repaired}}$ , are determined as follows:

$$P_{\text{original}} = 70686 \text{ mm}^2 \times 17.2 \text{ MPa}$$

$$P_{\text{original}} = 1216 \text{ kN}$$

$$P_{\text{repaired}} = 39270 \text{ mm}^2 \times (f'_{cg})_{\text{shell}}$$

$$P_{\text{repaired}} = 39270 \times 24.6 \text{ MPa}$$

$$P_{\text{repaired}} = 966 \text{ kN}$$

Since the design capacity of the repaired 300 mm diameter pile is less than the original strength of the pile, a single layer of GFRP wrap and 41 MPa grout are not adequate.

Two alternative methods for improving the capacity of the repaired pile are as follows:

- 1) Increase the strength of grout used to  $f'_g = 54 \text{ MPa}$ .

$$(f'_{cg})_{\text{shell}} = 0.6f'_g$$

$$(f'_{cg})_{\text{shell}} = 0.6 \times 54 \text{ MPa}$$

$$(f'_{cg})_{\text{shell}} = 32.4 \text{ MPa}$$

$$P_{\text{repaired}} = 39270 \text{ mm}^2 \times 32.4 \text{ MPa}$$

$$P_{\text{repaired}} = 1272 \text{ kN}$$

- 2) Use a double layer of GFRP wrap or prefabricated GFRP shell and lower grout strength,  $f'_g = 41$  MPa. Although the number of tests is limited, test results do indicate an increase in the strength of the grout shell with an increase in confining GFRP, even with a 200 mm diameter timber core. Based on test results, using 75% of  $f'_g$  for the strength of the grout shell, when confined with two layers of GFRP wrap, is considered to be conservative. Therefore,

$$(f'_{cg})_{\text{shell}} = 0.75 \times 41 \text{ MPa}$$

$$(f'_{cg})_{\text{shell}} = 30.75 \text{ MPa}$$

and,

$$P_{\text{repaired}} = 39270 \text{ mm}^2 \times 30.75 \text{ MPa}$$

$$P_{\text{repaired}} = 1208 \text{ kN}$$

Both alternatives result in a repaired pile capacity that meets or exceeds the design capacity of the original 300 mm timber pile. However, the use of higher strength grout is more cost effective. A second layer of GFRP wrap may be used for cases where the repair with a single layer has been completed and subsequent grout cylinder tests indicate that the cast-in-place grout is below the desired design strength,  $f'_g$ .



Table 4.1: Summary of 200 mm Overall Diameter Piles Tested in Axial Compression

GFRP Repair System	Timber or Core Condition	Timber or Void Diameter (mm)	Grout Strength ( $f'_g$ ) (MPa)	Max. Load (kN)	Ave. Max. Load (kN)	Specimen Mark
Control: Timber Only	Mild	200	-	1072	953 (STDEV=243)	2CT-M1
				806		2CT-M2
				701		2CT-M3
				1233		2CT-M4
				214		2CT-H1
	Heavy	200	-	58	184 (STDEV=198)	2CT-H2
				516		2CT-H3
				98		2CT-H4
				35		2CT-H5
				881		2F1-M1
Single Layer GFRP Wet-Wrap	Mild	100	41	882	857 (STDEV=42)	2F1-M2
				808		2F1-M3
				876		2F1-H1
	Heavy	100	41	1167	1003 (STDEV=149)	2F1-H2
				967		2F1-H3
				1230		2F1-V1
	Void	100	54	1174	1214 (STDEV=35)	2F1-V2
				1238		2F1-V3
				526		2F1-B1
	Bearing (Mild)	100/200	41	826	652 (STDEV=156)	2F1-B2
604				2F1-B3		
901				2F1-SB1		
Improved Bearing (Mild)	100/200	41	1068	956 (STDEV=97)	2F1-SB2	
			898		2F1-SB3	

Re-tested Piles

Bearing Specimens

Table 4.2: Summary of 300 mm Overall Diameter Piles Tested in Axial Compression

GFRP Repair System	Timber or Core Condition	Timber or Void Diameter (mm)	Grout Strength ( $f'_g$ ) (MPa)	Max. Load (kN)	Ave. Load (kN)	Specimen Mark
Control: Grout only	Mild	200	41	974	958 (STDEV=25)	3CG-M1
				938		3CG-M2
Single Layer	Mild	200	41	1243	1392 (STDEV=130)	3F1-M1
				1445		3F1-M2
				1487		3F1-M3
GFRP Wet-Wrap	Void	200	54	1443	1313 (STDEV=151)	3F1-V1
				1350		3F1-V2
				1147		3F1-V3
Double Layer	Mild	200	54	2671	2585 (STDEV=194)	3F2-M1
				2720		3F2-M2
				2363		3F2-M3
GFRP Wet-Wrap	Void	200	54	1616	1617 (STDEV=16)	3F2-V1
				1602		3F2-V2
				1633		3F2-V3
GFRP Shell	Mild	200	41	1871	1886 (STDEV=158)	3FS-M1
				2051		3FS-M2
				1737		3FS-M3
Re-tested Piles	Heavy	200	41	1080	898 (STDEV=258)	3FS-H1
				715		3FS-H2

Table 4.3: Maximum Grout Stress Assuming Load is Carried by Grout Shell Only:  
200 mm Diameter Piles

Specimen Mark	Max. Load (kN)	Assumed Max. Grout Stress ( $\sigma_g$ ) if $P_{total} = P_g$ (MPa)	Ave. Grout Stress ( $\sigma_g$ ) if $P_{total} = P_g$ (MPa)	Grout Strength ( $f'_g$ ) (MPa)	$\frac{\sigma_g}{f'_g}$	Predicted Confined Grout Strength ( $f'_{cg}$ ) (MPa)
2CT-M1	1072					
2CT-M2	806	-	-	-	-	-
2CT-M3	701					
2CT-M4	1233					
2CT-H1	214					
2CT-H2	58					
2CT-H3	516	-	-	-	-	-
2CT-H4	98					
2CT-H5	35					
2F1-M1	881	37				
2F1-M2	882	37	36	41	0.88	69
2F1-M3	808	34				
2F1-H1	876	37				
2F1-H2	1167	50	43	41	1.05	69
2F1-H3	967	41				
2F1-V1	1230	52				
2F1-V2	1174	50	52	54	0.96	84
2F1-V3	1238	53				
2F1-B1	526	22				
2F1-B2	826	35	28	41	0.68	69
2F1-B3	604	26				
2F1-SB1	901	38				
2F1-SB2	1068	45	41	41	1.00	69
2F1-SB3	898	38				

 Re-tested Piles

 Bearing Specimens

Table 4.4: Maximum Grout Stress Assuming Load is Carried by Grout Shell Only:  
300mm Diameter Piles

Specimen Mark	Max. Load (kN)	Assumed Max. Grout Stress ( $\sigma_g$ ) if $P_{total} = P_g$ (MPa)	Ave. Grout Stress ( $\sigma_g$ ) if $P_{total} = P_g$ (MPa)	Grout Strength ( $f_g$ ) (MPa)	$\frac{\sigma_g}{f_g}$	Predicted Confined Grout Strength ( $f'_{cg}$ ) (MPa)
3CG-M1	974	25	24	41	0.58	-
3CG-M2	938	24				
3F1-M1	1243	32				
3F1-M2	1445	37	35	41	0.85	61
3F1-M3	1487	38				
3F1-V1	1443	37				
3F1-V2	1350	34	33	54	0.61	75
3F1-V3	1147	29				
3F2-M1	2671	68				
3F2-M2	2720	69	66	54	1.20	91
3F2-M3	2363	60				
3F2-V1	1616	41				
3F2-V2	1602	41	41	54	0.76	91
3F2-V3	1633	42				
3FS-M1	1871	48				
3FS-M2	2051	52	48	41	1.20	79
3FS-M3	1737	44				
3FS-H1	1080	28	23	41	0.56	79
3FS-H2	715	18				

 Re-tested Piles

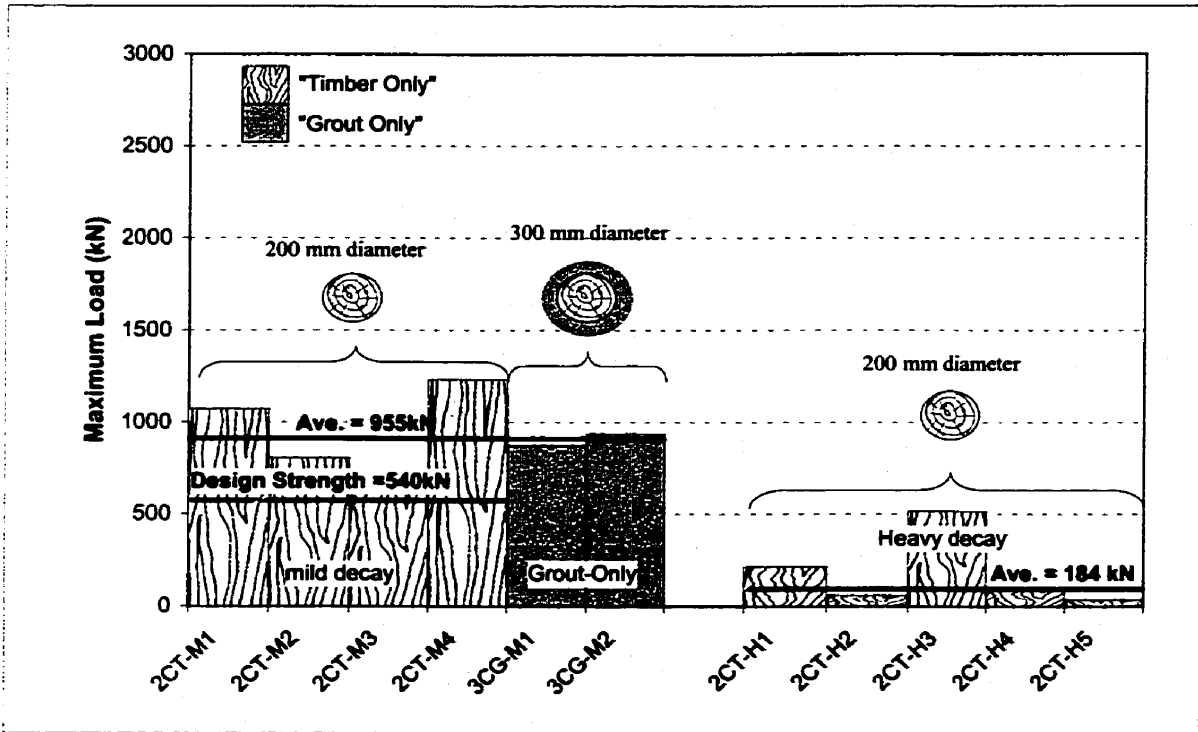


Figure 4.1(a): Maximum Load for all Control Pile Specimens

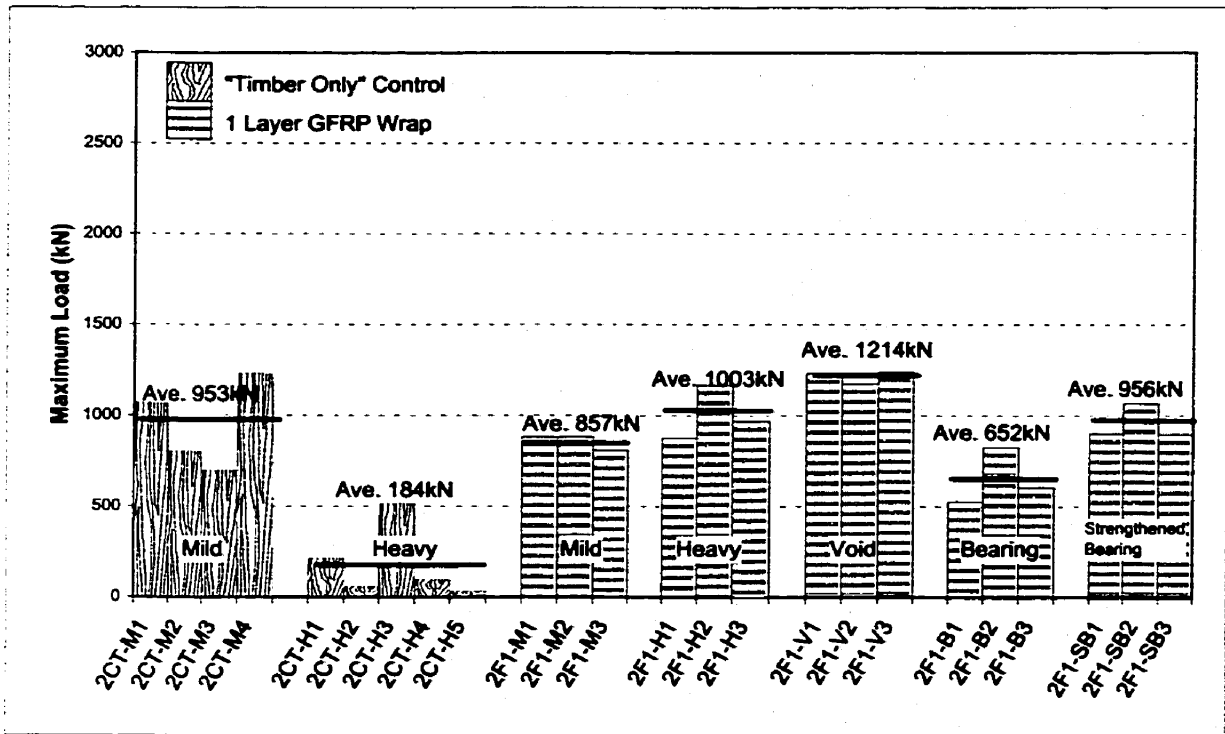


Figure 4.1(b): Summary of Test Results for 200 mm Overall Diameter Piles

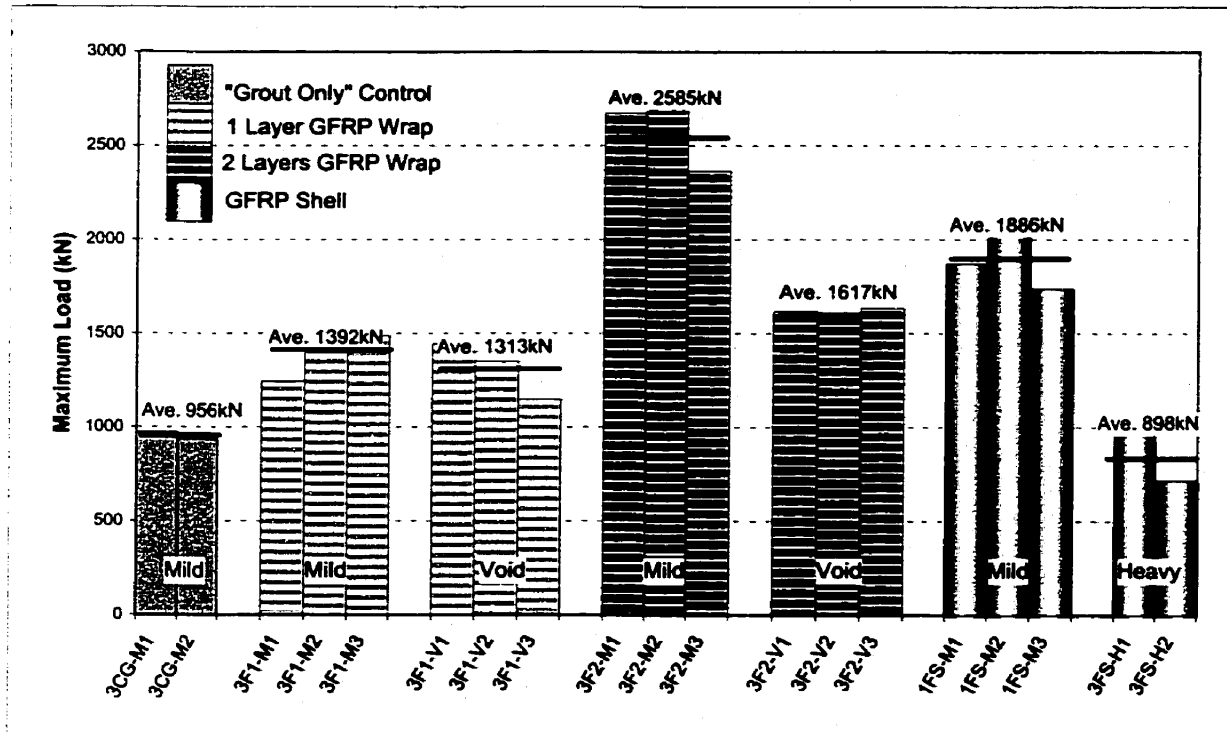


Figure 4.1(c): Summary of Test Results for 300 mm Overall Diameter Piles

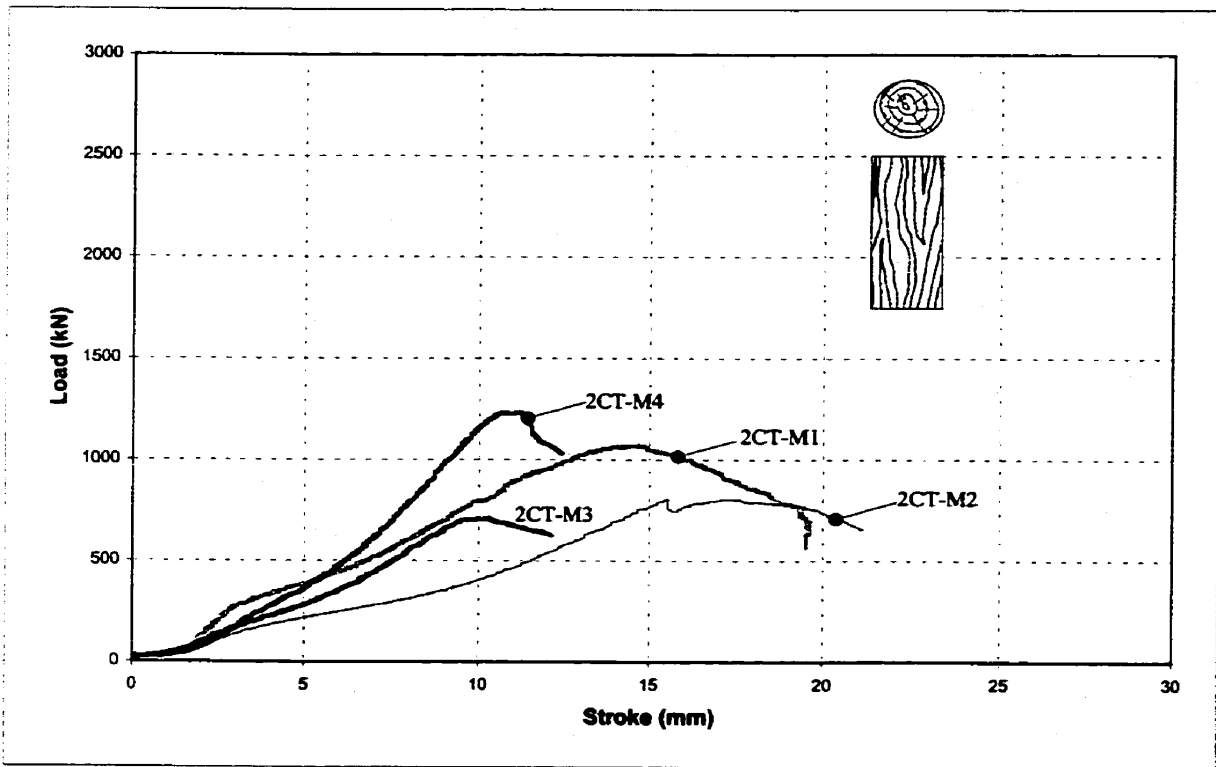


Figure 4.2(a): Load vs Stroke for Mildly Decayed "Timber Only" Control Specimens

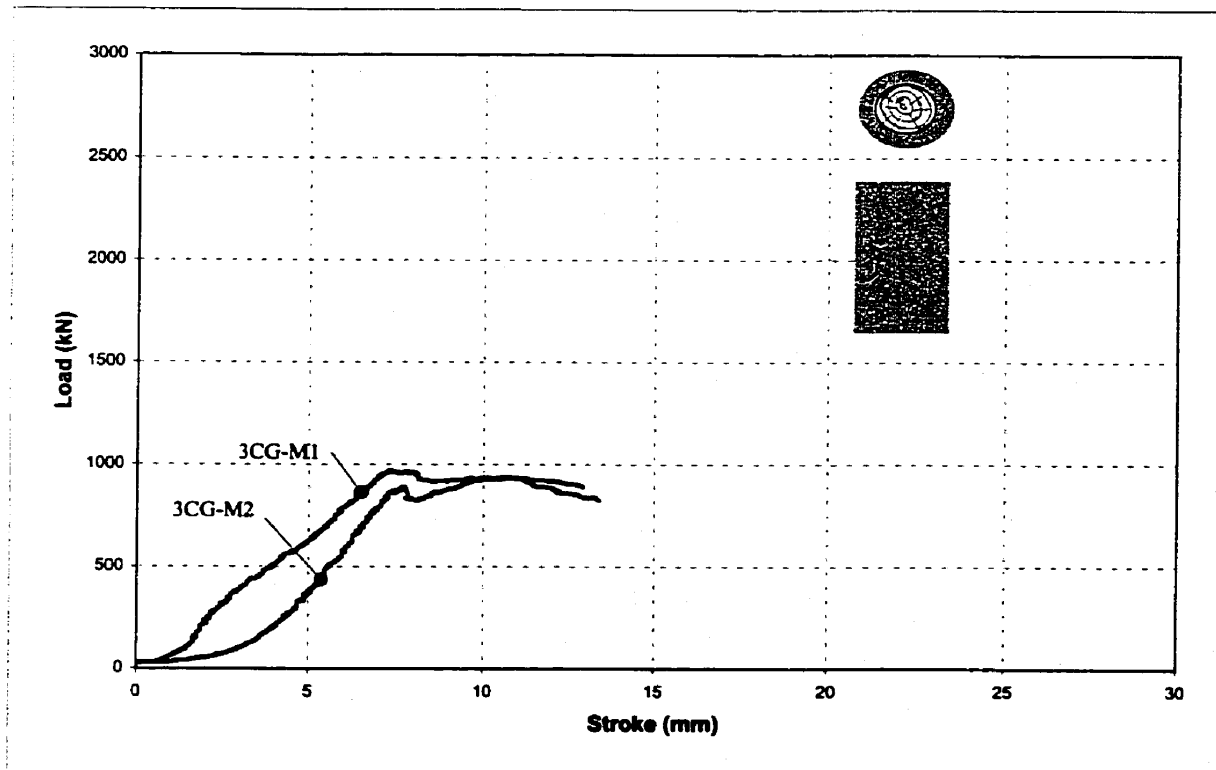


Figure 4.2(b): Load vs Stroke for "Grout Only" Control Specimens

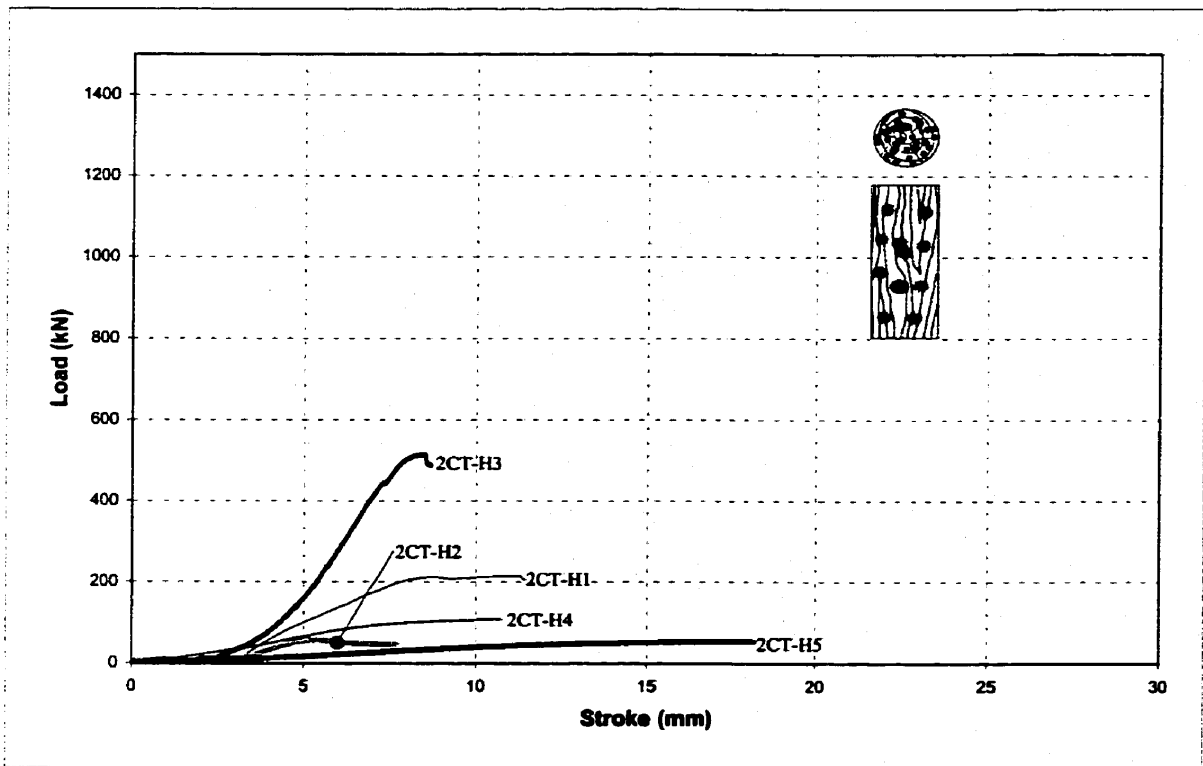
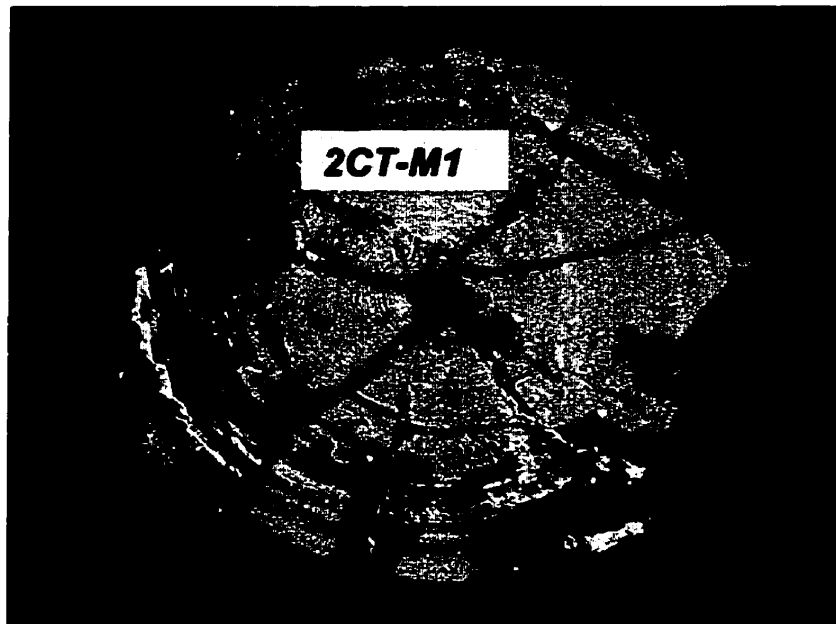
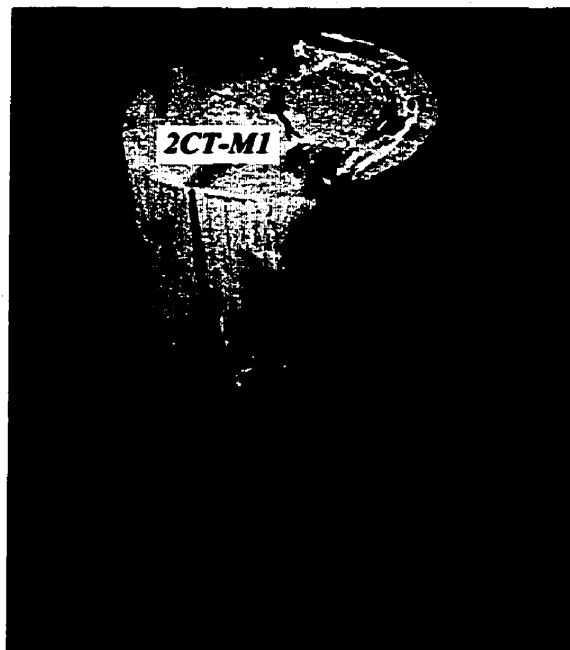


Figure 4.2(c): Load vs Stroke for Heavily Decayed "Timber Only" Control Specimens





*Figure 4.3(a): Cross-section "Timber Only" Control Pile After Failure*



*Figure 4.3(b): "Timber Only" Control Pile After Failure*

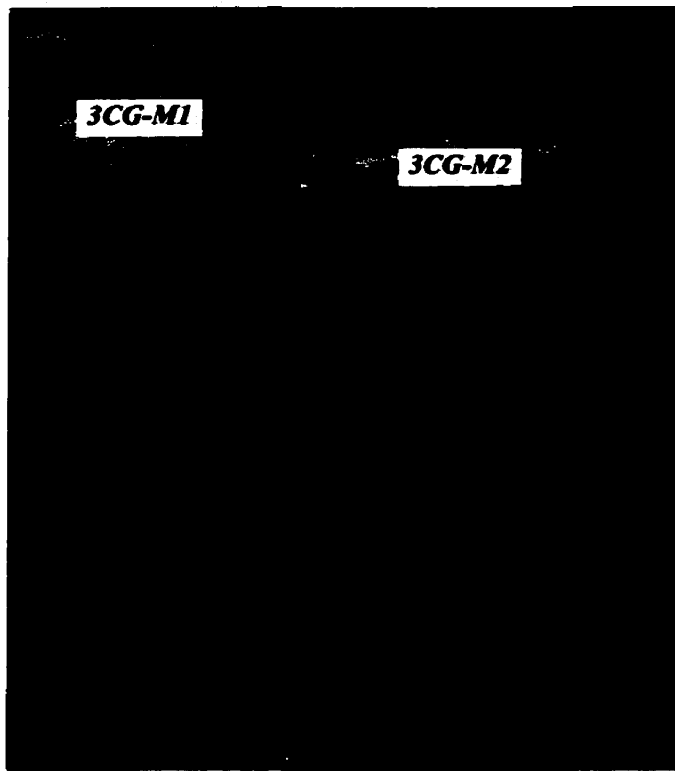


*Figure 4.4(a): "Grout Only" Pile Specimens After Failure*

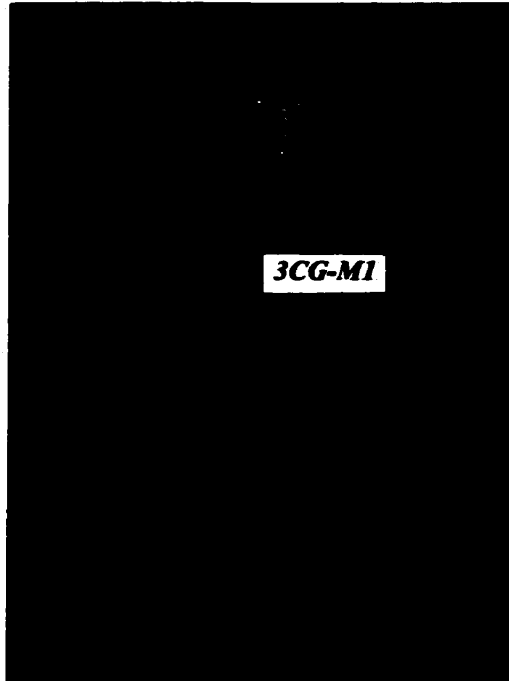


*Figure 4.4(b): Cracking of the Grout Shell After Curing*

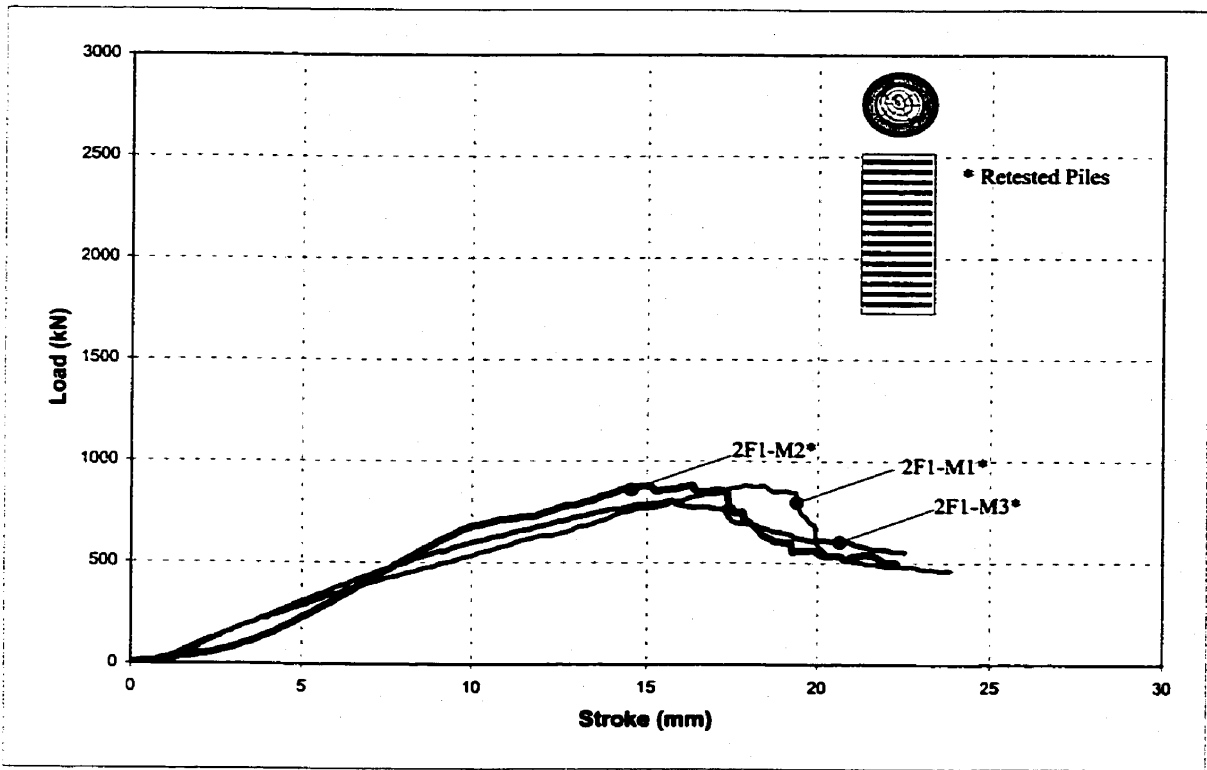


Figure 4.5(a): Load vs Stroke for Piles with a Single Layer of GFRP Wrap and Mildly Decayed Timber Core

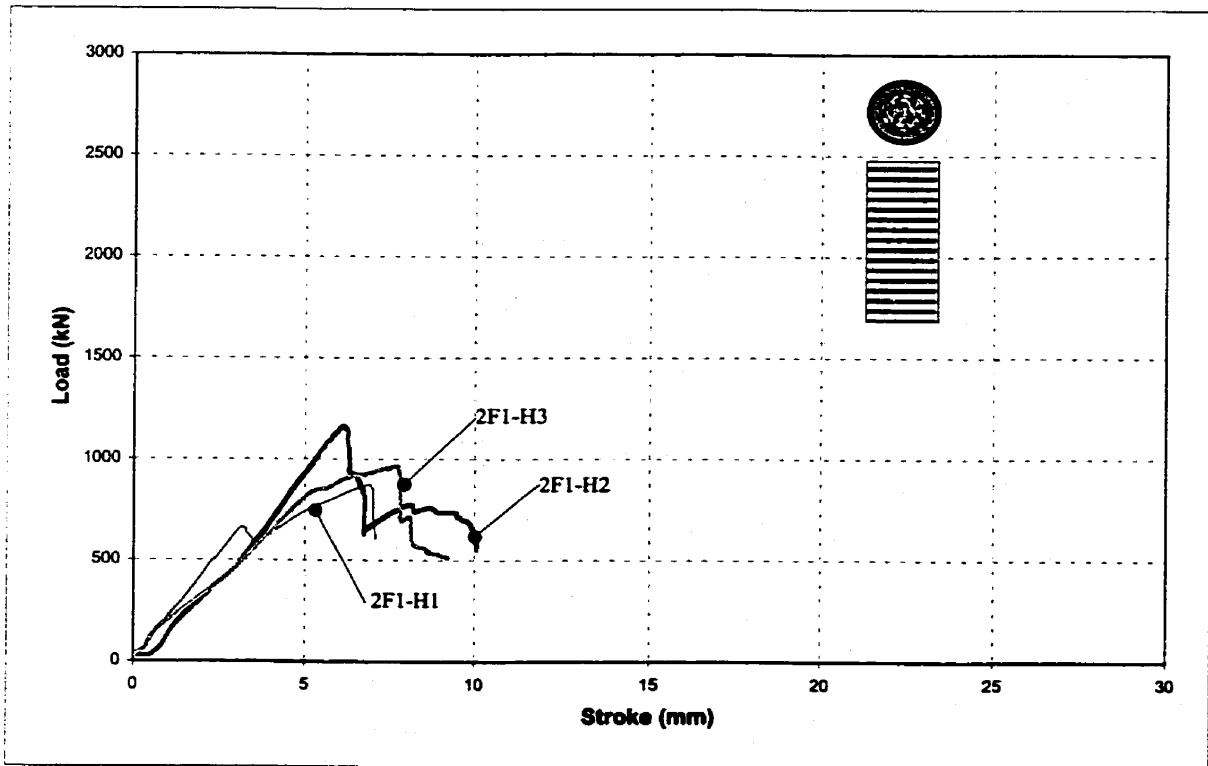


Figure 4.5(b): Load vs Stroke for Piles with a Single Layer of GFRP Wrap and Heavily Decayed Timber Core

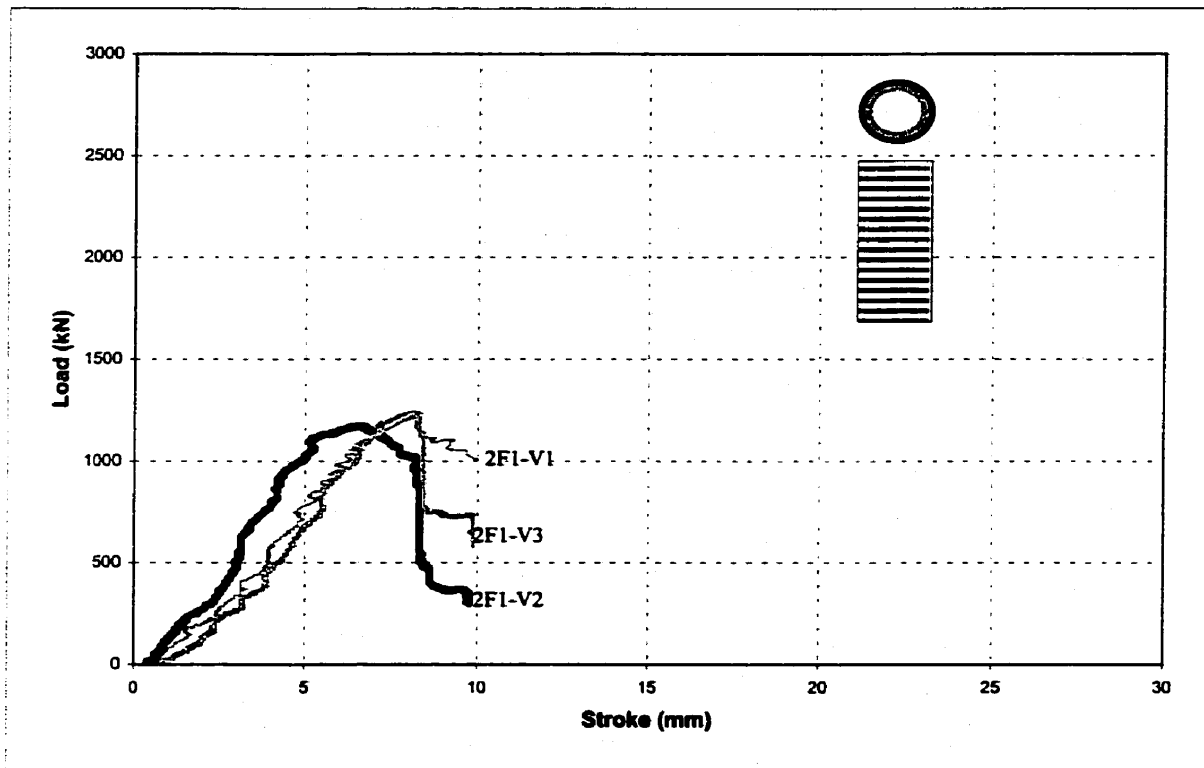


Figure 4.5(c): Load vs Stroke for Piles with a Single Layer of GFRP Wrap and Void Core

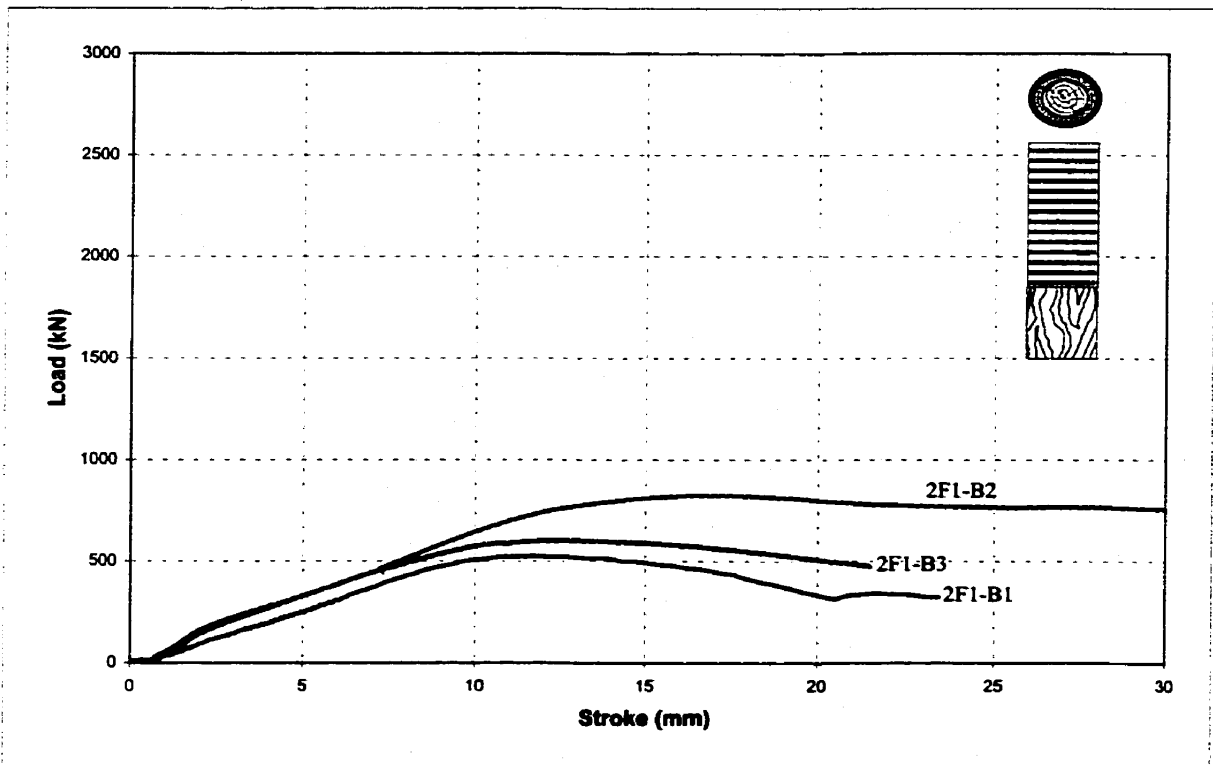


Figure 4.6(a): Load vs Stroke Curves for Bearing Specimens

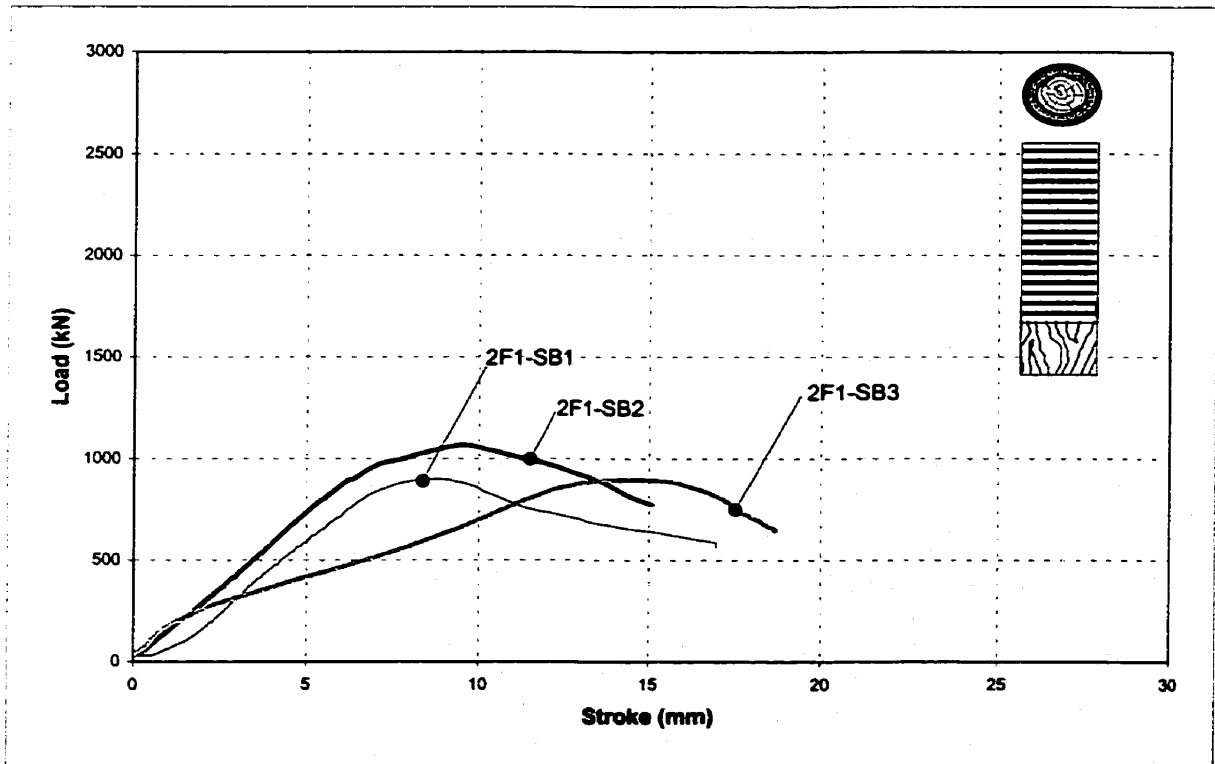
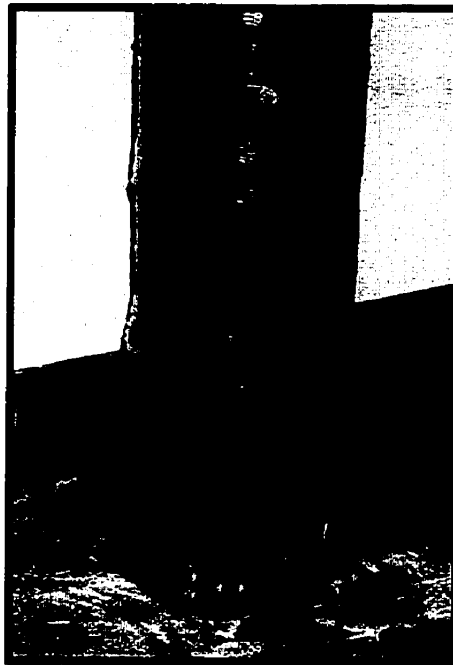


Figure 4.6(b): Load vs Stroke Curves for Piles with Strengthened Bearing Surface



*Figure 4.7: 200 mm Diameter Piles with a Single Layer of GFRP Wrap After Failure*



*Figure 4.8: Piles with Strengthened Bearing Surface After Failure*

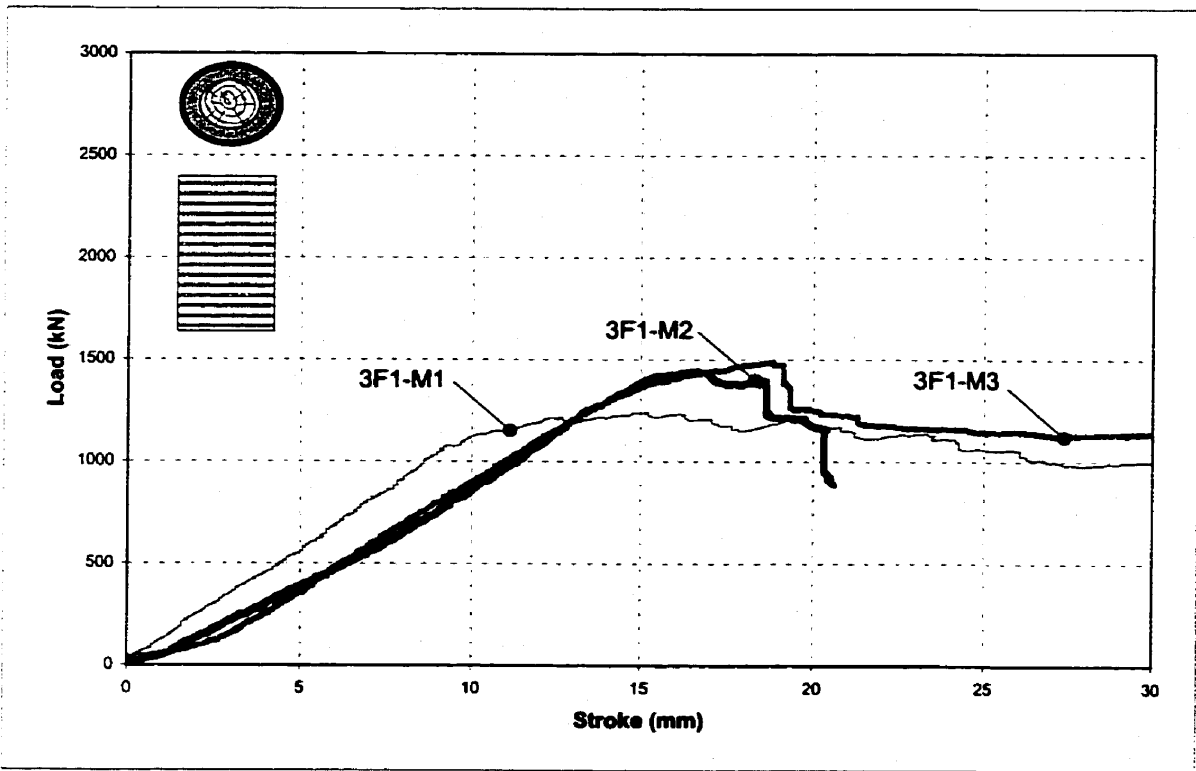


Figure 4.9(a): Load vs Stroke for 300 mm Diameter Piles with a Single Layer of GFRP Wrap and Mildly Decayed Timber Core

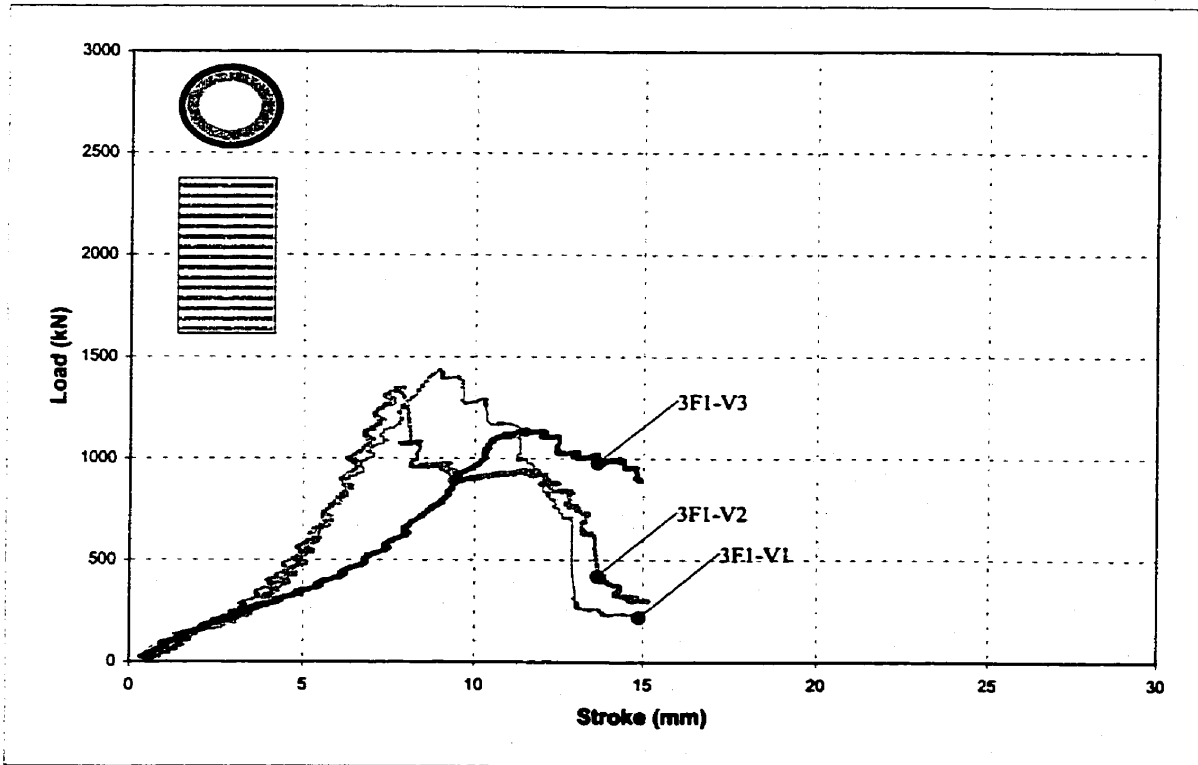


Figure 4.9(b): Load vs Stroke for 300 mm Diameter Piles with a Single Layer of GFRP Wrap and Void Core

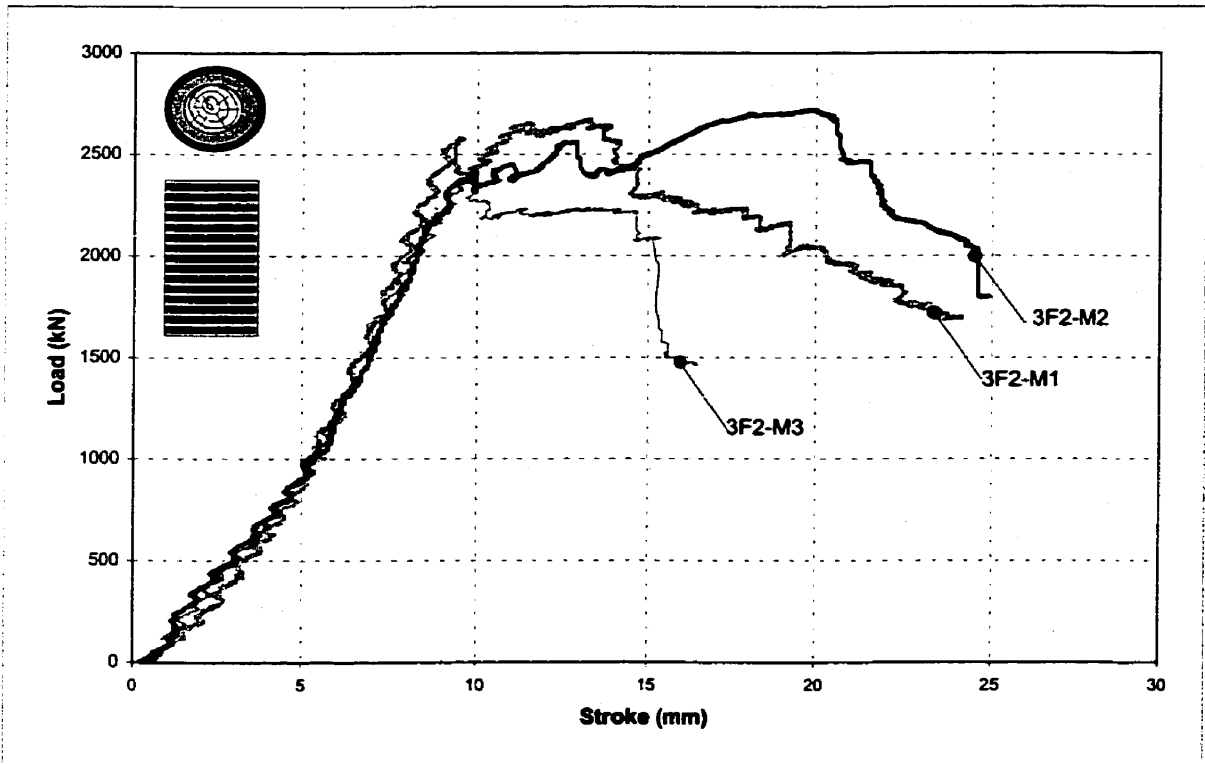


Figure 4.10(a): Load vs Stroke for 300 mm Diameter Piles with a Double Layer of GFRP Wrap and Mildly Decayed Timber Core

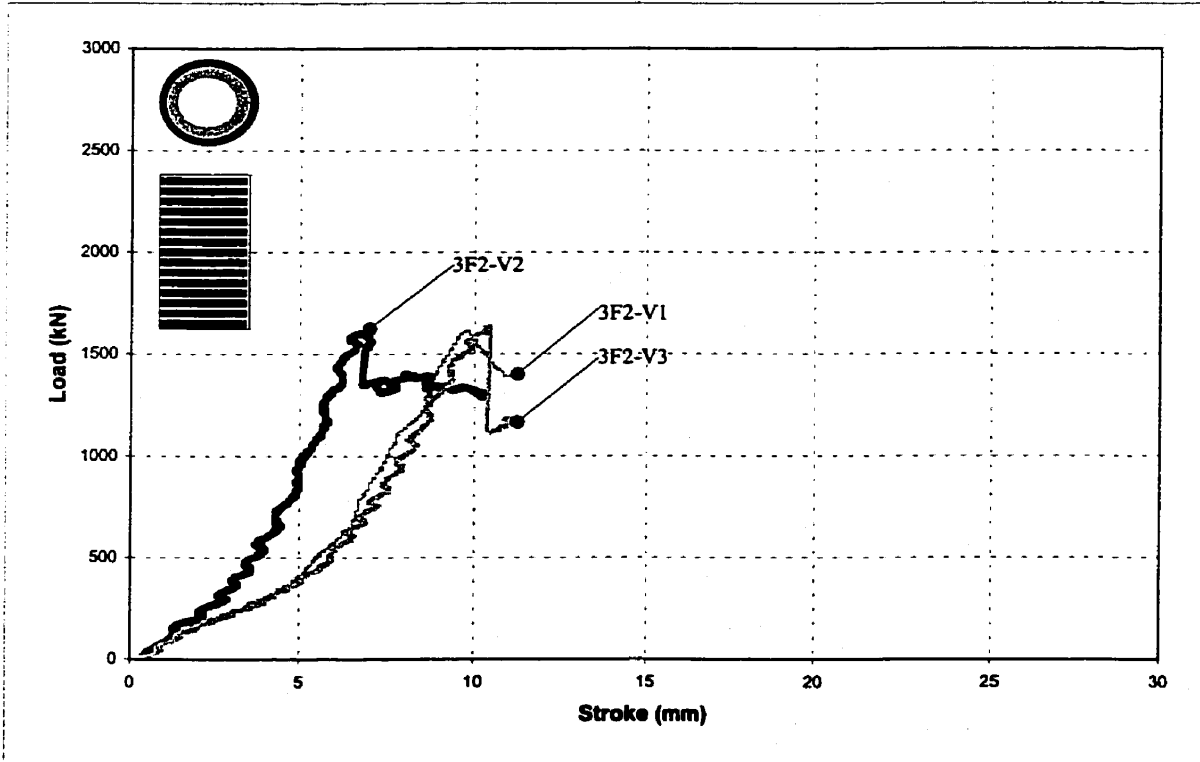


Figure 4.10(b): Load vs Stroke for 300 mm Diameter Piles with a Double Layer of GFRP Wrap and Void Core



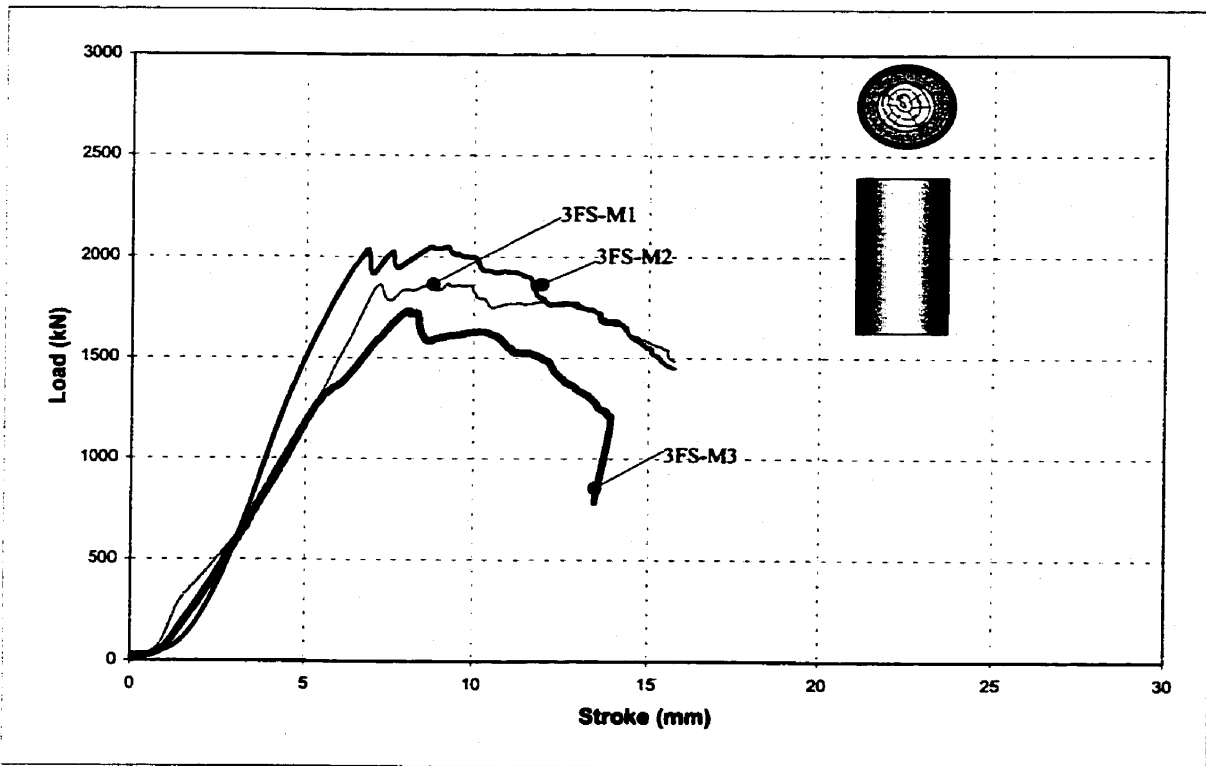


Figure 4.11(a): Load vs Stroke for 300 mm Diameter Piles With a Prefabricated GFRP Shell and Mild Decay Timber Core

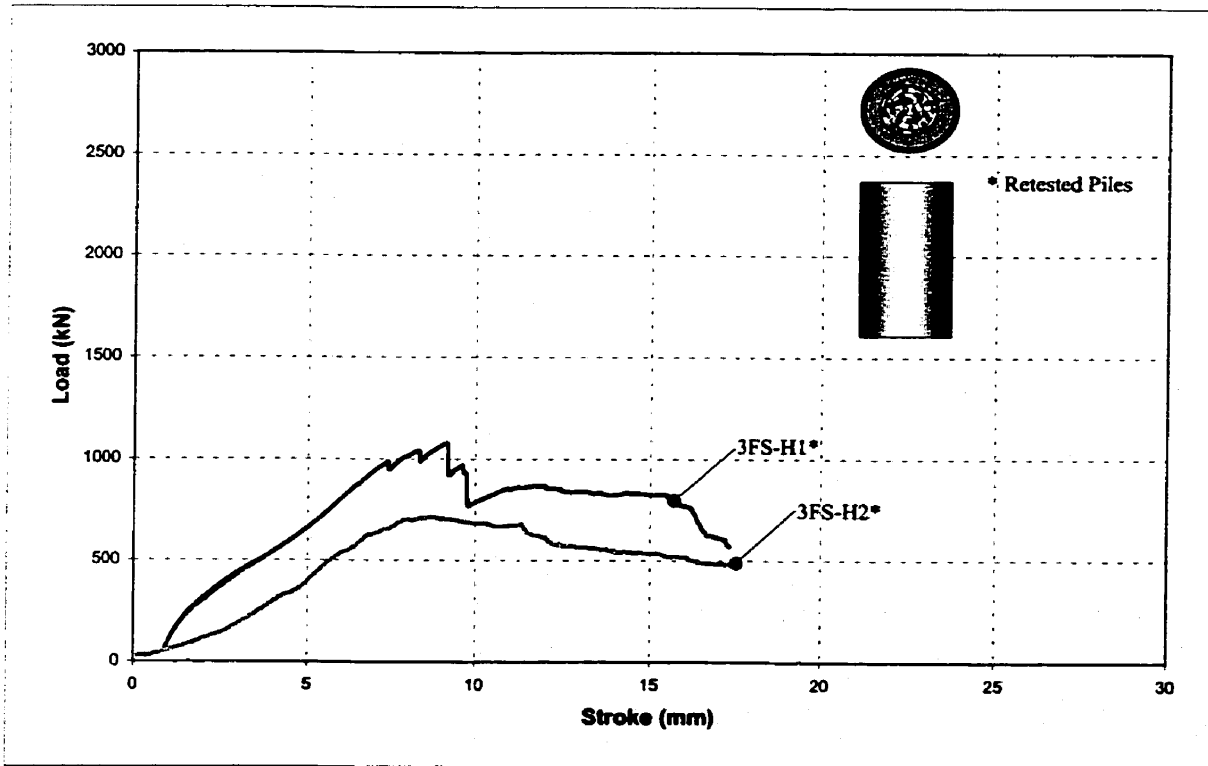


Figure 4.11(b): Load vs Stroke for 300 mm Diameter Piles With a Prefabricated GFRP Shell and Heavy Decay Timber Core



*Figure 4.12(a): 300 mm Diameter Piles with a Single Layer of GFRP Wrap and Void Core After Failure*



*Figure 4.12(b): Top View of 300 mm Diameter Piles with Single Layer of GFRP Wrap After Failure*



*Figure 4.13(a): Piles with a Double Layer of GFRP Wrap and Mildly Decayed Timber Core After Failure*

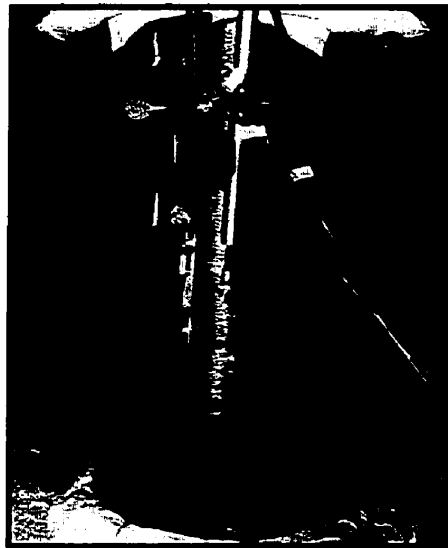


*Figure 4.13(b): Piles with a Double Layer of GFRP Wrap and Mildly Decayed Timber Core After Failure*

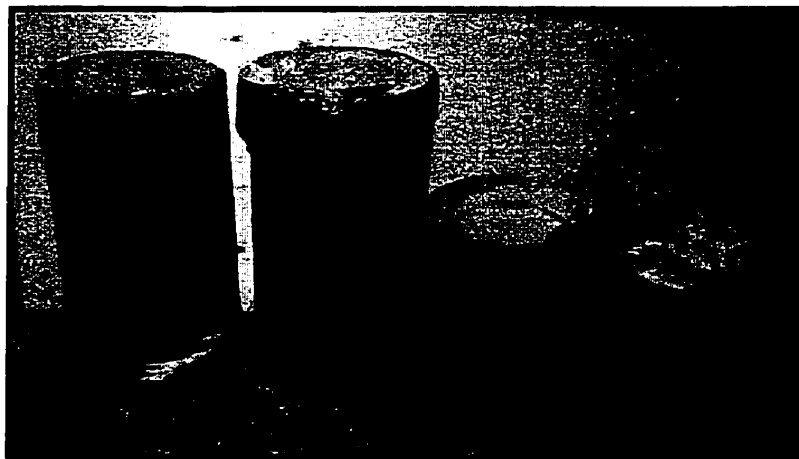


*Figure 4.14: Piles with a Double Layer of GFRP Wrap and Void Core After Failure*



*Figure 4.15: Pile with a Prefabricated GFRP Shell After Failure.*

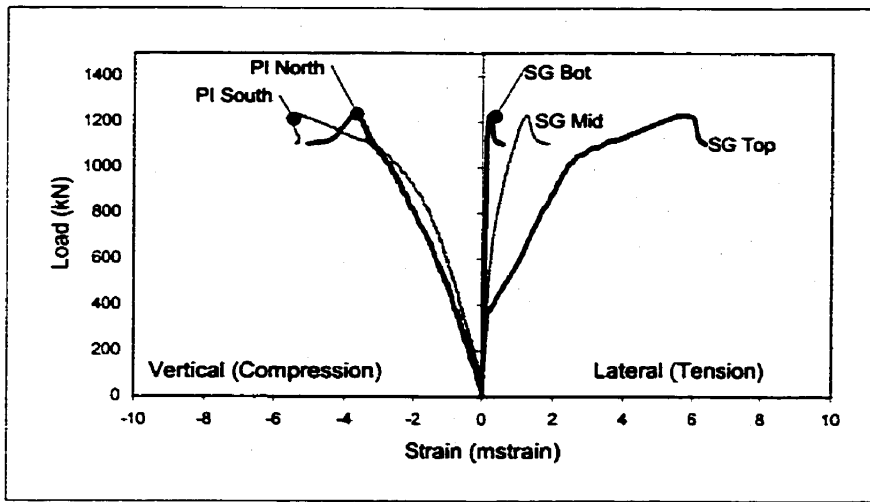


Figure 4.16(a): Load vs Strain Curves for 2F1-V1

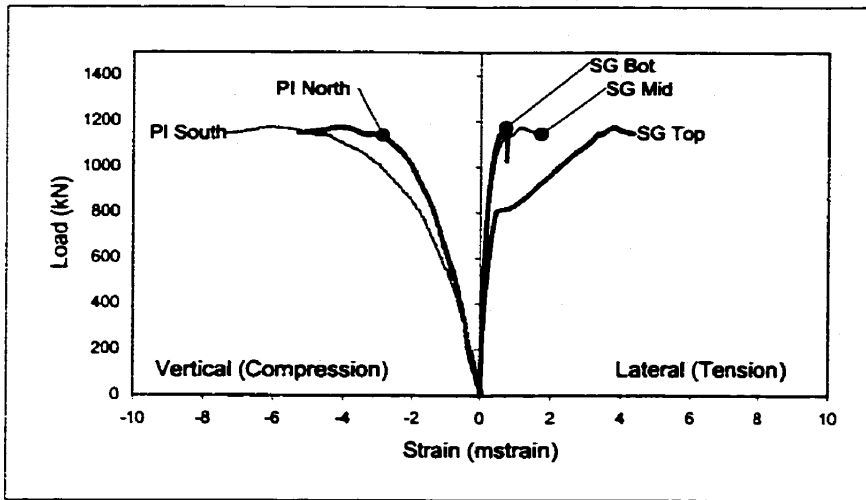


Figure 4.16(b): Load vs Strain Curves for 2F1-V2

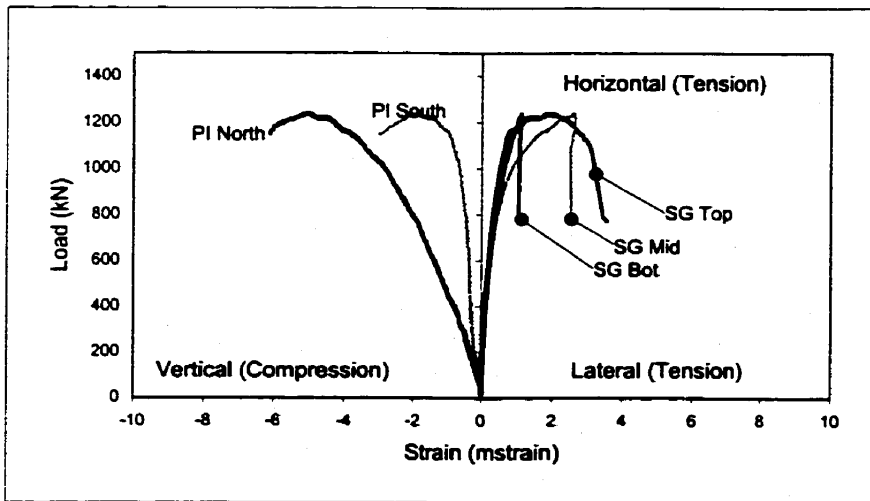


Figure 4.16(c): Load vs Strain Curves for 2F1-V3

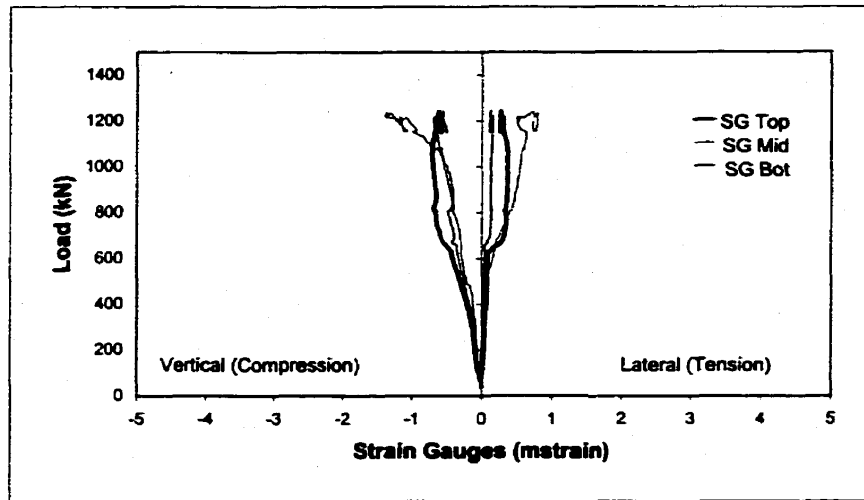


Figure 4.17(a): Load vs Strain Curves for 3F1-M1

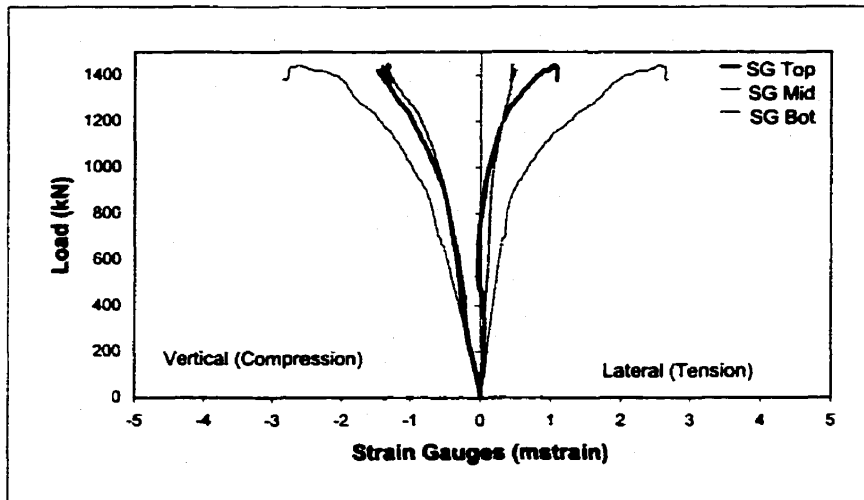


Figure 4.17(b): Load vs Strain Curves for 3F1-M2

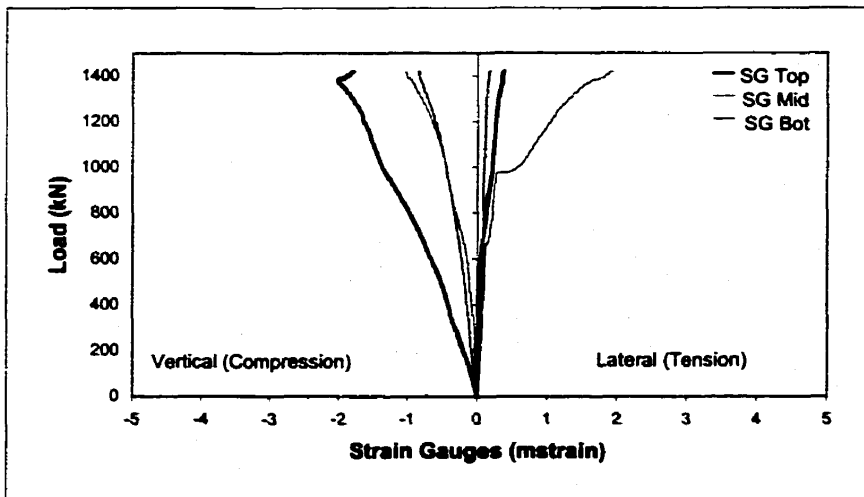


Figure 4.17(c): Load vs Strain Curves for 3F1-M3

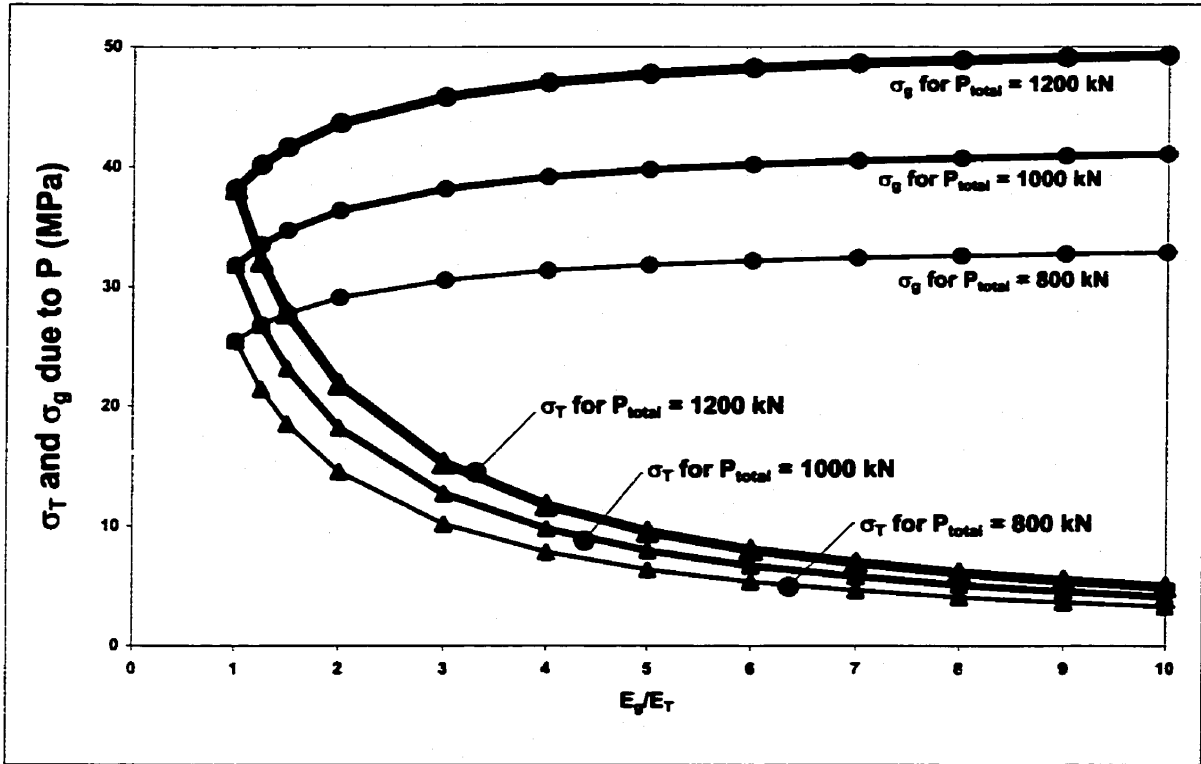


Figure 4.18: Stress in Timber Core,  $\sigma_T$ , and Grout Shell,  $\sigma_g$ , vs Material Stiffness Ratio  $E_g/E_T$

## **Chapter 5**

### **Test Results and Analysis:**

#### **Bending Series**

##### ***5.1 General***

Test results and analysis for the series of specimens tested in bending are presented and discussed in this chapter. A total of ten specimens were tested in the Bending Series, as described in Chapter 3. Three 200 mm diameter timber control specimens were tested and the results are compared with results for five 200 mm diameter piles repaired with two orthogonal layers of GFRP wrap. These repaired specimens were also designed to examine the behaviour of the transition zone between the repaired and unrepaired portions of the pile when subjected to bending. In addition, two 300 mm diameter specimens were tested. Table 5.1 presents a summary of test results and specimen parameters for all of the bending specimens. The bending moment at mid-span and at the failure location are given in Table 5.2 and Figure 5.1.



## 5.2 Bending Control Specimens

Three 200 mm diameter timber piles with only mild decay were tested for control purposes. The load versus mid-span deflection curves for the “timber only” bending control specimens is shown in Figure 5.2. The average ultimate load obtained for all three specimens was 120 kN, as shown in Table 5.1. The average mid-span moment at failure was 30 kNm, as shown in Table 5.2. As indicated in Table 5.1 and 5.2, a considerable variability in flexural capacity was observed for the “timber only” bending control specimens.

Figure 5.4 shows the typical mode of failure observed for the “timber only” bending control specimens. Each timber control specimen failed in tension at mid-span of the specimen, with no crushing of the timber observed on the compression side.

Table 5.3 presents the ultimate load at failure and the modulus of rupture at failure as calculated based on the test results. The modulus of rupture,  $f_r$ , was computed using the following equation.

$$f_r = \frac{M_f}{S} \quad (5.1)$$

Where,  $M_f$  = Bending moment at failure load

$S$  = Section modulus

Also provided for comparison in Table 5.3, is the specified strength,  $f_b$ , for Douglas Fir timber piles at the extreme fiber under bending stress, as obtained from

CAN/CSA-O86.1-M89. As shown in Table 5.3, the modulus of rupture calculated from the test data is 90% higher than the specified strength,  $f_b$ , given by CSA. As discussed in Chapter 4, a similar trend was observed for the axial compressive strength of the piles which was significantly greater than the design strength.

### **5.3 Transition Zone Between Repaired and Unrepaired Pile Lengths**

Five pile specimens with an overall diameter of 200 mm were repaired using the GFRP wet-wrap system, as described in Chapter 3, and were tested to failure. Two layers of GFRP wet-wrap sheets were applied with the glass fibers of each sheet in two different orthogonal directions, axial and lateral. The purpose of the lateral fibers around the circumference of the pile are to confine the cementitious grout shell, while the axial fibers are intended to carry the tensile stress due to bending. As described in Chapter 3, these bending specimens were designed to examine the behaviour and strength of the transition zone between the repaired and unrepaired zone of the piles.

For the 200 mm diameter repaired piles, failure did not occur at the location of maximum moment at mid-span, but rather at the transition zone between the repaired and unrepaired portions of the pile. The typical failure occurring in the transition zone is shown for four different specimens in Figures 5.5 through 5.8.

A photo of the trimmed timber prior to grout injection, a longitudinal cross-section of the repaired pile at failure and a sketch showing the location of GFRP rupture, are shown in Figures 5.9(a), (b) and (c), respectively. Failure typically was initiated at the cross-section where the 200 mm diameter of the timber pile is reduced to 100 mm as shown in Figure 5.9(a). Following the cracking of the timber and separation of the repaired section from the 200 mm diameter timber, as shown in Figure 5.9(b), the GFRP sheets began to rupture at the left end. The rupture of the GFRP sheet propagated in the axial

direction over the 200 mm length of GFRP overlapping the 200 mm diameter timber. As shown in Figure 5.7, the 200 mm length of GFRP sheet wrapped around the 200 mm diameter timber showed a tendency to slip out. It should be noted that the 800 mm long repaired zone remained relatively undamaged.

The load versus mid-span deflection curves for three of the 200 mm diameter repaired pile specimens are shown in Figure 5.3. Load versus mid-span deflection data for specimens 2LA-T-1 and 2LA-T-2 is not available, however, the mode of failure observed for these two specimens is similar to that observed for the other specimens in this group.

The average ultimate load obtained for the repaired 200 mm diameter piles was 154 kN, as shown in Table 5.1. However, the maximum moment at mid-span due to this ultimate load does not represent the maximum flexural capacity of the repaired portion of the pile, since failure occurred away from the mid-span in the transition zone between the repaired and unrepaired portion of the pile. A summary of the moment at failure occurring at both the mid-span and at the location of failure is given in Table 5.2.

As shown in Table 5.2, the average bending moment at failure for the repaired piles, occurring at the location of failure in the transition zone, was 23.1 kNm. This value is only 77% of the flexural capacity obtained for the “timber only” bending control specimens. Since the repaired portion remained undamaged, the flexural capacity of the repaired zone has not been determined, but is at least greater than the maximum mid-

span moment of 38.5 kNm, which is 28% higher than the capacity of the “timber only” bending control specimens.

## **5.4 Effect of Axial GFRP and Timber Core Condition**

In order to examine the effect of the axial GFRP wrap on the flexural behaviour of the piles, two pile specimens with an overall diameter of 300 mm were tested in bending. Specimen 3L-T was repaired using GFRP wrap fibers in only the lateral circumferential direction, while specimen 3LA-V was repaired using both axial and lateral fibers. The worst-case condition of complete deterioration of the timber core was also considered since specimen 3LA-V, was fabricated with a void core.

Both 300 mm diameter piles, 3L-T and 3LA-V, failed in flexure at mid-span. Specimen 3L-T, with no axial GFRP, failed due to flexural cracking of the grout shell. Figure 5.10 shows specimen 3L-T at failure. For specimen 3LA-V, failure occurred due to rupture of the axial GFRP fibers. A photo of specimen 3LA-V after failure is shown in Figure 5.11.

The load versus mid-span deflection curves for the two 300 mm diameter piles are shown in Figure 5.12. Since only one layer of fibers oriented in the lateral direction around the circumference of the pile was used for specimen 3L-T, it may be assumed that the GFRP wrap provided little or no enhancement to the flexural strength of the pile. As shown in Figure 5.12, pile 3L-T failed at a lower ultimate load when compared to pile 3LA-V with both lateral and axial fibers. The curve for specimen 3L-T shows a significant drop in flexural capacity after cracking of the grout shell at an ultimate load of 209 kN. After loss of the grout shell contribution, the timber core continued to sustain

an applied load of about 100 kN with increasing deflection, but with no increase in load-carrying capacity.

As shown in Figure 5.12, the application of axial GFRP fibers increased the flexural capacity of the pile significantly. Test results indicate that even without a timber core, the addition of a layer of axially oriented GFRP wrap can increase the load-carrying capacity by up to 53% when compared to pile 3L-T. However, without a timber core, the void core pile 3LA-V failed abruptly and completely at an applied load of 320 kN.

## **5.5 Flexural Strain Analysis**

The load versus flexural strain curves for the “timber only” bending control specimen 2C-T-1 and the load versus flexural strain curves for the repaired specimen 2LA-T-3 are shown in Figures 5.13 and 5.14 respectively. The instrumentation layout for the “timber only” bending control specimens and the 200 mm diameter repaired specimens are shown in Chapter 3, Figures 3.15(a) and (b) respectively. The load versus flexural strain curves for the other specimens tested in this experimental program are provided in Appendix B. The load versus flexural strain curves for specimen 3LA-V are shown in Figure 5.15 while the load versus flexural strain curves for specimen 3L-T are provided in Appendix B. The instrumentation layout shown in Figure 3.15(a) was used for both specimens 3LA-V and 3L-T.

The load versus flexural strain curves for one of the bending control specimens, at a distance of 175 mm from mid-span are shown in Figure 5.13. For this specimen, the maximum strain measured on the tension and compression sides of the specimen ranged from 2.3 to 5 millistrain respectively. However, for all three bending control specimens, the maximum flexural strain at mid-span, where failure occurred, ranged from 3.5 to 10.9 millistrain. As shown in the load versus flexural strain curves found in Figure 5.13 and Appendix B, considerable variability in the flexural strains and flexural capacity was observed for the “timber only” bending control specimens.

The load versus flexural strain curves for one of the 200 mm diameter repaired specimens at a distance of 175 mm from mid-span are shown in Figure 5.14. The



maximum strain measured on the tension side of the specimens ranged from 5.8 to 8 millistrain. The flexural strain curves for these repaired piles were higher when compared to the “timber only” bending control specimens at a distance 175 mm from mid-span. As discussed earlier, failure of these repaired specimens occurred at the transition zone. The strain measured at the failure zone typically ranged from 2 to 5 millistrain.

The load versus flexural strain curves for specimen 3LA-V are shown in Figure 5.15. As shown in Figure 5.15, the strain measured on the tension side was considerably higher than the strain on the compression side. The maximum strain measured at 175 mm from mid-span was 17.6 millistrain. The maximum strain at mid-span on the tension side, where failure occurred, was 14.1 millistrain. This strain reading is considered to be reasonably close to the maximum strain of 20 millistrain specified by the manufacturer.

Table 5.1: Summary of Results for Pile Specimens Tested in Bending

Overall Dia. (mm)	GFRP Repair System	Timber or Core Condition	Timber or Void Diameter (mm)	Grout Strength (MPa) ( $f'_g$ )	Ult. Load (kN)	Ave. Ult. Load (kN)	Specimen Mark
200	Control:				98		2C-T-1
	Timber	Mild	200	-	137	120	2C-T-2
	Only				126		2C-T-3
	Lateral				-		2LA-T-1
	& Axial	Mild	100/200	63	146		2LA-T-2
	GFRP				158	154	2LA-T-3
					158		2LA-T-4
							2LA-T-5
	Lateral GFRP	Mild	200	63	209	209	3L-T
	Lat. & Axial	Void	200	63	320	320	3LA-V

Table 5.2: Summary of Moment at Failure for Pile Specimens Tested in Bending

Overall Dia. (mm)	GFRP Repair System	Ult. Load (kN)	Ave. Ult. Load (kN)	Mid-Span Moment (kNm)	Ave. Mid-Span Moment (kNm)	Failure* Moment (kNm)	Ave. Failure* Moment (kNm)	Specimen Mark
	Control:	98		24.5		24.5		2C-T-1
	Timber	137	120	34.3	30.0	34.3	30.0	2C-T-2
	Only	126		31.5		31.5		2C-T-3
200		-		-		-		2LA-T-1
	Lateral	-		-		-		2LA-T-2
	& Axial	146		36.5		21.9		2LA-T-3
	GFRP	158	154	39.5	38.5	23.7	23.1	2LA-T-4
		158		39.5		23.7		2LA-T-5
300	Lateral GFRP	209	209	52.3	52.3	52.3	52.3	3L-T
	Lat. & Axial	320	320	80	80	80	80	3LA-V

\*All of the loads and moments given in Table 4.2 occurred at failure. "Failure moment" refers to the moment at failure in the location of failure, which in some cases is not the mid-span moment.

Table 5.3: Estimated Modulus of Rupture and Specified Strength for "Timber Only" Bending Control Specimens at Mid-Span

Specimen Mark	Ult. Load (kN)	Modulus of Rupture ( $f_r$ ) (MPa)	Ave. Modulus of Rupture ( $f_r$ ) (MPa)	Specified Strength ( $f_b$ ) (MPa)	$\frac{f_r}{f_b}$	Ave. $\frac{f_r}{f_b}$
2C-T-1	98	31.2		20.1	1.6	
2C-T-2	137	43.7	38.3	20.1	2.2	1.9
2C-T-3	126	40.1		20.1	2.0	

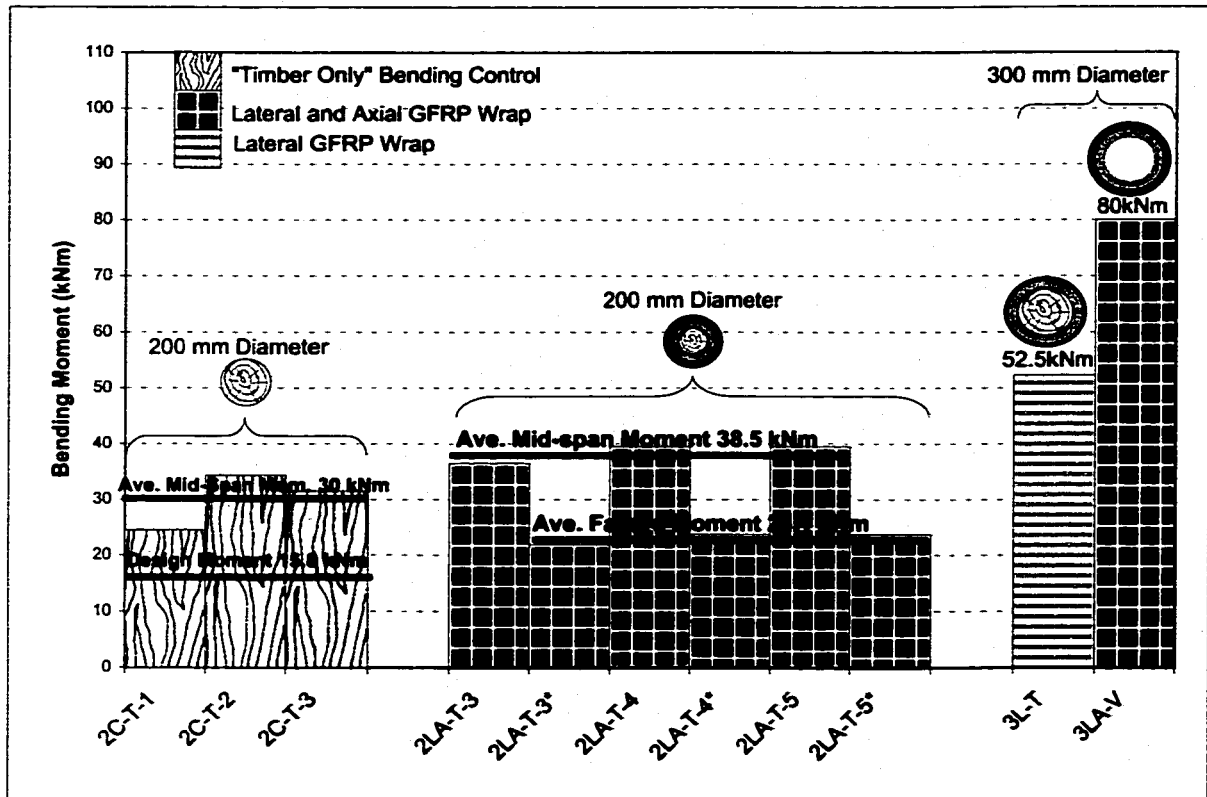


Figure 5.1: Summary of Bending Moment at Mid-Span and at Location of Failure

Note: Asterisk (\*) Denotes Bending Moment of the Specimen at Location of Failure

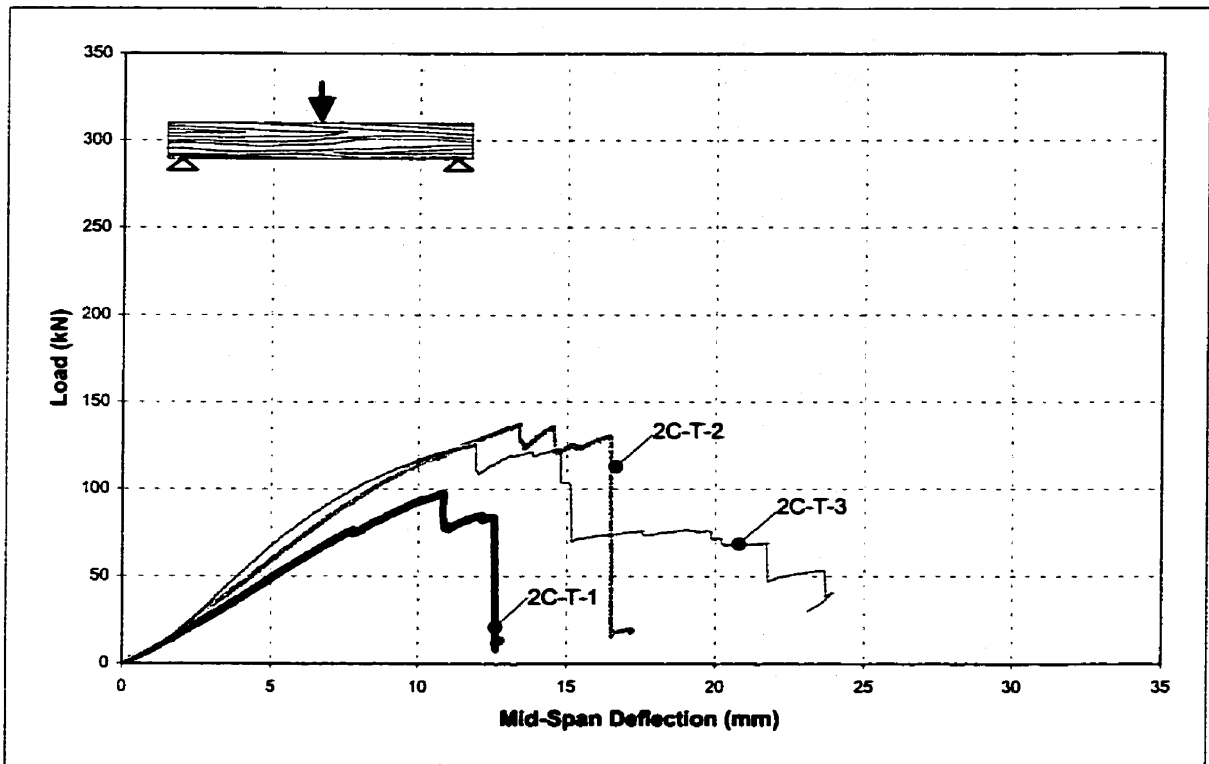


Figure 5.2: Load vs Mid-Span Deflection Curves for 200 mm Diameter "Timber Only" Bending Control Specimens

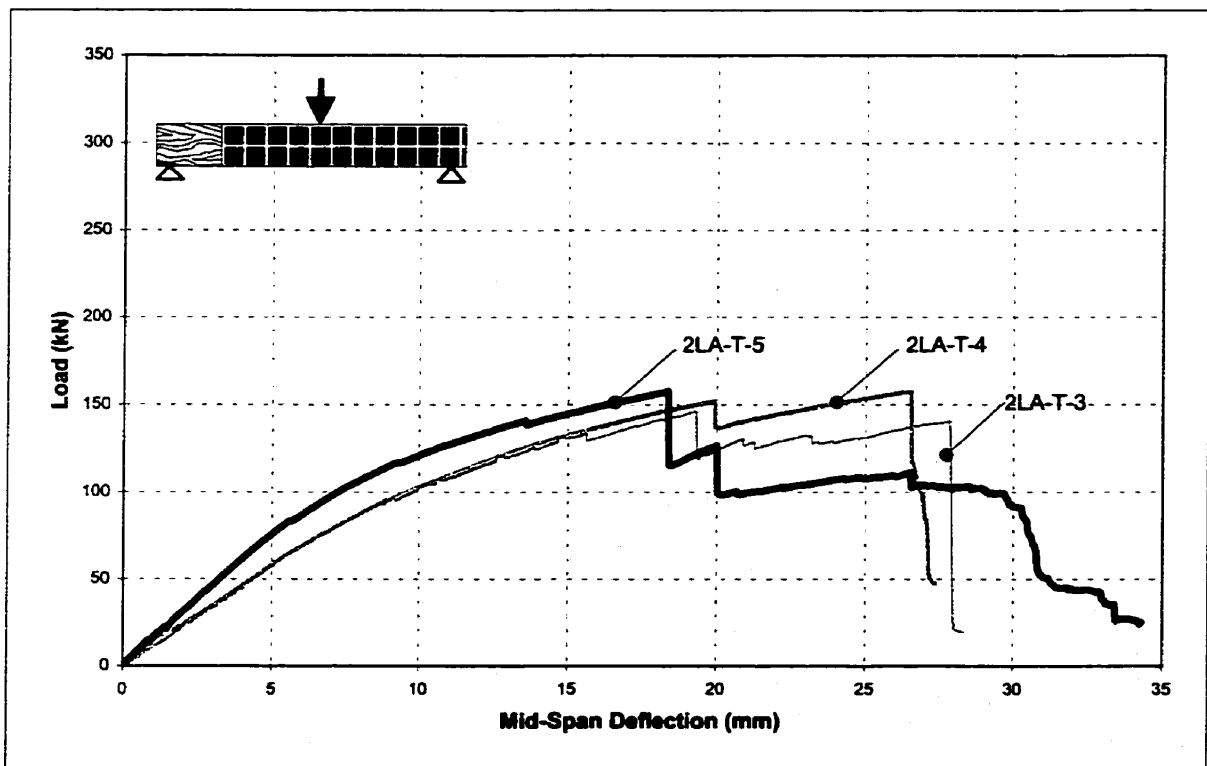
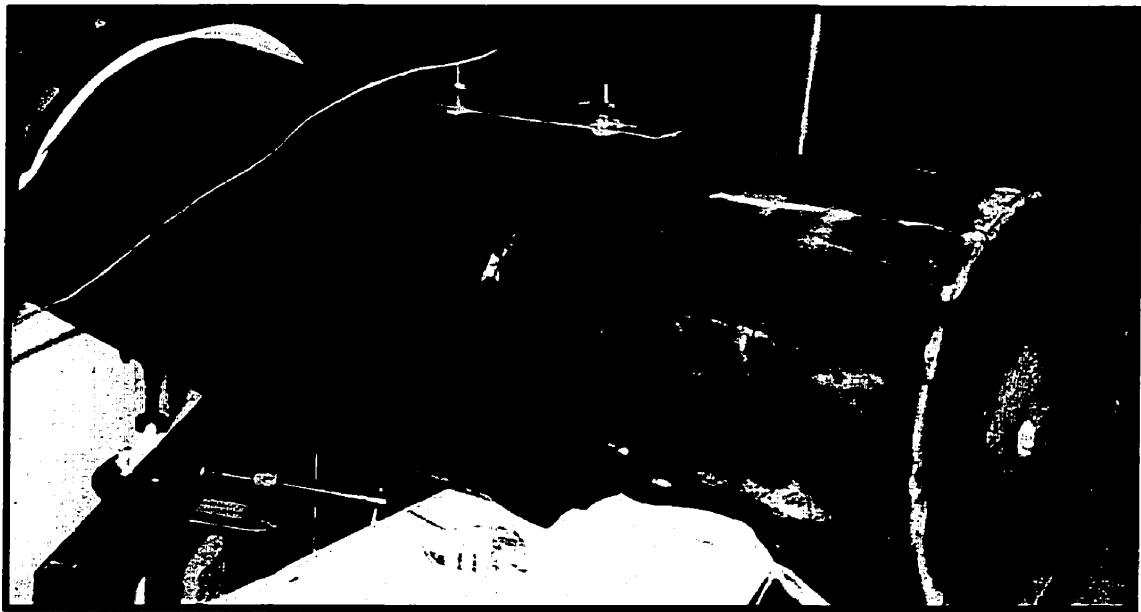


Figure 5.3: Load vs Mid-Span Deflection Curves for 200 mm Diameter Repaired Specimens Examining the Transition Zone



*Figure 5.4: "Timber Only" Bending Control Specimen at Failure 2C-T-2*



*Figure 5.5: Failure at Transition Zone for Specimen 2LA -T-1*

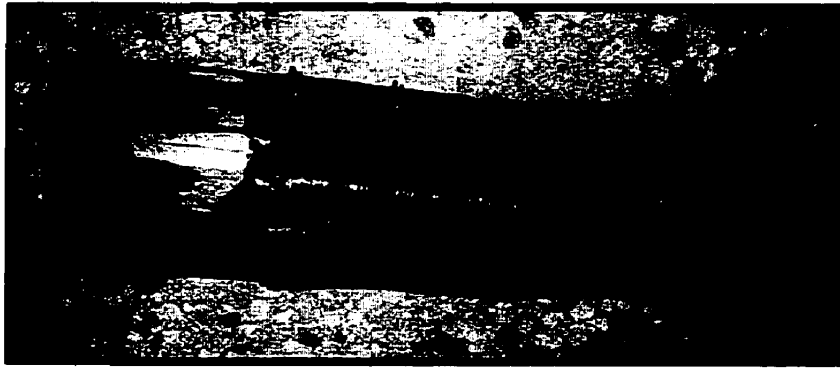


*Figure 5.6: Failure at Transition Zone for Specimen 2LA-T-3*

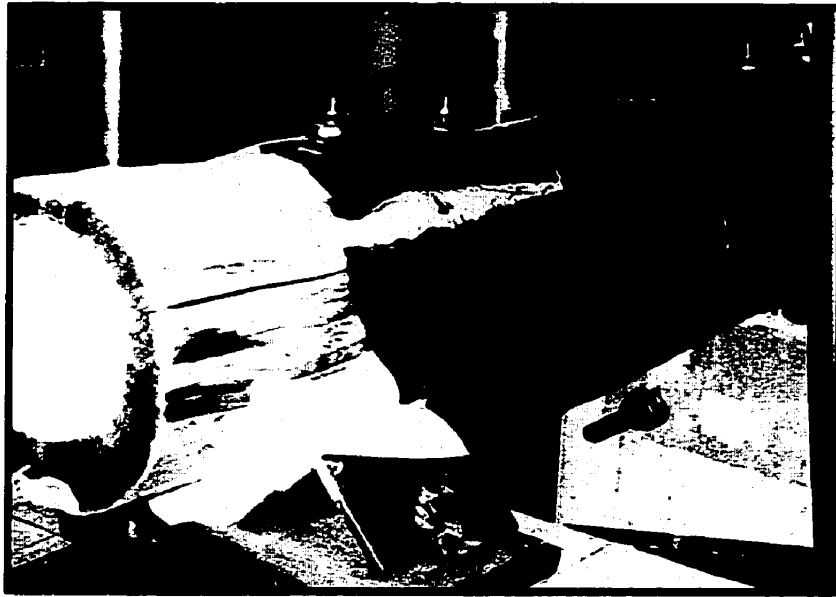


*Figure 5.7: Failure at Transition Zone for Specimen 2LA-T-4*

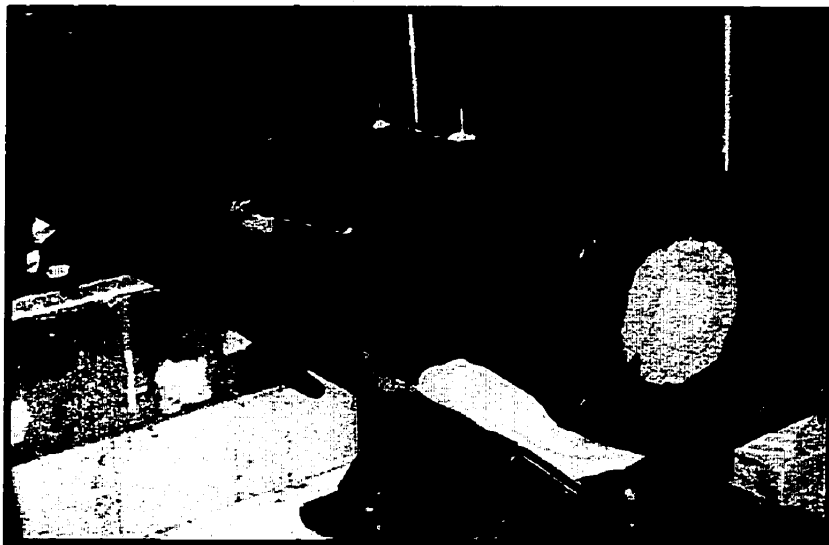


*Figure 5.8: Failure at Transition Zone for Specimen 2LA-T-5*

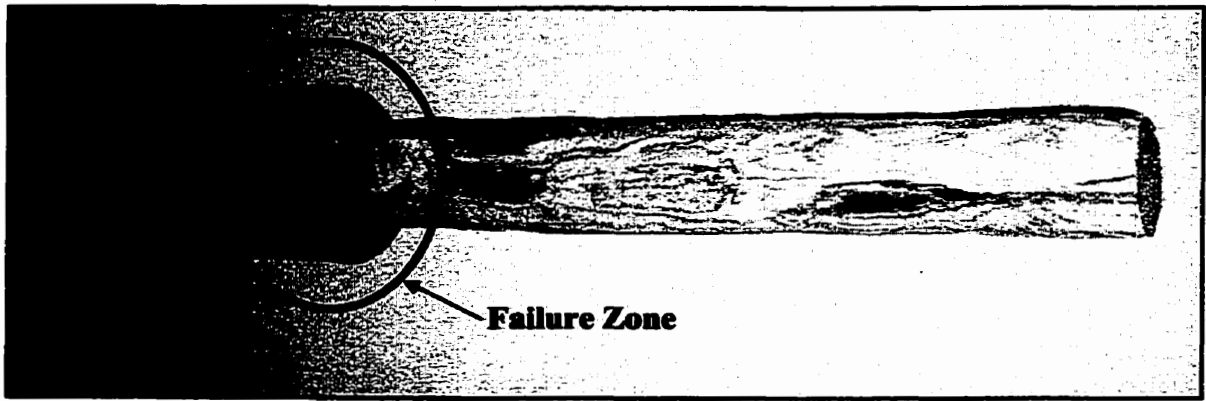


Figure 5.9(a): Photo of Trimmed Timber Pile Before Grout Injection

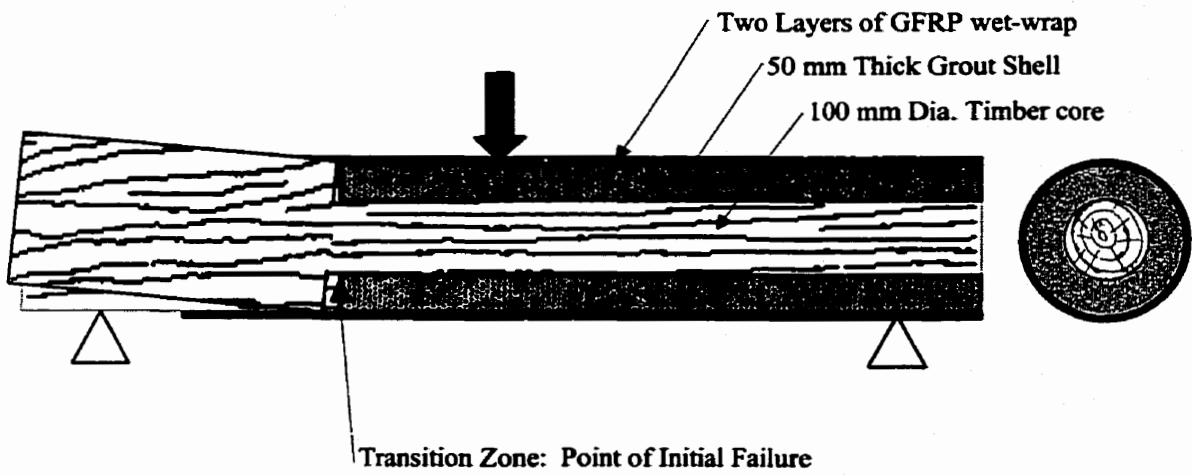


Figure 5.9(b): Schematic of Longitudinal Cross-Section of Repair Specimen at Failure

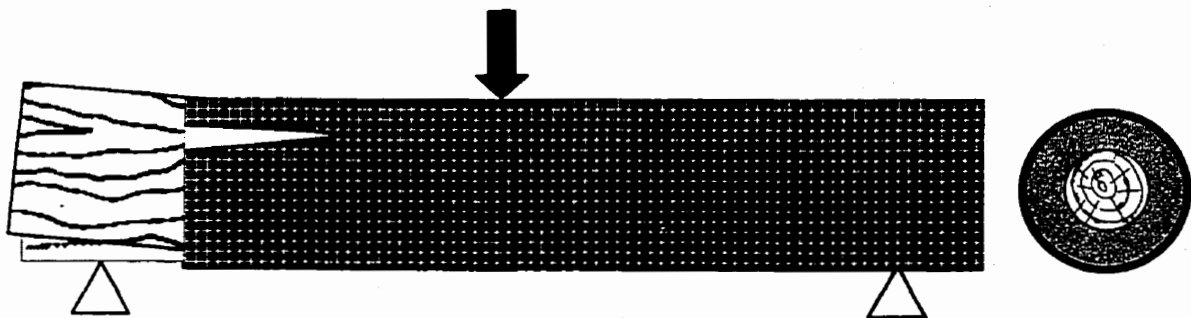


Figure 5.9(c): GFRP Sheet Ruptured Over 200 mm Length





*Figure 5.10: Specimen 3L-T with Lateral GFRP Wrap and Timber Core at Failure.*



*Figure 5.11: Specimen 3LA-V with Axial and Lateral GFRP Wrap and Void Core at Failure*

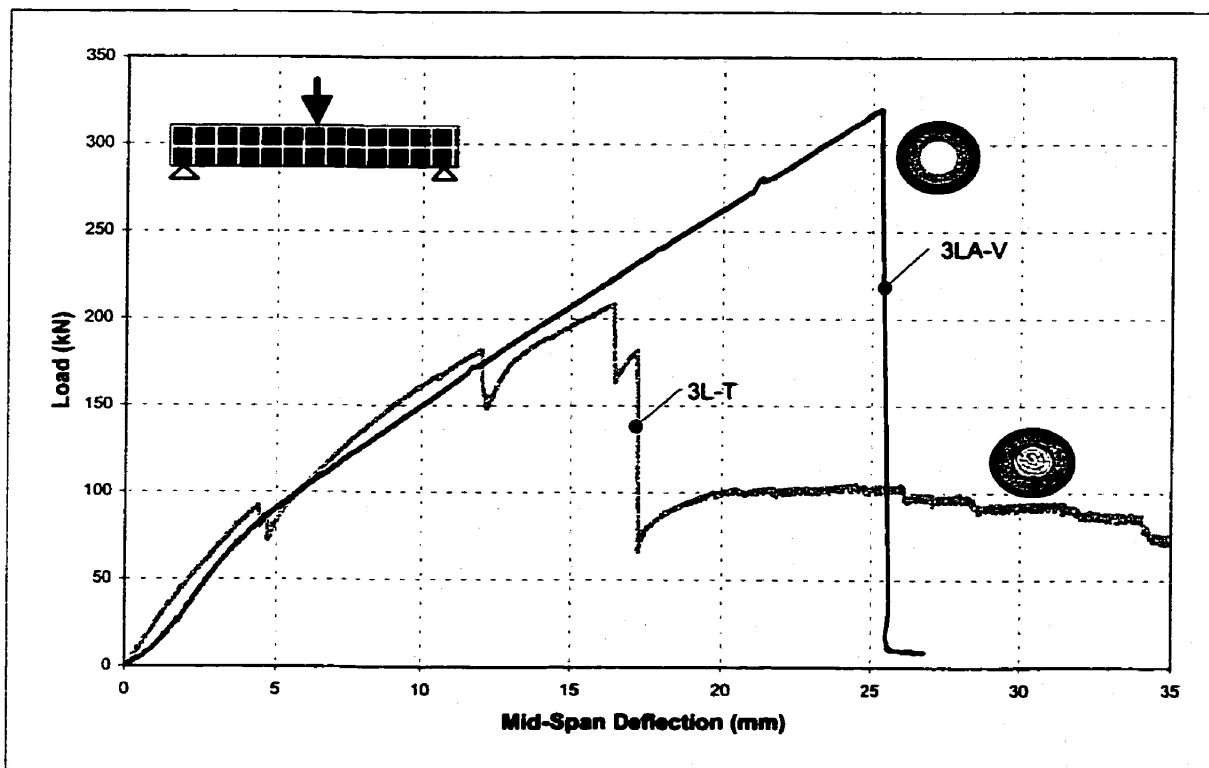


Figure 5.12: Load vs Mid-Span Deflection Curves for 300 mm Diameter Piles Tested in Bending

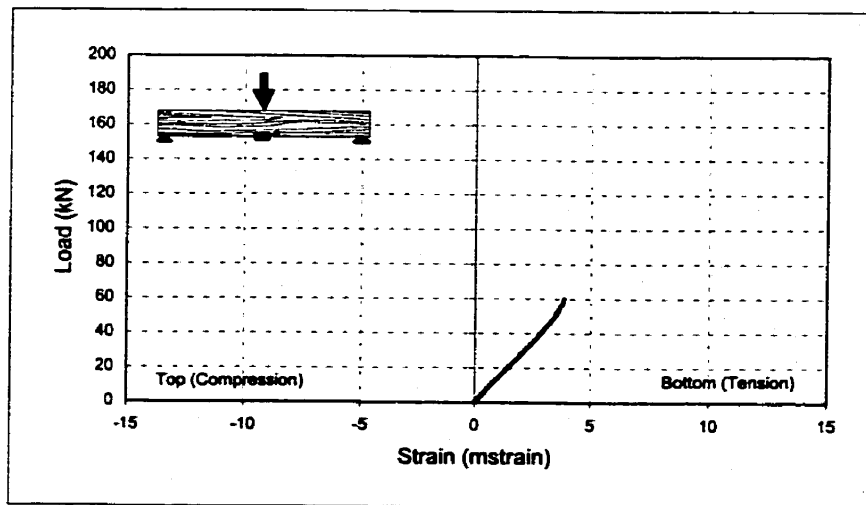
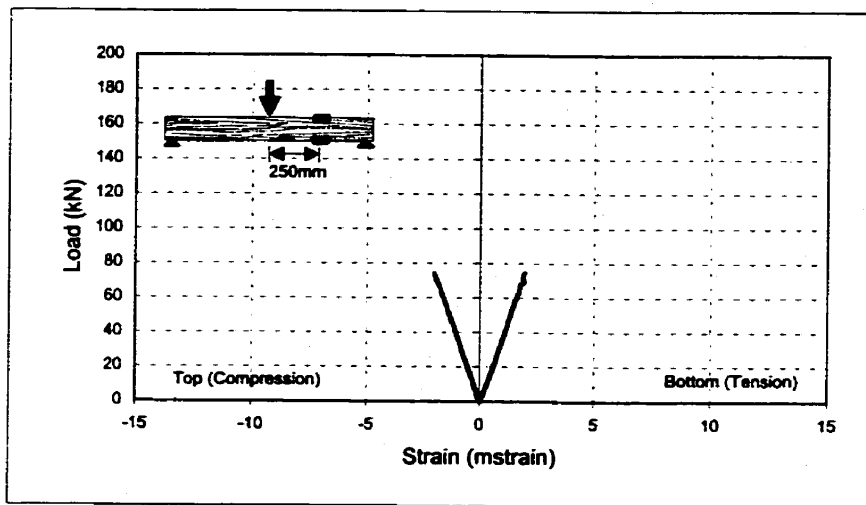
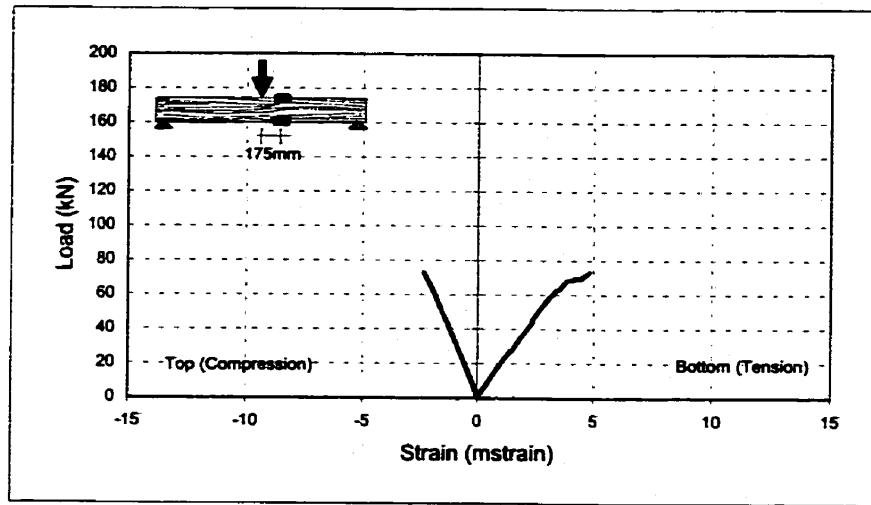


Figure 5.13: Load vs Flexural Strain Curves for 2C-T-1

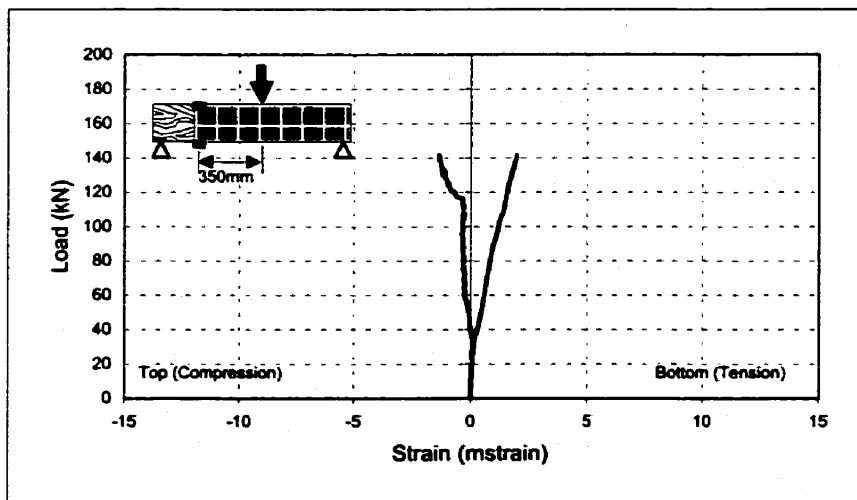
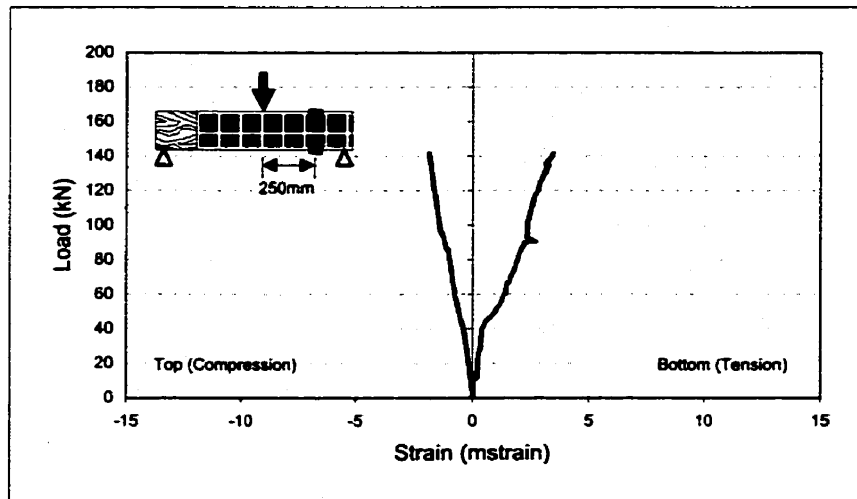
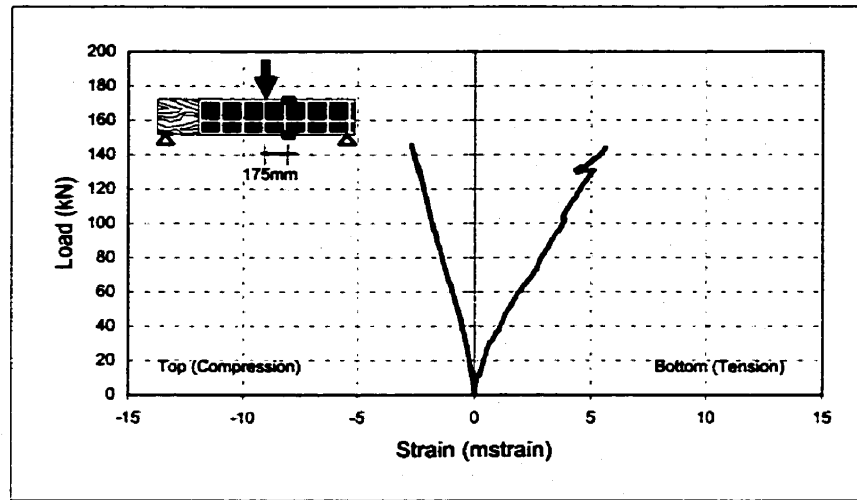


Figure 5.14: Load vs Flexural Strain Curves for 2LA-T-3

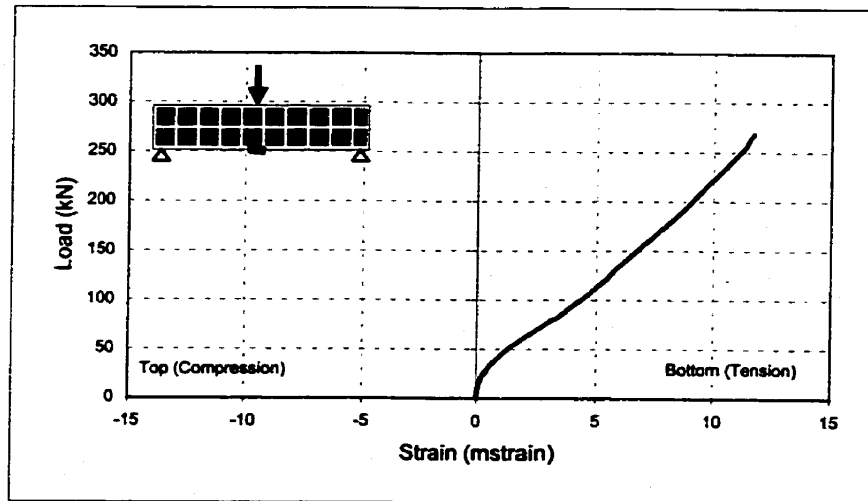
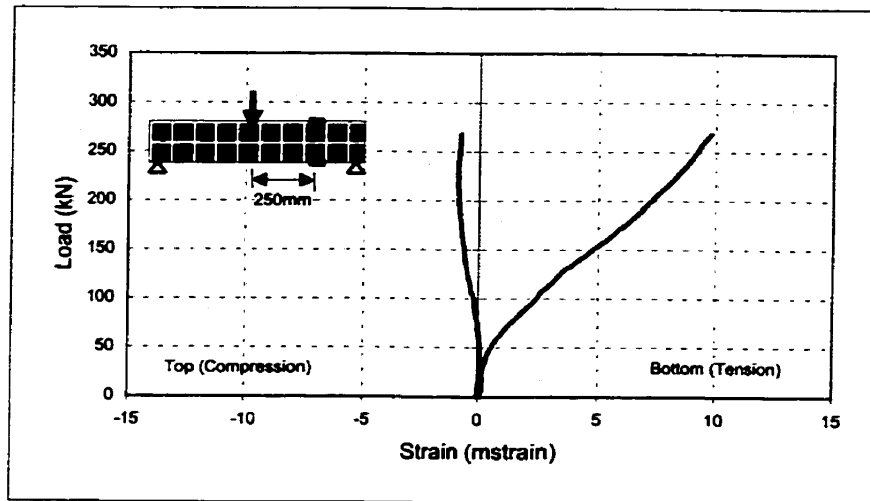
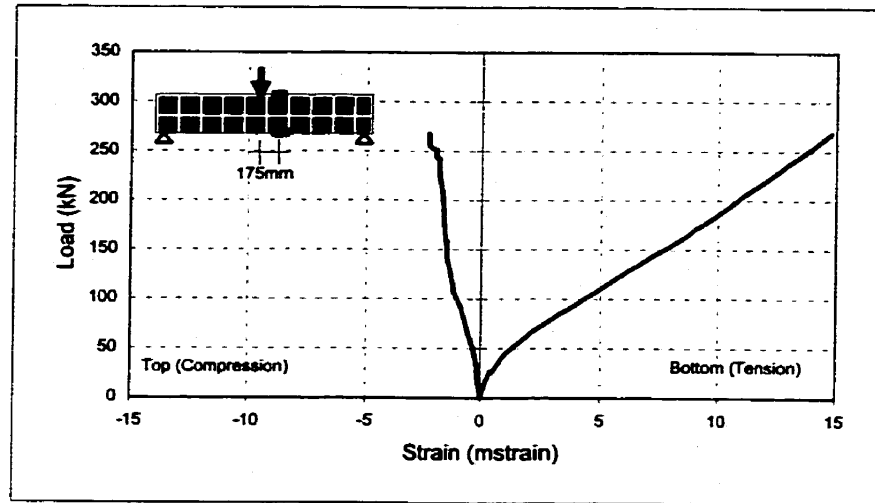


Figure 5.15: Load vs Flexural Strain Curves for 3LA-V

## **Chapter 6**

### **Summary and Conclusions**

#### **6.1 Summary**

The main objective of this study was to evaluate a repair scheme that can restore or improve the original capacity of deteriorated timber piles. The use of external GFRP confinement systems and cementitious grout to repair heavily decayed timber piles was examined and an experimental program was conducted to evaluate the strength and behaviour of the repaired timber piles. A total of 53 pile specimens were fabricated and tested in axial compression and bending.

In order to examine the load-carrying capacity of the repaired piles, a total of 43 timber piles repaired using two different external GFRP systems were tested in axial compression. The effect of various levels of confinement on the behaviour of the repaired piles was examined using three different GFRP configurations: single and double layers of GFRP wet-wrap and a prefabricated GFRP shell. Furthermore, in order

to examine the load transfer behaviour between the repaired and unrepaired zone, bearing specimens were fabricated and tested using the GFRP wet-wrap system. In order to determine the effect that the condition of the timber core has on the behaviour of the repaired piles, three different levels of timber deterioration were examined. Timber piles with only mild decay, timber piles with heavy decay and simulating the worst case of completely deteriorated timber, pile specimens with a void core were tested.

The flexural behaviour of the repaired piles was examined using 10 specimens tested in bending. The bending tests included “timber only” bending control specimens as well as timber piles repaired using the GFRP wet-wrap system with various orientations of the fibers. The major area of focus was examining the flexural capacity of the transition zone between the repaired and unrepaired lengths of pile.

General trends in the behaviour of the repaired piles were identified, and the effect of various parameters was assessed. A summary of key observations is provided in the following section. In order to facilitate field application of this repair technique, a simplified design procedure was developed and detailed design recommendations are made in the following section. And finally, recommendations for further research are made in order to provide for optimization of the repair technique and refinement of the design procedure.

## **6.2 Conclusions and Design Recommendations**

Based on the results of this experimental program, the following conclusions and design recommendations can be drawn:

1. A single layer of GFRP wet-wrap with the fibers oriented laterally around the circumference of the pile provides enough confinement to restore a timber pile repaired with a 50 mm thick grout shell to its original axial capacity or greater, satisfying the required design capacity.
2. The application of a grout shell and FRP confinement system tends to reduce the variability in axial capacity of the repaired piles.
3. Since a large portion of the applied axial load is carried by the stiff grout shell, bearing failure in the sound timber below the grout shell must be avoided. In order to provide sufficient bearing area, a minimum thickness of 50 mm must be used for the grout shell. The bearing surface of the timber must be strengthened using epoxy impregnation and confining GFRP wrap, or some other technique shown to be effective.
4. A double layer of GFRP wrap and prefabricated GFRP shells with increased fiber content when used for confinement, are effective in increasing the axial capacity of the piles beyond that obtained for piles with a single layer of GFRP wrap.



5. Although the GFRP systems used were effective in confining the grout shell, the strain in the FRP at failure was significantly lower than the rupture strain reported by the manufacturers. This behaviour should be accounted for when applying or developing more refined models for prediction of the pile capacity.
6. As was observed by other researchers, the effectiveness of the confinement provided by the FRP system is reduced with an increase in core size. In addition, the presence of sound timber in the core may enhance the effectiveness of the confinement provided by the external FRP system.
7. Based on the test data available to date, a simplified designed approach is recommended. It is both reasonable and conservative to assume that the applied axial load is carried entirely by the stiff grout shell. Due to the presence of the void or timber core, only 60% of the grout cylinder strength,  $f_g$ , should be used to calculate the strength of the confined grout shell. For piles with a greater degree of confinement, such as a double layer of GFRP wrap, the strength of the grout shell may be increased to  $0.75f_g$ , but should be confirmed with further testing and a statistical analysis.
8. The presence of axial GFRP sheets is effective in increasing the flexural capacity of the repaired piles. However, the transition zone between the repaired and unrepaired lengths of pile has a lower flexural capacity than the repaired zone and the original

timber pile. The transition zone should therefore be located at a depth with lower applied moment.

9. Additional design recommendations based on observations made during specimen fabrication include: the use of shoring while removing decayed timber around the circumference of the pile, pre-wetting of the timber core prior to grout injection to control the amount of moisture absorbed by the timber and removed from the grout mix.

### **6.3 Recommendations for Further Research**

In order to optimize the repair technique and refine the proposed design approach, it is proposed that further research be conducted in the following areas:

1. Development of an improved method for strengthening the timber bearing area below the grout shell, in order to more effectively transfer the applied axial load to the sound timber below the repaired zone.
2. The transition zone between the repaired and unrepaired portions of the pile cannot sustain high moment. Therefore a method for improving the flexural capacity of the transition zone should be developed.
3. In principle, if axial compression is the controlling design load, then the continuous fibers of the GFRP system should be oriented in the hoop direction for maximum confinement. On the other hand, if applied moment is the dominating design factor, the continuous fibers of the GFRP system should be oriented in the axial direction of the pile. Therefore, fibers oriented in other directions such as  $\pm 45^\circ$  to the axis of the piles may provide the optimum design solution. Further testing should be conducted to examine more optimal fiber orientations, and to quantify the effect of different fiber orientations on the pile capacity.

4. Refinement of Mander's model or the development of other reliable models for predicting the confined grout strength may be conducted based on additional testing and parametric analysis. Parameters to be considered include: the strain that can be achieved in the confining FRP system at failure, the effect of confining solid grout cylinders in comparison to solid concrete cylinders, and the effect of core size and core condition on the efficiency of the confining external FRP system.
  
5. The durability of the proposed repair technique should be assessed through accelerated wet-dry and freeze-thaw cycling in the laboratory and monitoring of trial field applications.

## References

1. ACI Committee 351, (1999), "*Grouting between Foundation and Bases for Support of Equipment and Machinery*", ACI 351.1R-99, American Concrete Institute.
2. American Society of Civil Engineers (ASCE), "*Practical Guide for the Selection, Design, and Installation of Piles*", By Committee on deep foundation of the ASCE Geotechnical division, (1984), New York, New York.
3. Armstrong, R. M., "*Structural Properties of Timber Pile*", Behaviour of Deep foundations. ASTM STP 670, Raymond Lundgren, Ed., American Society for testing and materials, 1979, pp. 118 – 152.
4. Avent, Richard R., "*Durability of Posted and Epoxy-Grouted Timber Piles*", Journal of Structural Engineering, 115(4), ASCE, April 1989, pp. 826 - 833.
5. Avent, Richard R., "*Repair of Timber Bridge Piling by Posting and Epoxy Grouting*" Transportation Research Record, 1053, 1986, pp. 70 - 79.
6. "*Bridge Piling can be Protected; FRP Jackets Stop Deterioration*", Better Roads, May 1980, 50(5), pp. 20 - 25.
7. Buslov, Valery M. and Scola, Philip T. "*Inspection and Structural Evaluation of Timber Pier: Case Study*", Journal of Structural Engineering, 117(9), ASCE, September 1991, pp. 2725 - 2741.
8. Canadian Institute of Timber Construction (CITC), (1962), "*Pressure Treated Timber Piles: a Manual for Architects and Engineers*", Ottawa, Canada.
9. Canadian Wood Council (CWC), (1991), "*Wood Piles: Design, Protection, Field Procedures, Specification, Case Study*", Ottawa, Ontario.

10. Canadian Standards Association (CSA), (1989), "*Engineering Design in Wood*", (CAN/CSA-O86.1-M89), Rexdale, Ontario, Canada, 1989.
11. Fam A. Z., Rizkalla, S. H., "*Behavior of Axially Loaded Concrete-Filled Circular Fiber-Reinforced Polymer Tubes*", ACI Structural Journal, V 98, No. 3, May-June 2001.
12. Fam, A. Z. "*Concrete-Filled Fiber Reinforced Polymer Tubes for Axial and Flexural Structural Members*", Ph.D. thesis, University of Manitoba, Winnipeg, Manitoba, July 2000.
13. Fardis, Michael. N., and Khalili, Homayoun, "*Concrete Encased in Fiberglass-Reinforced Plastic.*" J. American Concrete Institute, No. 78 – 38, November – December 1981, pp 440 – 446.
14. Findlay, W. P. K., "*Timber: Properties and Uses*", Granada Publishing Limited, London, 1975.
15. Freas, Alan, "*Evaluation, Maintenance and Upgrading of Wood Structures: a Guide and Commentary.*" American society of civil engineers, New York, New York, 1982.
16. Gentile, C. J., "*Flexural Strengthening of Timber Bridge Beams Using FRP*", M.Sc. thesis, University of Manitoba, Winnipeg, Manitoba, January 2000.
17. Gerke, Richard C., "*New Process Restores Timber Piles.*" Ocean Industry, 4(5) May, 1969, pp. 92 - 93.
18. Grefsheim, Frank D., "*Timber Pile Study, Existing Structures.*" Conference proceeding, Deep Foundations, ASCE, 1980, pp. 166 - 181.

19. "Gribbles' Attack Collapses Bridge ... But Polyester Sleeves Thwart Them", Better Roads, April 1980, pp. 10 – 14.
20. Johnston, G. H., "Pile Construction in Permafrost", National Research Council Canada, Proceedings: Permafrost International Conference, November 1963, pp 477 - 480.
21. Kosmatka, Steven H., "Cementitious Grouts and Grouting", Portland Cement Association (PCA), USA, 1990
22. MacGregor, J. G. (1997) "Reinforced Concrete Mechanics and Design", 3<sup>rd</sup> Ed., Prentice Hall, Upper Saddle River, NJ.
23. Madsen, B. (1992), "Structural Behaviour of Timber", Timber Engineering LTD., North Vancouver, British Columbia, Canada.
24. Mander, J. B., Priestley, M. J. N. And Park, R., "Theoretical Stress-Strain Model for Confined Concrete", Journal of Structural Engineering, ASCE, Vol. 114 No. 8, August 1988, pp 1804 – 1826.
25. Master Builders Inc., "Composite Strengthening System: Engineering Design Guidelines", 2<sup>nd</sup> Ed., September 1998, Baltimore, MD.
26. Michel, Samaan and Mirmiran, Amr, "Model of Concrete Confined by Fiber Composites." Journal of Structural Engineering, Vol. 124, No. 9, 1998, pp 1025 – 1031.
27. Mirmiran, A., Shahawy, M., "Behaviour of Concrete Columns Confined by Fiber Composites", Journal of Structural Engineering, Vol. 123, No. 5, 1997, pp 583 – 590.

28. Mirmiran, A., Shahawy, M., "A New Concrete-Filled Hollow FRP Composite Column", *Composites: Part B: Engineering, Special Issue on Infrastructure*, Elsevier Science Ltd., Vol. 27B, No. 3 – 4, June 1996, pp 263 – 268.
29. Nanni, Antonio and Bradford, Nick M., "FRP Jacketed Concrete under Uniaxial Compression", *Construction and Building Materials*, Elsevier Science Ltd., Vol. 9 No. 2, 1995, pp 115 – 124.
30. Picher, F., Rochette, P., and Labossiere, P., 1996, "Confinement of Concrete Cylinders with CFRP", *Proceedings of the 1<sup>st</sup> International Conference on Composites in Infrastructure*, H. Saadatmanesh and M. R. Ehsani, eds., University of Arizona, Tucson, Ariz., pp. 829-841.
31. Railway and Truck Structures (1973), "Now: Grout-Filled Timber Piles", February 1973, Vol. 69, No. 2, pp 28-29, Simmons-Boardman Pub. Corp., Bristol, Conn. USA.
32. Ruddick, John N. R., (1999), "An Assessment of Decay in House Piles Supporting Buildings Managed by the Inuvik Housing Authority," Technical Report Submitted to Mr. Garry Smith, Maintenance Manager, Inuvik Housing Authority, July 22, 1999.
33. Sedziak, H. P., Shields, J. K., Johnston, G. H., "Condition of Timber Foundation Piles at Inuvik, N. W. T.", Canadian Forestry Service, Department of the Environment, December 1973.
34. Stumes, Paul, "W.E.R. System Manual – Structural Rehabilitation of Deteriorated Timber", Published by the Association for Preservation Technology, 1979, Ottawa, Canada.
35. US ARMY (1985), "Pile Construction", Field Manual, FM 5-134, Washington, DC.



## **Appendix A**

**(Load vs Strain Curves for Axial Compression Series)**

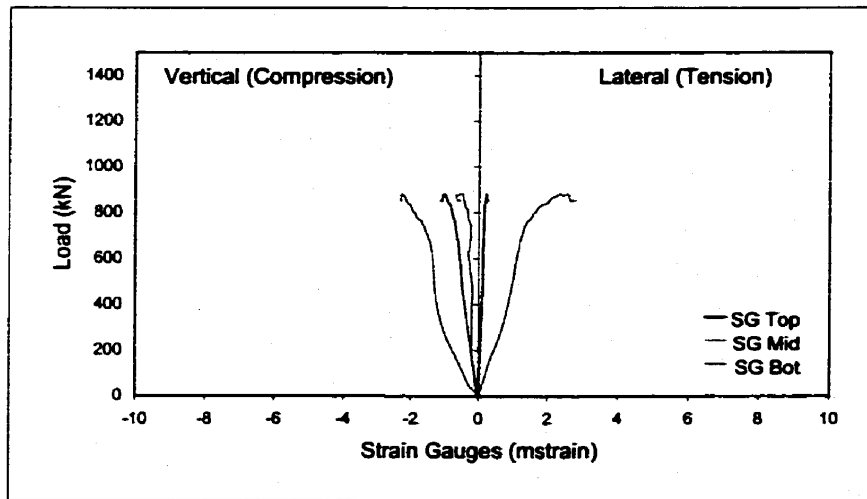


Figure A1(a): Load vs Strain Curves for 2F1-M1

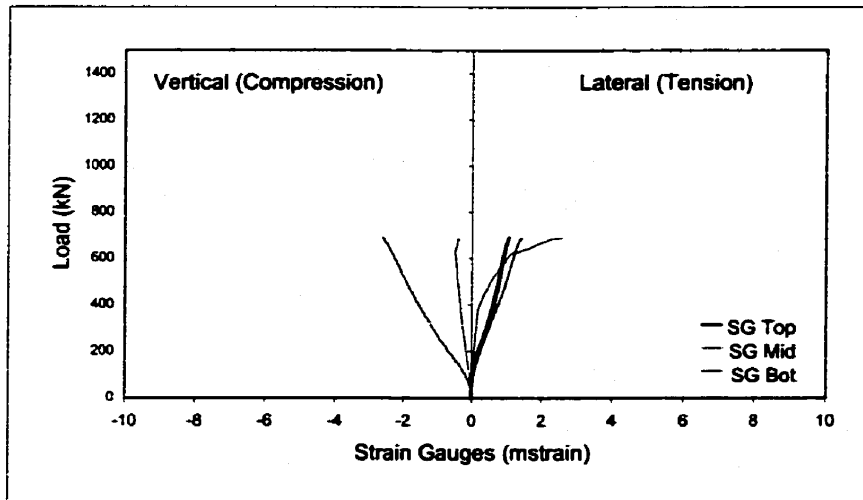


Figure A1(b): Load vs Strain Curves for 2F1-M2

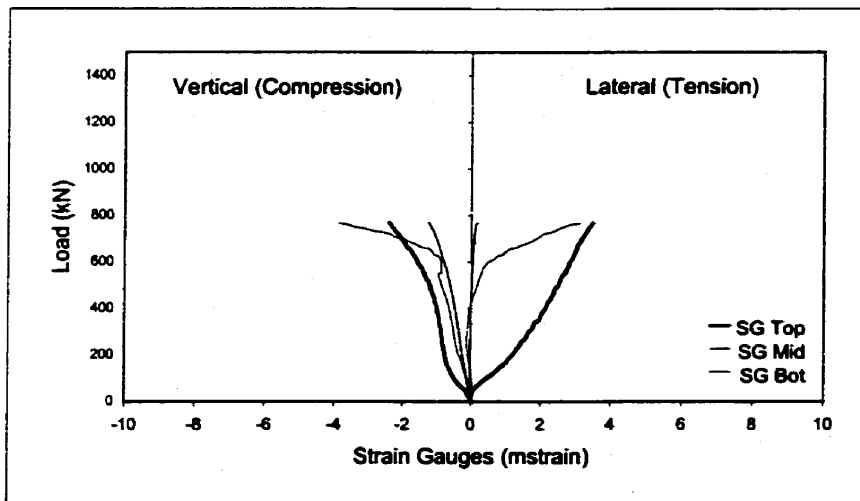


Figure A1(c): Load vs Strain Curves for 2F1-M3

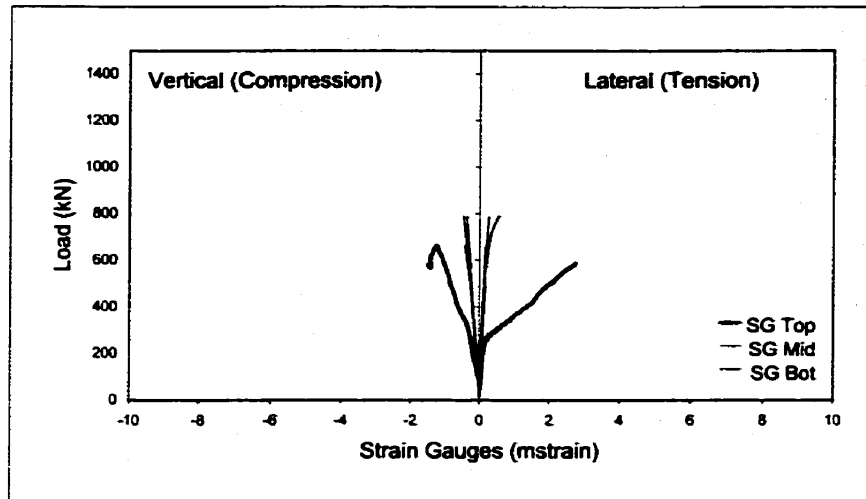


Figure A2(a): Load vs Strain Curves for 2F1-H1

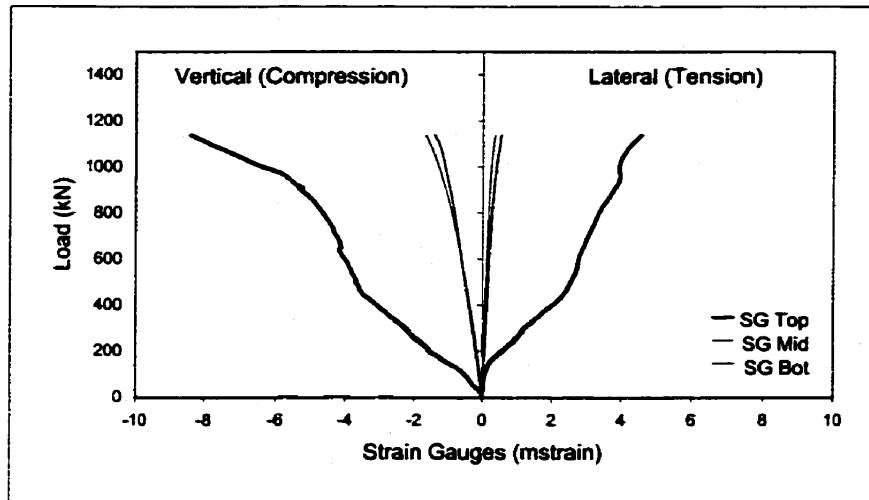


Figure A2(b): Load vs Strain Curves for 2F1-H2

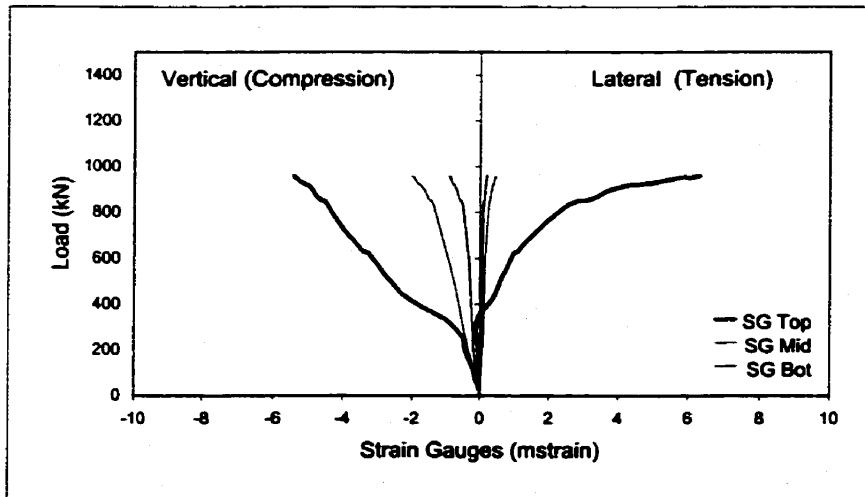


Figure A2(c): Load vs Strain Curves for 2F1-H3

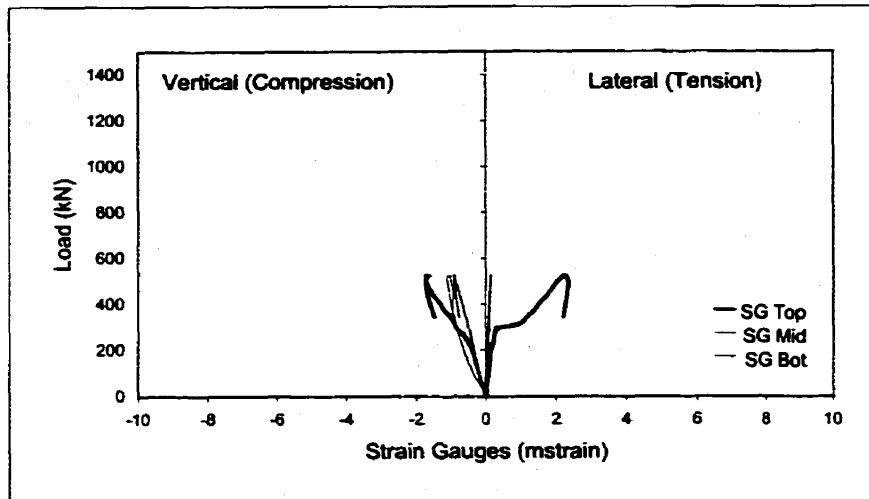


Figure A3(a): Load vs Strain Curves for 2F1-B1

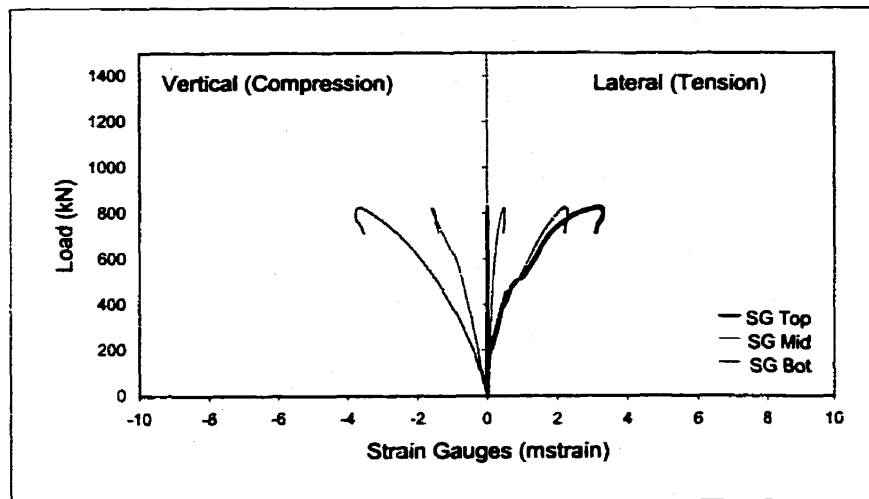


Figure A3(b): Load vs Strain Curves for 2F1-B2

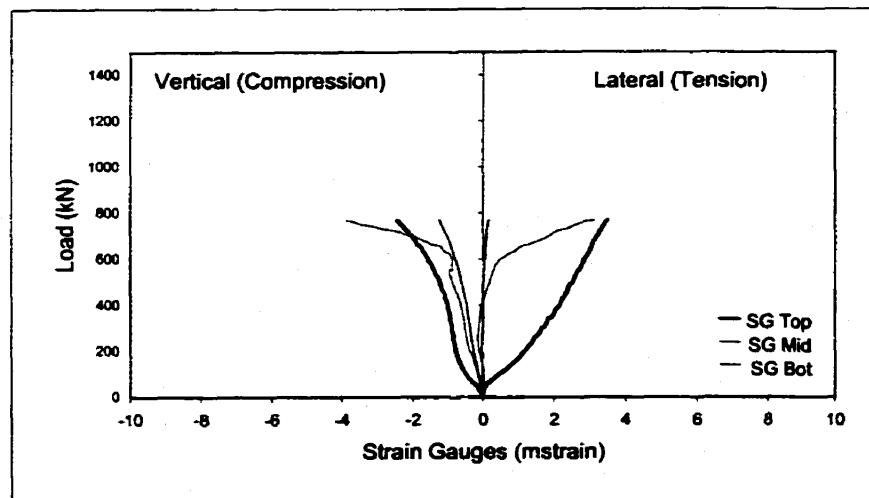


Figure A3(c): Load vs Strain Curves for 2F1-B3

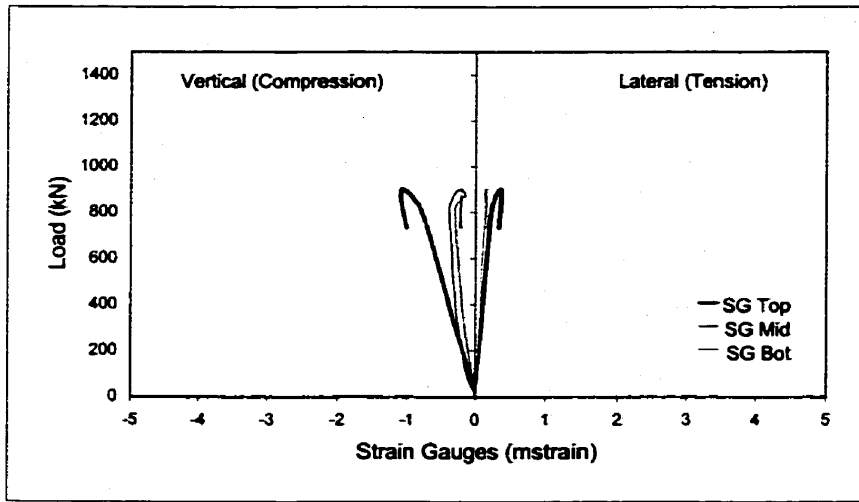


Figure A4(a): Load vs Strain Curves for 2F1-SB1

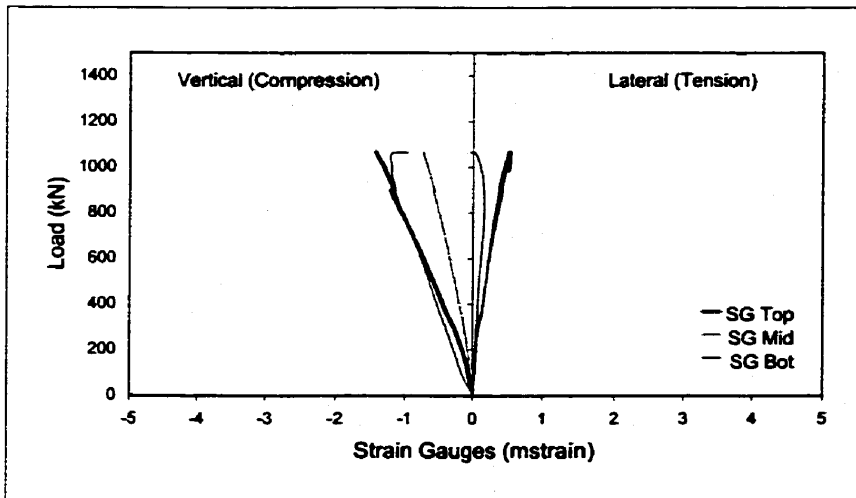


Figure A4(b): Load vs Strain Curves for 2F1-SB2

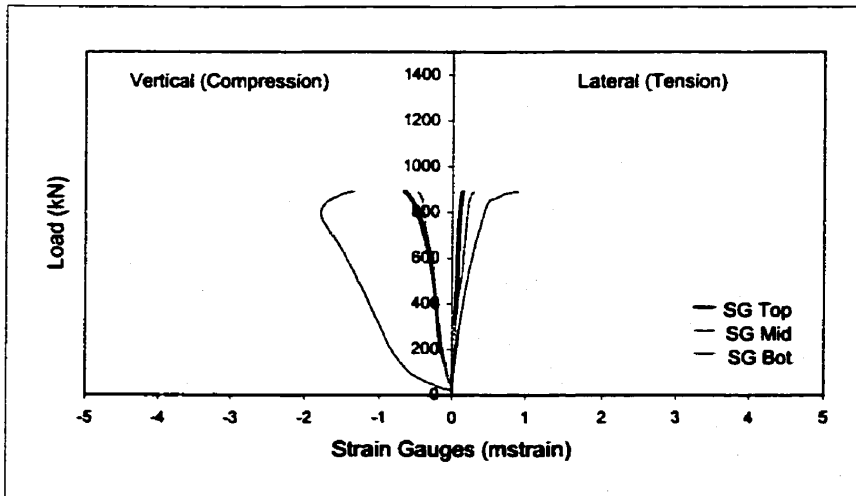


Figure A4(c): Load vs Strain Curves for 2F1-SB3

No Data

Figure A5(a): Load vs Strain Curves for 3F1-V1

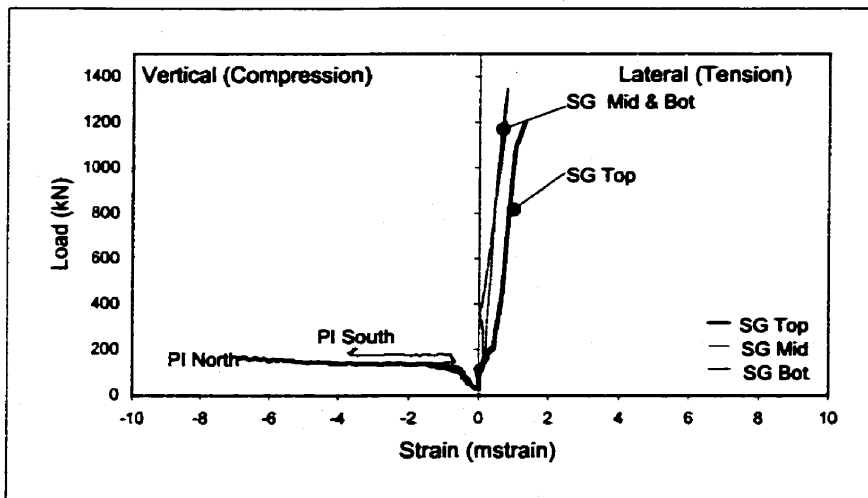


Figure A5(b): Load vs Strain Curves for 3F1-V2

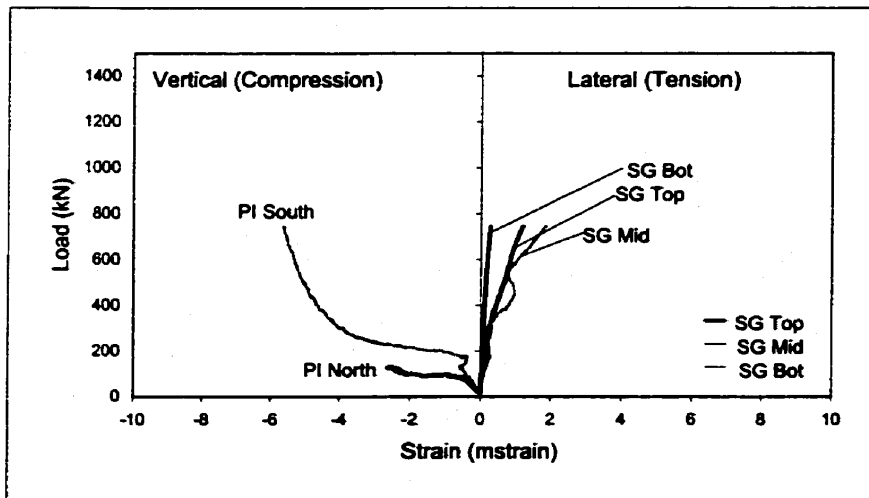


Figure A5(c): Load vs Strain Curves for 3F1-V3

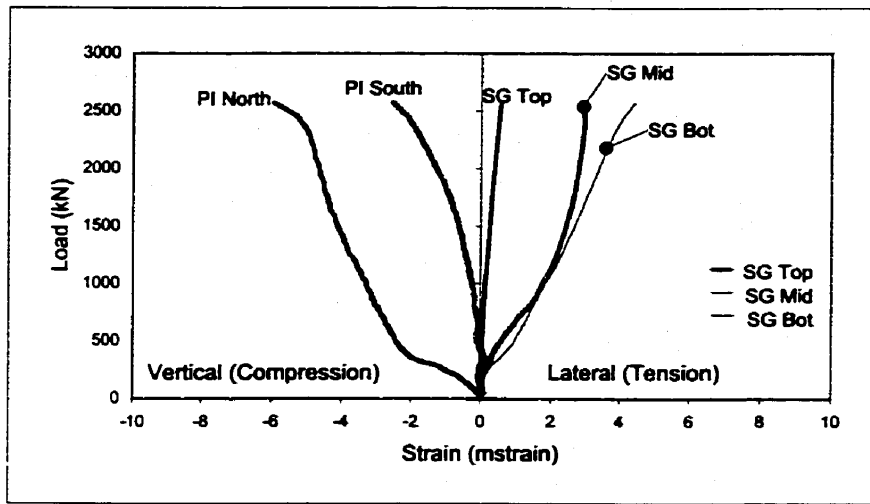


Figure A6(a): Load vs Strain curves for 3F2-M1

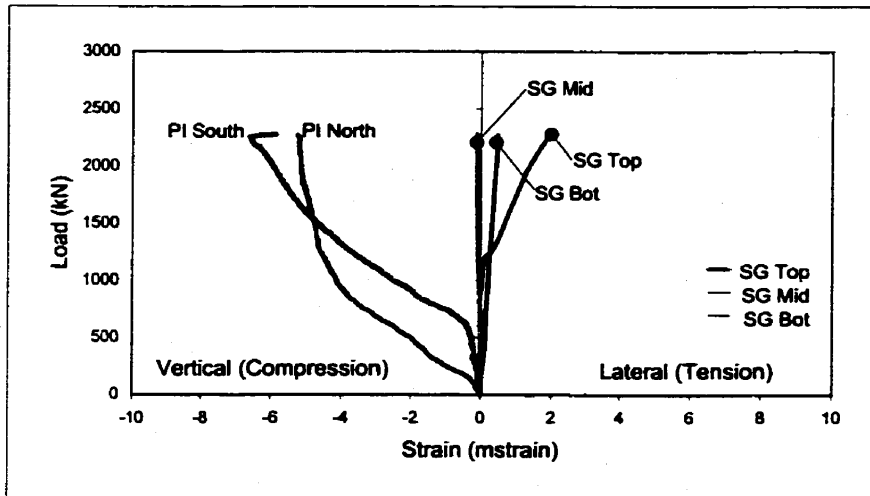


Figure A6(b): Load vs Strain curves for 3F2-M2

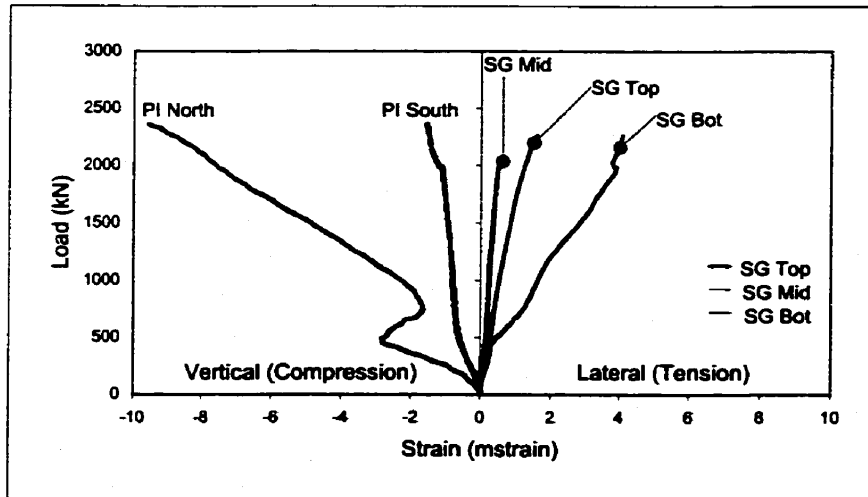


Figure A6(c): Load vs Strain curves for 3F2-M3

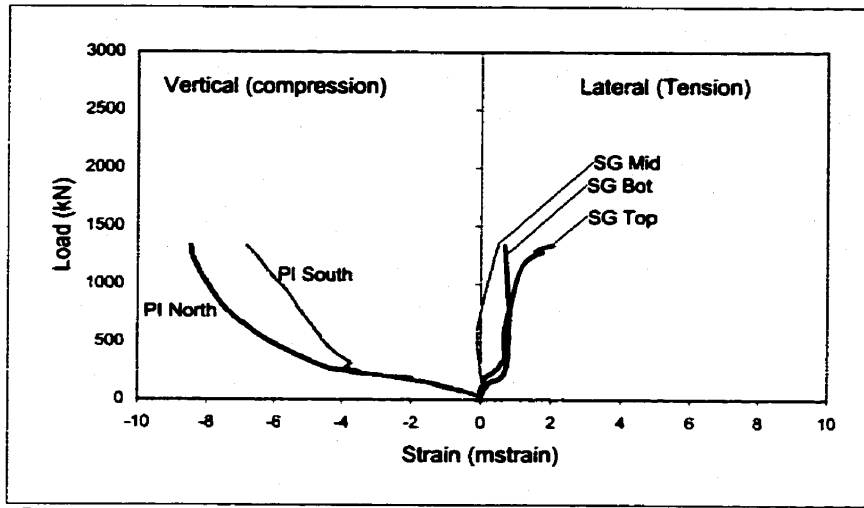


Figure A7(a): Load vs Strain Curves for 3F2-V1

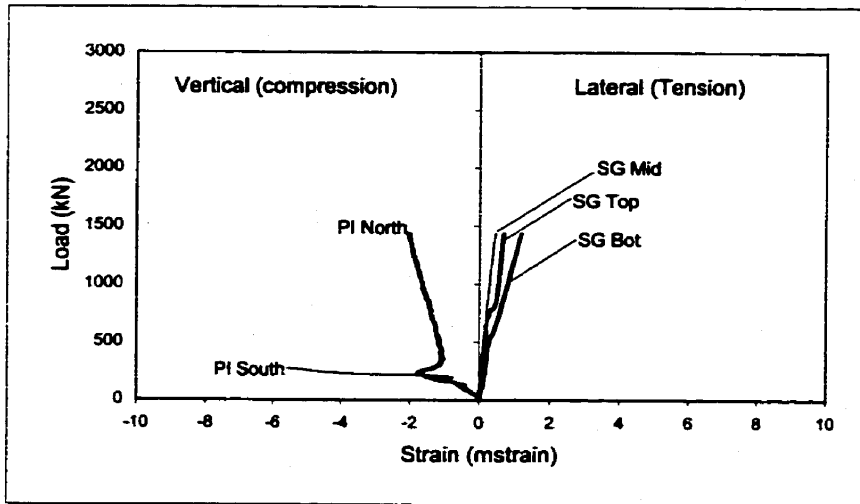


Figure A7(b): Load vs Strain Curves for 3F2-V2

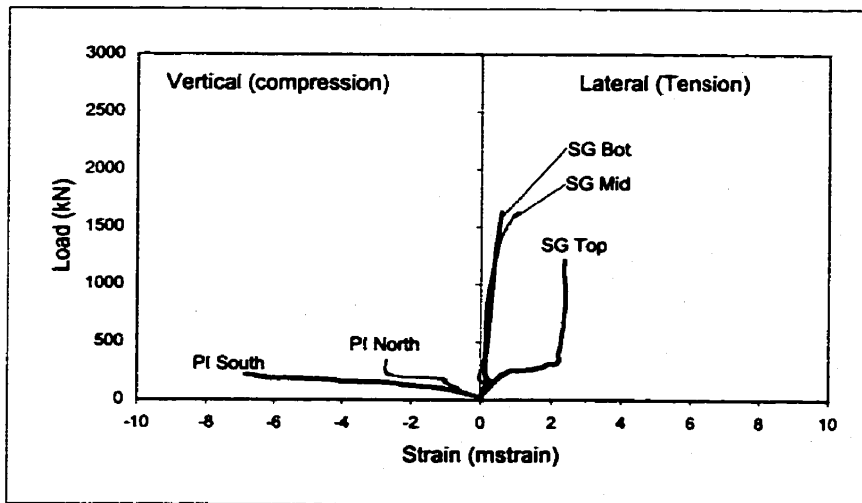


Figure A7(c): Load vs Strain Curves for 3F2-V3



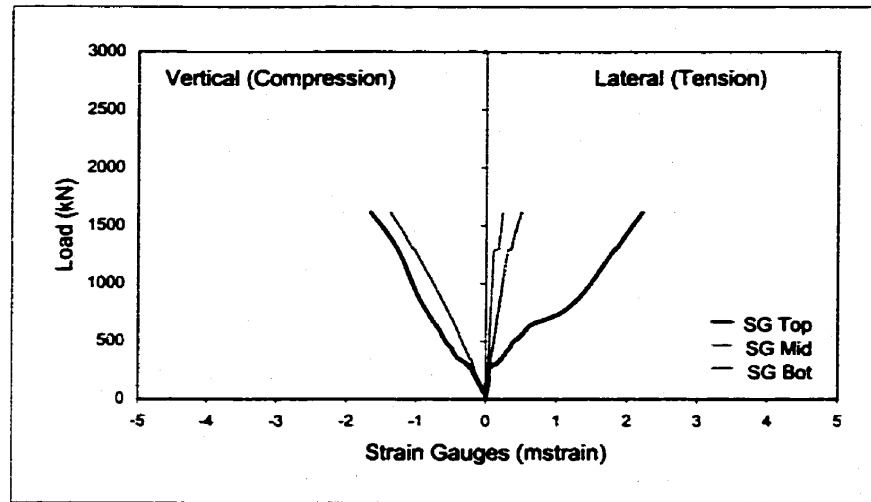


Figure A8(a): Load vs Strain Curves for 3FS-M1

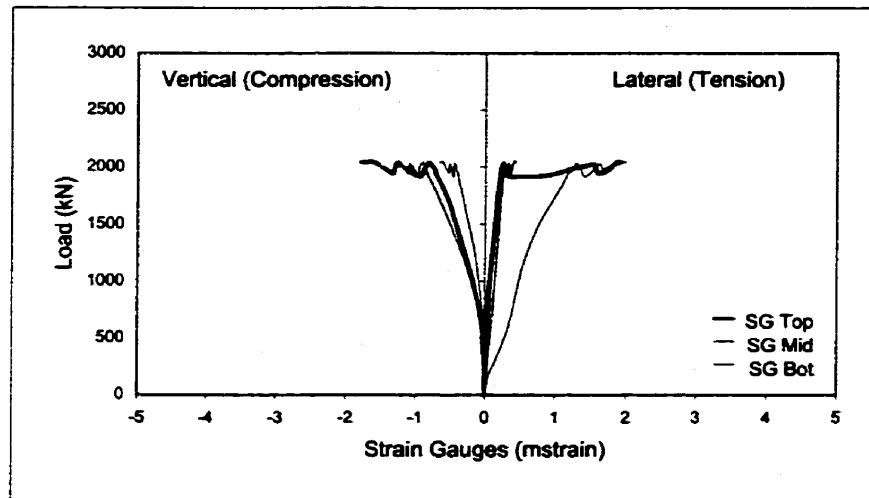


Figure A8(b): Load vs Strain Curves for 3FS-M2

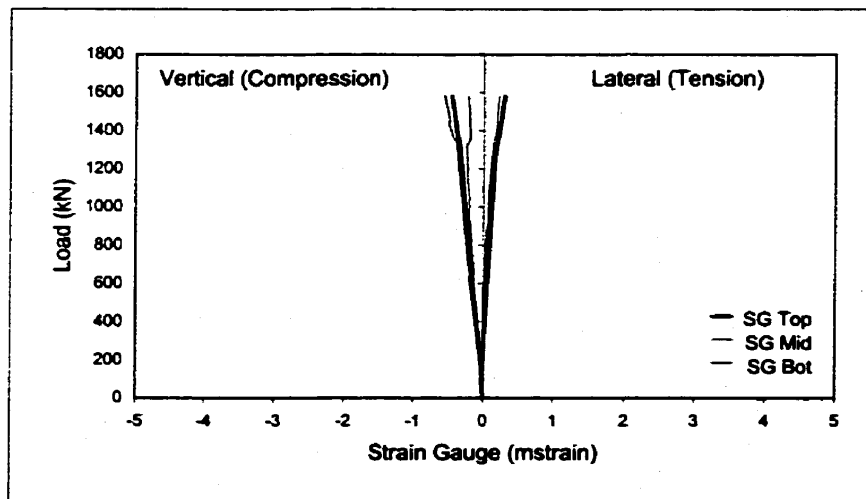


Figure A8(c): Load vs Strain Curves for 3FS-M3

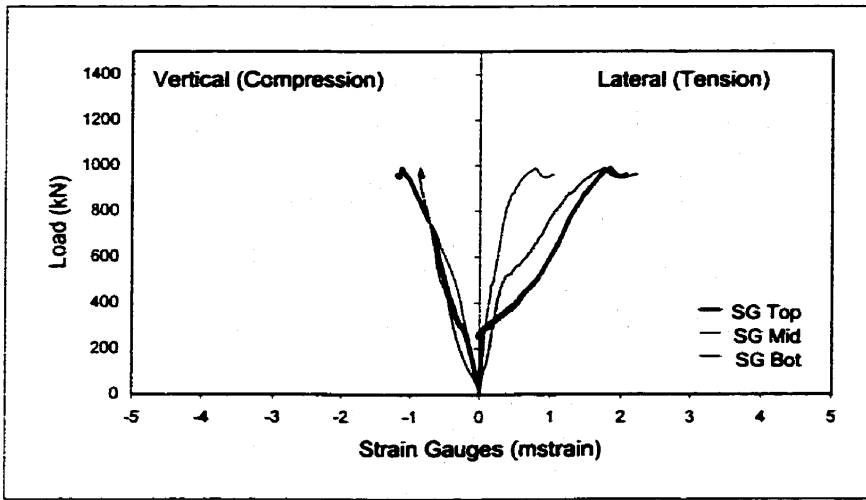


Figure A9(a): Load vs Strain Curves for 3FS-H1

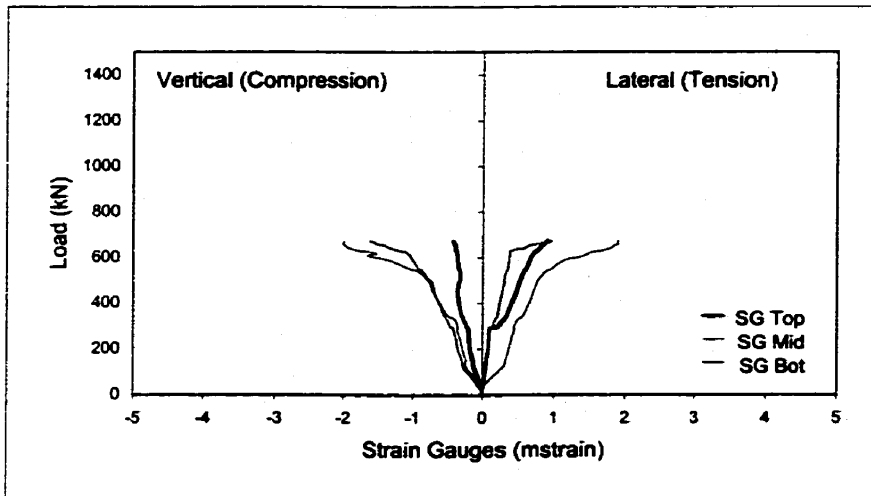


Figure A9(b): Load vs Strain Curves for 3FS-H2

## **Appendix B**

**(Load vs Flexural Strain Curves for Bending Series)**

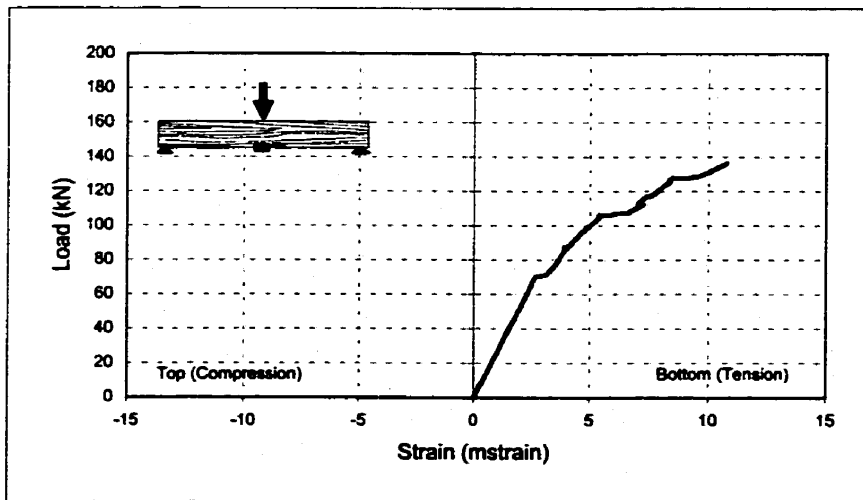
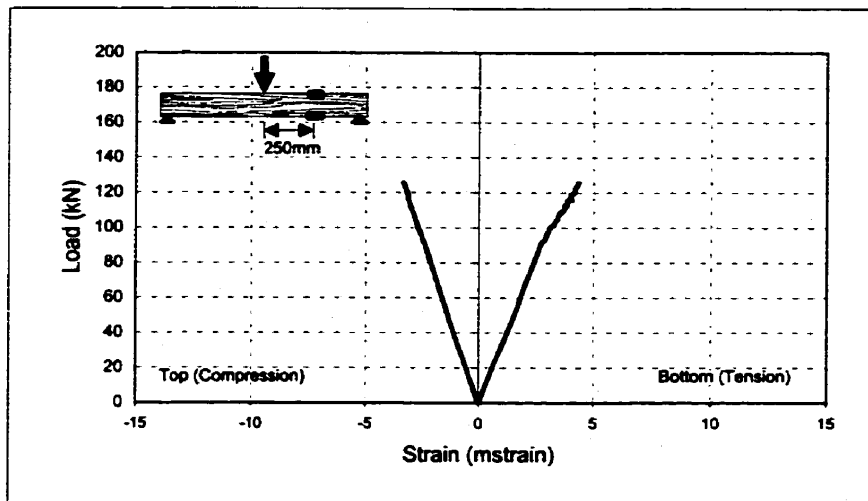
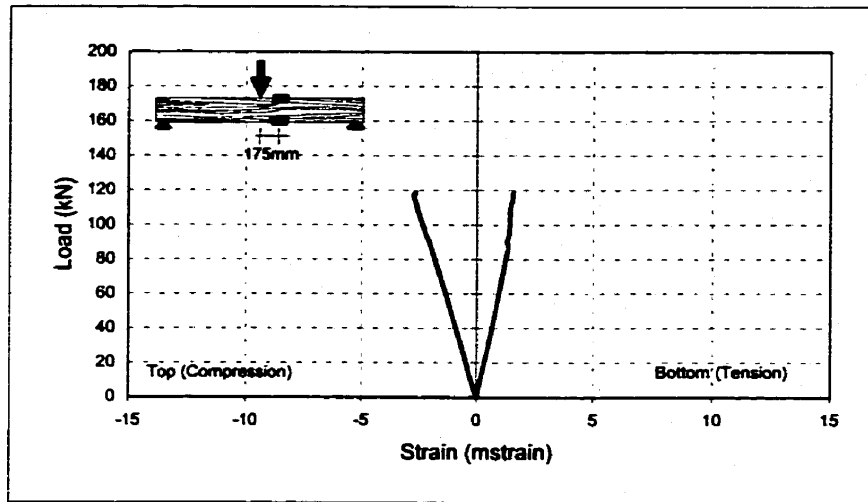


Figure B1: Load vs Flexural Strain Curves for 2C-T-2

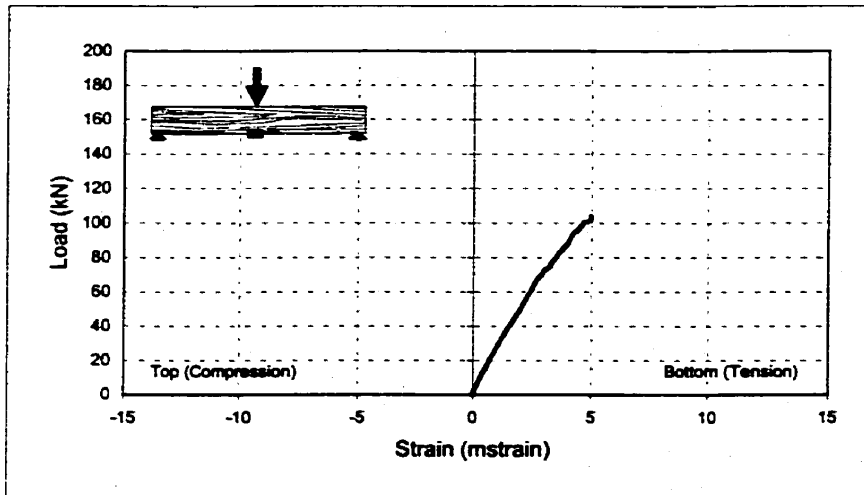
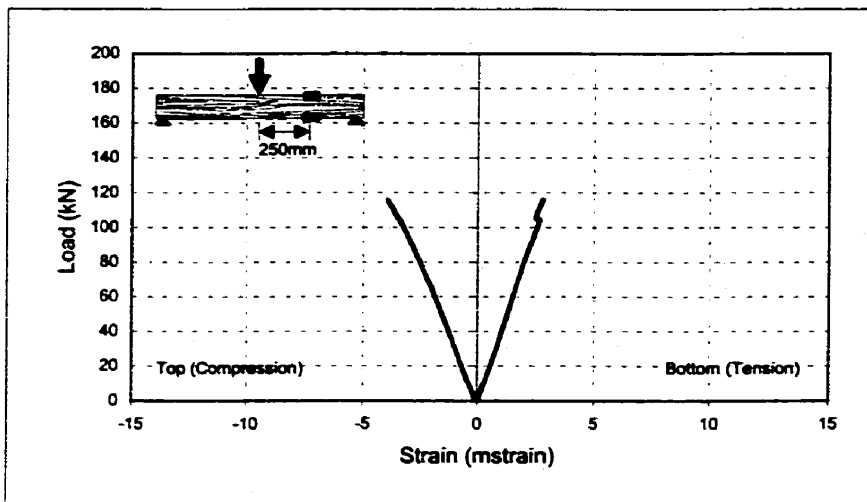
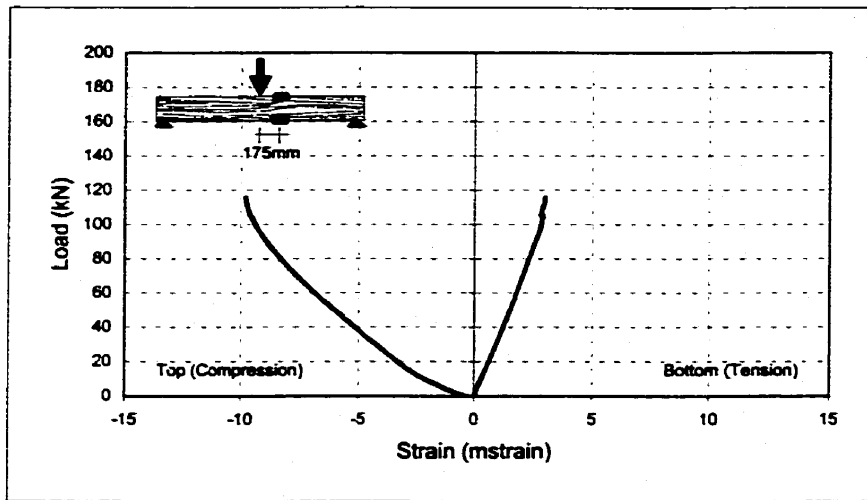


Figure B2: Load vs Flexural Strain Curves for 2C-T-3

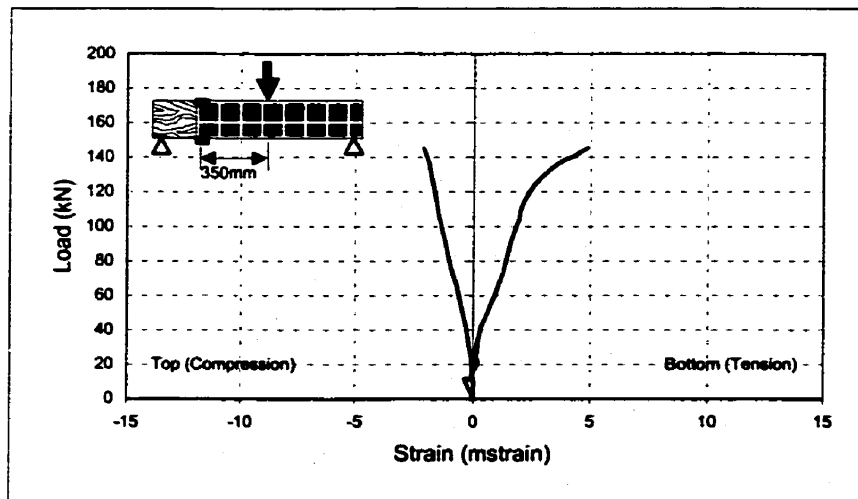
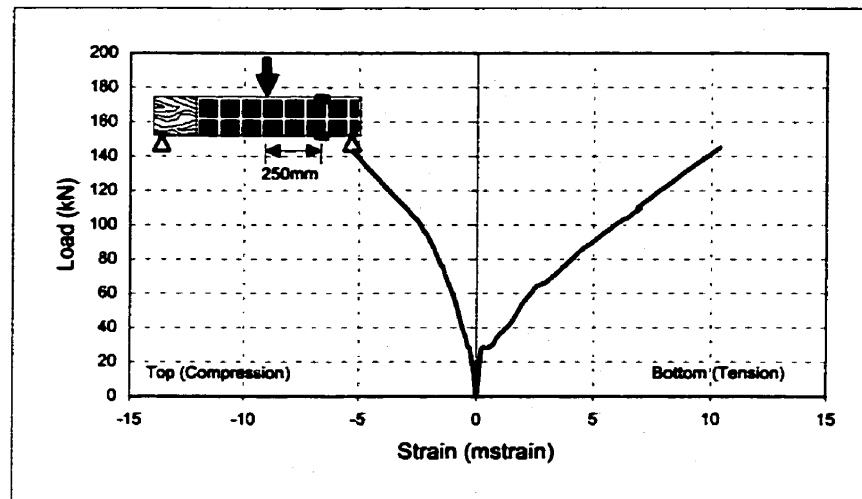
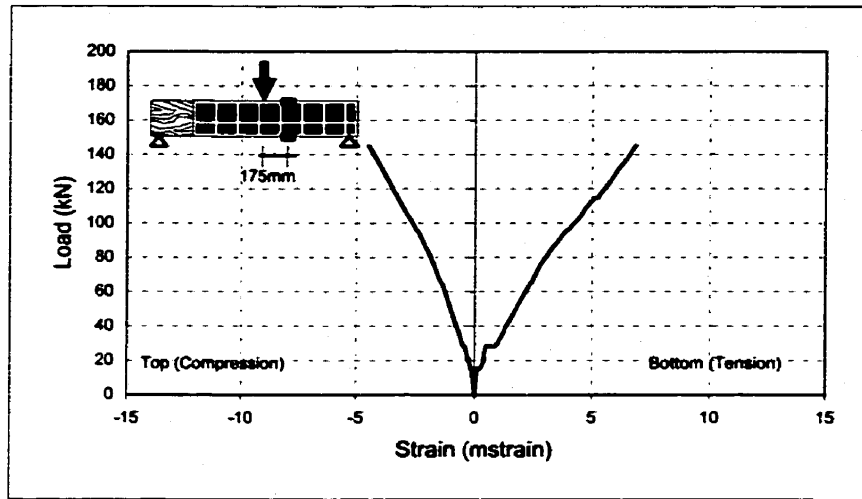


Figure B3: Load vs Flexural Strain Curves for 2LA-T-4

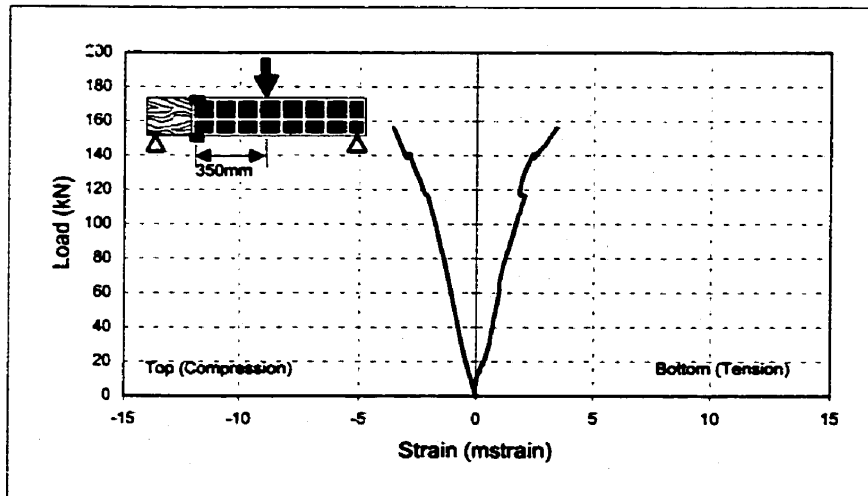
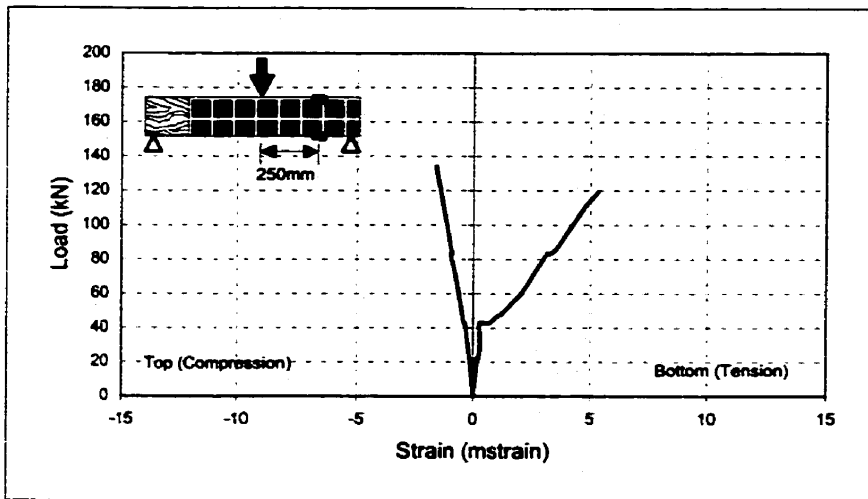
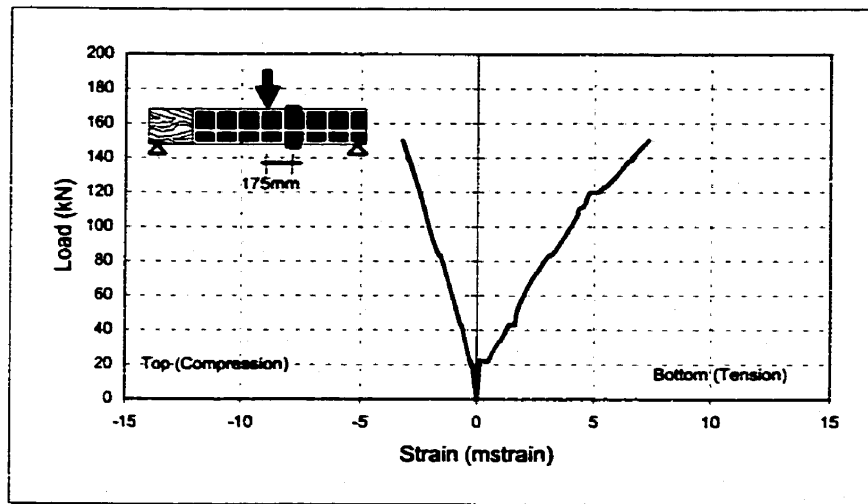


Figure B4: Load vs Flexural Strain Curves for 2LA-T-5

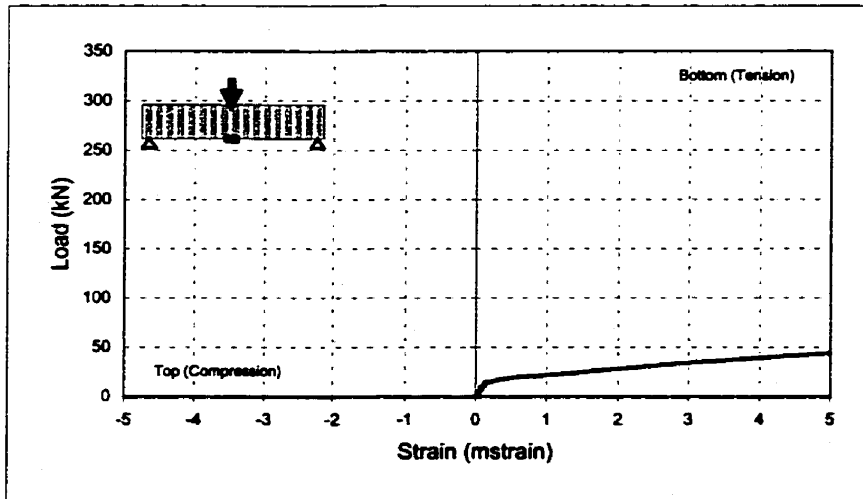
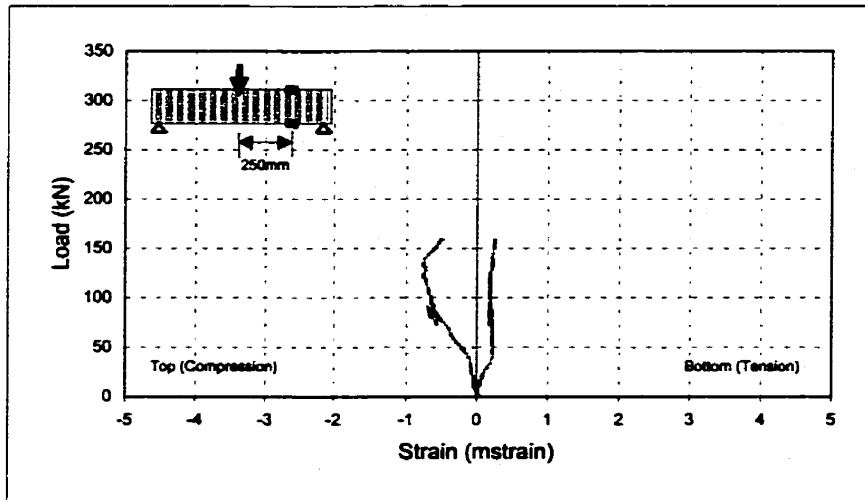
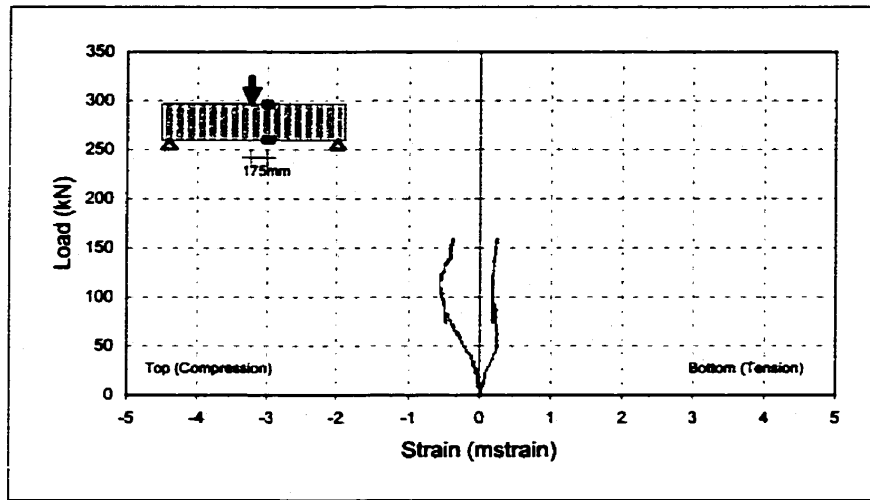


Figure B5: Load vs Flexural Strain Curves for 3L-T